

LEXNET Low EMF Exposure Future Networks

Deliverable D6.2: Report on validation, Part-B

Contractual delivery date: M36 Actual delivery date: M36

Document Information

Version	V1.0	Dissemination level	PU
Editor	Y. Corre (Siradel)		
Other authors	M. Wilson, Y. Far G. Vermeeren (In P. Zimmermann (M. Lalam (Sagen S.M. Anwar, M. L J. Stéphan, M. Br	ninds) Orange) ncom) e Henaff, Y. Toutain (Satimo) au, G. Gougeon, Y. Lostanle)
	Y. Fernández, A. Sánchez (TTI) P. Chambers, T. Brown (UniS)		

PROPRIETARY RIGHTS STATEMENT

This document contains information, which is proprietary to the LEXNET Consortium. Neither this document nor the information contained herein shall be used, duplicated or communicated by any means to any third party, in whole or in parts, except with prior written consent of the LEXNET consortium.



	L. Díez, L. Rodríguez de Lope, R. Agüero (UC) M. Popović, J. Milinković, S. Nikšić, M. Koprivica, A. Nešković (TKS)
Abstract	This deliverable presents the validations and proofs of concept of methodologies and technical solutions elaborated in the LEXNET project. Part-A details the developed EMF measurement tools and their characterization. Different methods for the Exposure Index (EI) assessment are implemented and demonstrated in various environments. In Part-B, a set of promising low EMF components and techniques are evaluated from both QoS and EMF metrics, either through laboratory tests, large-scale real cellular testbeds, or system-level simulations.
Key words	El assessment validation, testbed, low EMF solutions, demonstration

Project Information

Grant Agreement n°	318273
Dates	1 st November 2012 – 31th October 2015

Document approval

Name	Position in project	Organisation	Date	Visa
Joe Wiart	Coordinator	Orange	19/11/2015	OK

Document history

Version	Date	Modifications	Authors
V1.0	18/11/2015		All



Table of contents

<u>1</u>	INTRODUCTION	<u> 7</u>
<u>2</u>	EVALUATION RESULTS AT A GLANCE	8
<u>3</u>	LOW EMF NETWORK TOPOLOGIES	10
3.1	SMALL CHANGES IN NETWORK TOPOLOGIES	10
3.1.1	Evaluated solution	
3.1.2	Test setup	
3.1.3	Evaluation results	
3.2	SMALL-CELL OFFLOADING	
3.2.1	Evaluated solution	
3.2.2	Evaluation results	
3.2.3	Conclusion	17
3.3	SMALL-CELL DENSIFICATION	18
3.3.1	Evaluated solution	
3.3.2	Test setup	19
3.3.3	Evaluation results	22
3.4	SWITCHING OFF 2G VOICE	25
<u>4</u>	LOW EMF COMPONENTS	27
4.1	LTE RF FRONT-END AND ANTENNA TESTBED FOR SMALL-CELL BS	27
4.1.1	Evaluated solution	
4.1.2	Test setup	
4.1.3	Evaluation results	32
4.2	BEAMFORMING ANTENNA TESTBED	
4.2.1	Evaluated solution	
4.2.1	Test setup	
4.2.2	Evaluation results	
4.2.3	Concluding remarks	44
4.3	LARGE-SCALE BEAMFORMING SIMULATION	44
4.3.1	Evaluated solution	
4.3.2	Test setup	45
4.3.3	Evaluation results	47
<u>5</u>	LOW EMF NETWORK TECHNIQUES	49
5.1	WI-FI OFFLOADING	49
5.1.1	Evaluated solution	
5.1.2	Test setup	
5.1.3	Evaluation results from coverage-based simulations	
5.1.4	Evaluation results from dynamic simulations	
5.2	SCHEDULED ON/OFF PROPAGATION IN A WIRELESS MESH NETWORK	
5.2.1	Evaluated solution	
5.2.2	Test setup	
5.2.3	Evaluation results	66
<u>6</u>	CONCLUSION AND RECOMMENDATIONS	<u>72</u>
<u>7</u>	REFERENCES	7 <u>5</u>
<u>APPENDI</u>	X A1: INTERNAL REVIEW	77
<u>APPENDI</u>	X A2: SCHEDULED ON/OFF PROPAGATION	<u>78</u>
	X A3: WI-FI ABSTRACTION MODEL FOR OFFLOADING STUDIES	



Executive Summary

This deliverable presents the validations and proofs of concept of solutions developed in the framework of the LEXNET project. Following the organisation of the project itself, the document distinguishes two main parts.

The first part (Part-A) focuses on the Exposure Index (EI) assessment validation. This concerns how the global metric defined in the framework of the project can be practically implemented to provide the full picture of a population Electromagnetic Field (EMF) exposure from all the wireless standards considered in LEXNET. The characteristics and validation of the three EMF measurement tools developed in LEXNET are detailed (or reminded when already described in the first WP6 deliverable): the low cost dosimeters deployed in the city of Santander; the selective wearable dosimeter version integrated from individual WP3 sub-components; and a connected measurement device (i.e. with an active wireless communication) that capture downlink (DL) and uplink (UL) key parameters. Part-A also presents the implementation and demonstration of El assessment methodologies based on dosimeters, network monitoring tools, drive-test equipment, multi-source database, or simulations, and finally how and by whom they could be exploited to evaluate the LEXNET global metric. In particular, the demonstrations include two real-life measurement campaigns leading to the El assessment in large-scale cellular networks: in the cities of Santander (involving drive test, dosimeter measurements, simulations and a smart city infrastructure) and Belgrade (involving network monitoring and drive test).

Compared to Part-A that aims to provide absolute values of EI, the second part of the deliverable (Part-B) re-uses the EI metric but for relative exposure reduction evaluation applied to a set of low EMF techniques. Some of the components and radio link techniques studied in WP4 have been selected for such demonstration. The LTE superdirective antenna combined with a low noise receiver are integrated into a demonstrator; characterization, laboratory radio-link tests and simulations show how this solution can fulfil dense deployment of low EMF small-cell base stations. Besides, the smart beamforming test bench demonstrates how to reduce the Specific Absorbtion Rate (SAR) for mobile or laptop usages.

Part-A also illustrates how a change in a cellular network topology, i.e. adding a macro-cell or micro-cell, affects the user QoS and EMF exposure. We understand from those use cases how the installation of new antennas can reduce the population exposure. The analysis on topologies is broadened with system-level simulations on dense urban small-cell deployments, in addition to the macro co-channel layer, and considering the contribution from the wireless NLOS small-cell backhaul.

Wi-Fi offloading is also evaluated, showing how the offloading policy and the Wi-Fi AP deployment influence the network performance and exposure.

Finally, exposure reduction in WLAN-managed networks is addressed thanks to an optimized AP deployment design, and gateways that propagate scheduled on/off commands to APs.



List of acronyms

Abbreviation	Meaning
3GPP	Third Generation Partnership Project.
ABS	Almost Blank Subframe
ADC	Analog to Digital Converter
ANDSF	Access Network Discovery and Selection Function
AP	Access Point
BB	Base Band
BS	Base Station
BTS	Base Transceiver Station
CDF	Cumulative Distribution Function
CL	Cell Load
CPU	Central Processing Unit
CRE	Cell Range Extension
DBDC	Dual Band Dual Concurrent
DCR	Direct Conversion Receiver
DL	DownLink
DBDC	Dual Band Dual Concurrent
EMF	ElectroMagnetic Field
eNB	Evolved Node B
FBS	Femtocell Base Station
GRE	General Routing Encapsulation
GSM	Global System for Mobile communications
GWC	GateWay Controller
HetNet	Heterogeneous Network
HSPA	High Speed Packet Access
ICT	Information and Communications Technologies
IF	Intermediate Frequency
IP	Internet Protocol
ISM	Industrial, Scientific and Medical
KPI	Key Performance Indicator
LNA	Low Noise Amplifier
LOS	Line Of Sight
LTE	Long Term Evolution
LTE-A	LTE-Advanced
MC	Macro Cell
MeNB	Macro eNB
MIMO	Multiple Inputs Multiple Outputs



NF Noise Figure

NLOS Non Line Of Sight
NTP Network Time Protocol

OLSR Optimized Link-State Routing

OS Operating System
P2MP Point to Multi-Points

P2P Point to Point

PCB Printed Circuit Board
POC Proof Of Concept
PPP Point-to-Point Protocol
QoS Quality of Service
RAN Radio Access Network
RAT Radio Access Technology

RB Resource Block
RF Radio Frequency

RMSE Root Mean Square Error

RSRP Reference Signal Received Power

Rx Receiver

SAR Specific Absorption Rate

SC Small Cell
SCeNB Small Cell eNB

SINR Signal to Interference Plus Noise Ratio

SNR Signal to Noise Ratio

SotA State of the Art

SSID Service Set IDentifier

STA STAtion

Tx Transmitter

UE User Equipment

UL UpLink

USB Universal Serial Bus

UMTS Universal Mobile Telecommunications System

WAN Wide Area Network

WARP Wireless Open Access Research Platform

Wi-Fi Wireless Fidelity

WLAN Wireless Local Area Network

WP Work Package

WSN Wireless Sensor Network



1 Introduction

This document is the second part of Deliverable D6.2. Part-A was devoted to the validation of EI assessment tools and methodologies. Part-B addresses the validation of various promising low EMF technologies, which were previously identified or elaborated by the LEXNET partners [D4.2] [D5.2], by means of demonstrations and performance evaluations. Hence, the main objective is to assess the EI reduction obtained from those technologies, while keeping an appropriate Quality of Service (QoS).

Section 2 provides a summary of all the evaluation results, including the EI reduction factor obtained for each evaluated technology.

The details are given in sections 3-5, where each evaluated technology is reported as follows:

- Short description of the technology (details are in general available in [D4.2] or D5.2].
- Description of the test setup, including a hardware, middleware or software demonstrator, and a test platform able to compute QoS and exposure metrics. Some of the test platforms are similar to the ones presented in [D6.2-A].
- Presentation of QoS and EMF evaluation results.

More precisely, section 3 is devoted to the investigation of three different low EMF topologies: installation of new macro or micro cells in poor-coverage areas (section 3.1); activation of a micro cell in a hotspot area (section 3.2); and large-scale densification based on a small-cell layer (section 3.3). Section 3 finishes with a discussion on 2G switch off, which has not been practically evaluated but is a critical step towards EI significant reduction (section 3.4).

The evaluation of low EMF radio components is given in section 0, including: small-cell RF front-end demonstrator with a compact steerable directive antenna and a configurable low-noise receiver (section 4.1); advanced beamforming antenna demonstrator (section 4.2); and large-scale deployment of small-cells with beamforming or beamsteering antennas (section 4.3).

Finally, low EMF network techniques are studied in section 5: LTE to Wi-Fi offloading in an urban environment (section 5.1); and Management of Wi-Fi AP on/off in a typical office scenario (section 5.2).

The conclusions are drawn in section 6, highlighting the benefits we expect from some of the evaluated technologies in terms of EMF exposure.



EVALUATION RESULTS AT A GLANCE

We introduced in [D6.2-A, section 2] the four main scenario classes that were addressed in the LEXNET validation and demonstration task: Traditional 3GPP outdoor cellular network; Smart city with traditional 3GPP outdoor cellular networks and sensing capabilities; Managed WLAN, mainly in large environments; and Smallcell offloading in heterogeneous networks (including 3GPP small-cells and Wi-Fi access points).

Smart city was a major use case in the El assessment demonstration. However there was no possibility to change the cellular network infrastructure (it is a real network in exploitation) or resource management policies in the smart city environment.

The distribution of the technology evaluations in the three remaining scenario classes is illustrated in Figure 1.

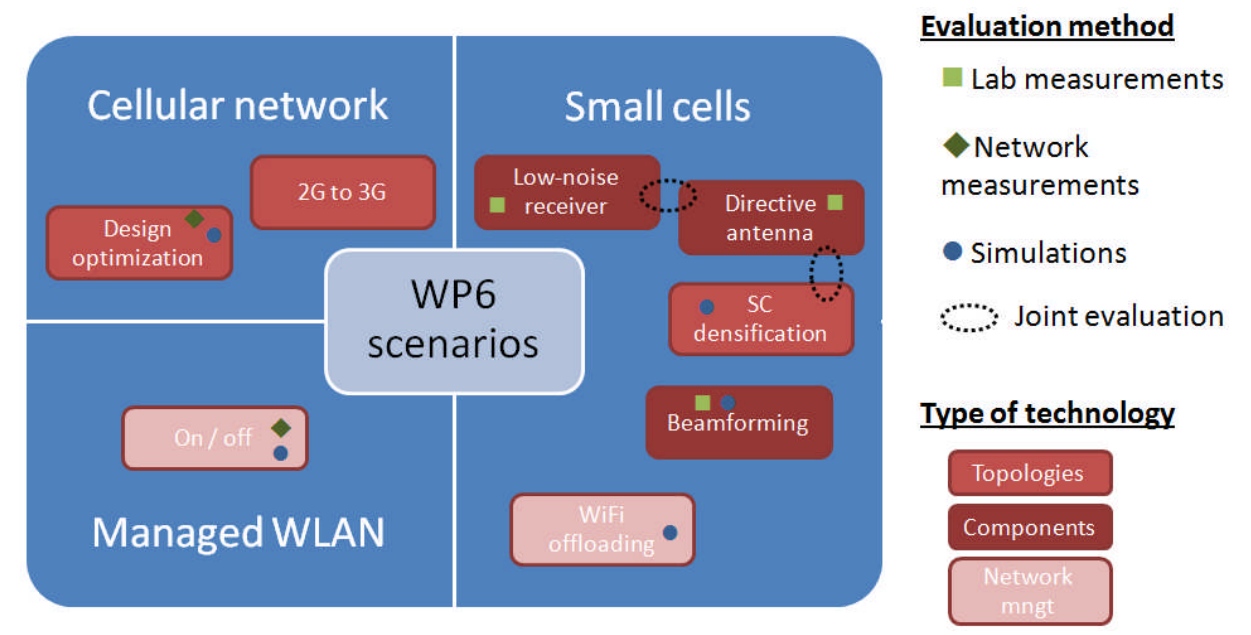


Figure 1: Scenarios for Lexnet technology demonstration.

New topologies have been evaluated in urban cellular networks, either based on trial measurements or simulations. Switching off the 2G voice and migrating towards 3G has not practically been tested but is discussed in the document.

The low EMF radio components have been demonstrated by the development and characterization of hardware prototypes and laboratory measurements; and have been validated for an indoor small-cell scenario.

Besides, the low EMF network management has been mostly evaluated by simulation, but completed by laboratory validation in case of the scheduled deactivation of wireless routers.

As shown in the diagram, some technologies were evaluated together. First, the steerable directive antenna and low-noise receiver have been integrated into a unique demonstrator, characterized in a laboratory scenario. Second, the measured properties of the directive antenna have been introduced in a system-level simulator to assess its performance in a dense small-cell deployment.



The main results are summarized in Table 1, while the details and complementary evaluations are given in sections 3-5.

The test scenario in Table 1 is described by a short description, the baseline situation (i.e. before implementation of the LEXNET evaluated technology) and the proposed improvement. The results on EI are composed of three reduction factors, i.e. on DL-EI, UL-EI and total EI. All components are not necessarily available.

Table 1: Summary on evaluation results.

Technology	Section	Test scenario	QoS	El reduction
Design optimization	3.1	Simulation. <u>Baseline:</u> Existing LTE urban cellular network. <u>Improvement:</u> adding micro-cells to improve the network performance in poor-coverage areas.	High local improvement And in macro area: DL peak Thr × 1.2 UL peak Thr × 1.0	In macro area: DL ≈ UL ÷ 1.6 EI ÷ 1.6
Design optimization 3.2 <u>Baseline:</u> 2G/3G poor coverage hotspot area.		Measurement in a marketplace. <u>Baseline:</u> 2G/3G poor coverage in a hotspot area. <u>Improvement:</u> Activation of a micro-cell	High local improvement	No change in macro area, except 3G DL ÷ 1.3. In micro area: 2G DL × 1.3 2G UL ÷ 5.9 3G DL ≈ 3G UL ÷ 46 (2G+3G) EI ÷ 5.8
Small-cell densification	3.3	Simulation. <u>Baseline:</u> Traditional LTE macro urban network. <u>Improvement:</u> Deployment of a cochannel dense small-cell layer.	DL peak Thr × 2.4 UL peak Thr × 1.5	DL ÷ 2.3 UL ÷ 4.4 EI ÷ 4.3
Low-noise receiver	4.1	Laboratory testbed, with short-range useful link. No interference. <u>Baseline:</u> UL sensitivity with traditional receiver. <u>Improvement:</u> UL sensitivity with configurable low-noise receiver	SNR × 1.3	UL ÷ 1.3 at constant SNR
Beamforming antennas	4.2	Laboratory testbed with a short-range radio link. Implementation of probes to capture the SAR evolution vs antenna radiation. <u>Baseline:</u> Beamforming with traditional single-stream null steering. <u>Improvement:</u> Beamforming with a new two-stream "hybrid" approach.	Equipment lab validation here. See [D4.3] for evaluation results	Equipment lab validation here. See [D4.3] for evaluation results
Small-cells with steerable directive antenna	4.3	Simulation. <u>Baseline:</u> Dense urban small-cell deployment with omni antennas. <u>Improvement:</u> Installation of beamforming or beamsteering antennas at the SC base station	With the steerable directive antenna: DL peak Thr × 1.2 UL peak Thr × 1.5	DL ÷ 6.3 UL ÷ 1.2
Wi-Fi offloading	5.1	Simulation. <u>Baseline:</u> Urban LTE macro-cell network. <u>Improvement:</u> Offloading of some applications towards existing Wi-Fi APs.	From the offloading "reference" scenario: DL peak Thr × 1.8 UL peak Thr ≈	From the offloading "reference" scenario: DL ÷ 2.5 UL ≈ EI ÷ 1.8
Wi-Fi APs with on/off scheduling	5.2	Middleware implementation. Laboratory validation and Evaluation into a real environment. <u>Baseline:</u> APs always switched on. <u>Improvement:</u> AP on/off management according to meeting schedule.	Unchanged	DL ÷ 1.1 UL ≈ EI ≈

Version: V1.0



10

3 Low EMF NETWORK TOPOLOGIES

This section discusses the most relevant results of studies that evaluate, either by simulation or measurement, the impact of topology changes in cellular networks: installation of an additional macro-cell or additional micro-cells in an existing network; deployment of a dense small-cell layout for massive traffic offloading in a two-tier network.

3.1 Small changes in network topologies

The evaluation reported in this section does not rely on a new technology or design optimization technique; and it does not necessarily aim at demonstrating an exposure decrease. The objective is actually to illustrate how the radio-planning tool can help the operator to characterize the evolution of EI when making simple and local modifications in the topology of an existing network.

3.1.1 Evaluated solution

Radio-planning simulations, as introduced in [D3.3] and demonstrated in [D6.2-A, section 6.4], can be used by cellular operators to assess the network KPI evolution, including the novel EI.

Two kinds of network topology modifications are illustrated here:

- Adding a new macro site in an area suffering from poor service coverage;
- Deploying few micro cells in the same area.

3.1.2 Test setup

The test is conducted in a real LTE network in Santander downtown, which was already simulated in [D62-A, section 6.4]. The study area is covered by 13 LTE cells. As shown in Figure 2 in the dotted circle, a part of the area under analysis of size 200m×70m, low-quality coverage is offered to deep-indoor users (actually a lower coverage quality is correlated with a lower DL exposure level).

We then assume that the operator is willing to locally improve the network coverage, by either adding a 2-sector macro eNodeB, or adding three micro cells distributed in the streets of the low-quality area. The properties of the macro eNodeB are similar to the ones already deployed in the study area: transmit power of 40 W; directive antenna with 6° down-tilt; located 3m above a dominant rooftop. The small-cells have omni-directional antennas transmitting at a maximum power of 5W, and are assumed to be located on lampposts, 8m above the ground.

What is expected in both tested situations are a local increase in the DL exposure (close to the new antennas) and a reduction of the UL exposure. However, the evolution of the global exposure over the whole Santander downtown area (2230mx1430m in this study) is far less obvious and is characterized exploiting simulation advantages.

Version: V1.0



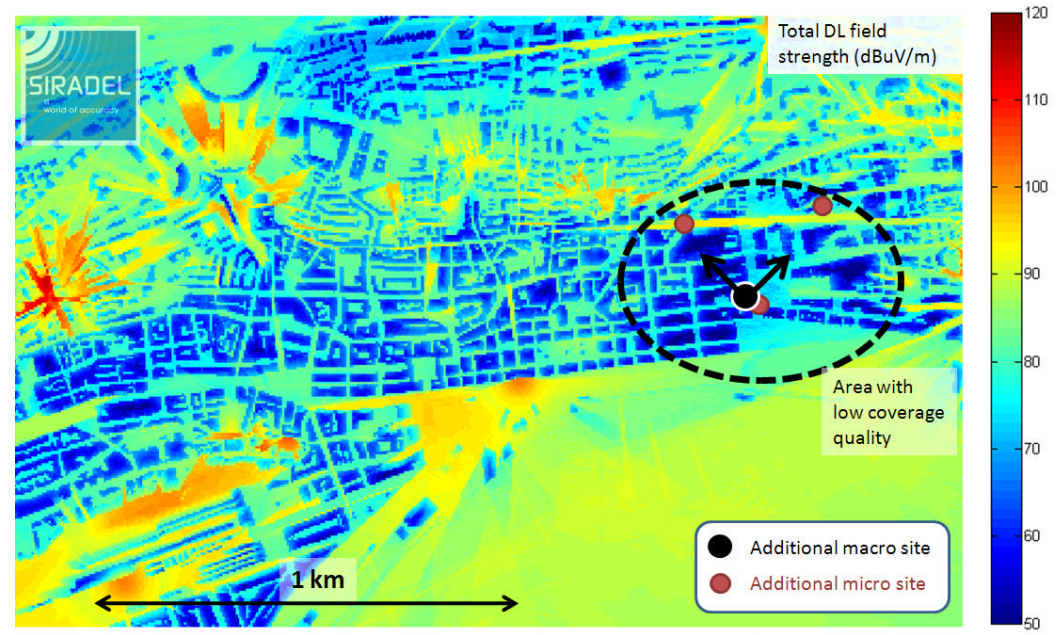


Figure 2: Total DL field strength from an existing LTE network in Santander; and position of an the additional sites under test.

The QoS and EMF metrics are predicted within the downtown area represented in Figure 2. However the simulation takes also into consideration the interference coming from all cells located in the vicinity of this study area, as they play a significant role in the calculation of both the SINR and the EMF values. The whole predicted Santander scenario is actually composed of 53 cells, in addition to the 13 cells mentioned here above.

The same kind of topology evolution (i.e. adding some macro or micro eNodeB in low-quality coverage areas) is assumed to be reproduced over the whole Santander city; therefore the DL cell load variations predicted in the study area are applied to all neighbouring cells. This leads to a general evolution of the interference levels, which means that the results below are valid only if the evaluated topology modification is generalized over the whole city (i.e. 1 additional macro 2-sector site or 3 additional micro sites for 13 existing macro cells).

3.1.3 Evaluation results

Figure 3 plots the difference observed between the reference network and the one resulting after deploying the new base stations, for two of the metrics of interest:

- The DL total field strength;
- The UL throughput, which is correlated to both the evolution of QoS and UL exposure.

In order to carry out a thorough analysis, those metrics are predicted over two different surfaces:

- A limited area around the new base stations (200m around the macro site, 100m around each micro site)
- The whole study area shown in Figure 2.



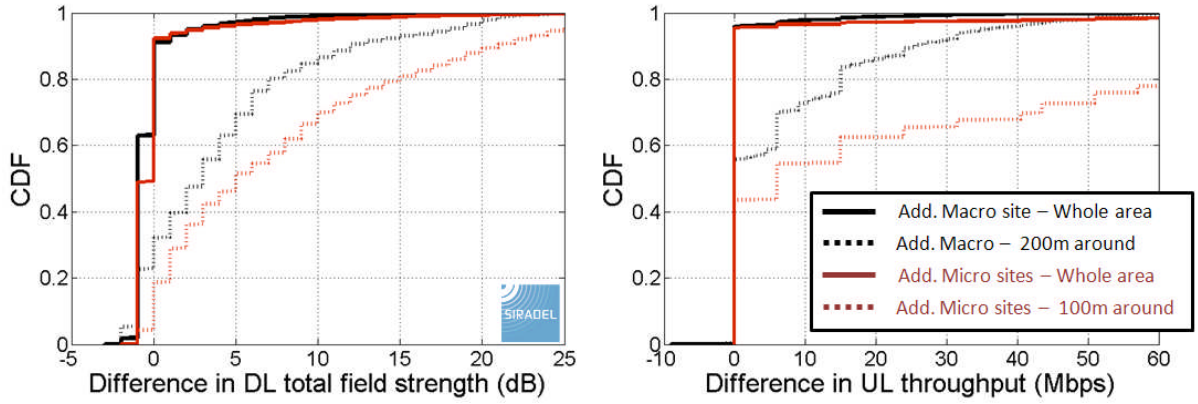


Figure 3: Evolution of the DL total field strength and UL throughput.

The evolution in the new cell's vicinity is the expected one. We can see that the global behaviour is more interesting. When adding the macro site, the DL field strength is increased in 9% of locations; is unchanged in 22% of locations; and is reduced in 69% of locations. The mean variations given in Table 2 show that the whole-area DL field strength, or DL exposure, is divided by 1.15. The mean DL exposure does not change when the micro sites are added.

The global reduction in the DL field strength means that the local increase is more than compensated at a larger scale. Actually this comes from the general cell load reduction. Figure 4 shows the statistical distribution of those cell loads. In the initial network, two cells (among 13) have more than 50% of the overall load. But the service area that is covered by those cells is significantly reduced with the introduction of the new base stations; therefore their load is strongly reduced. Then, the interference levels decrease in the nearby cells, the link performance benefits from it, and finally (if the same user traffic is kept) the cell loads over the whole test area decrease. The average reduction is of 7 dB.

Table 2: El variations when adding new base stations in poor-coverage areas.

	Adding a 2-sec	ctor macro site	Adding 3 micro-cells		
	Whole area	200 m around new site	Whole area	100 m around each new site	
DL throughput	× 1.10	×1.63	×1.18	×2.61	
UL throughput	× 1.01	× 1.19	× 1.03	× 2.61	
EI - DL contribution	÷ 1.15	× 4.95	÷ 1.01	×10.8	
EI - UL contribution	÷ 1.09	÷ 2.37	÷ 1.64	÷ 320	
El	÷ 1.09	÷ 2.28	÷ 1.61	÷ 305	

Version: V1.0



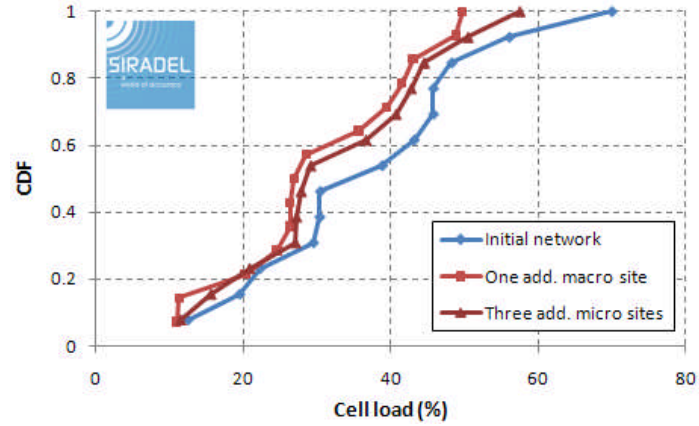


Figure 4: Reduction in DL cell loads.

The UL throughput is only changed very locally, i.e. at 3% of locations. However, this local improvement is observed within an area that was initially suffering from low performance. Hence, the throughput improvement and the reduction of the UL transmit power lead together to a whole-area UL exposure divided by 1.09 or 1.64 with the new macro site or micro sites, respectively.

The ratio obtained between DL and UL contributions in section [D6.2-A, section 6.4] is used here to evaluate the impact on the El. The major contribution is coming from UL; thus the global El evolution follows the trend observed on the UL link direction.

Finally, a traditional network with new antennas installed in poor-coverage areas leads (as expected) to a large increase in the local DL field strength, but a significant decrease in the local EI (where the UL is the major contributor). At a larger-scale, both DL and UL exposure reductions are observed.

3.2 Small-cell offloading

Small-cell offloading is evaluated in a live network using microcells in GSM and UMTS technologies, as an illustrative example of the small cells group with highest transmit powers.

3.2.1 Evaluated solution

The scenarios that are evaluated are described in [D6.2-A, section 3.4]. The aim is to compare the EI with the micro layer turned on and off, over the coverage area of observed macro sites ("macro area") and over the coverage area of the micro sites ("micro area").

The observed macro and micro sites have the characteristics shown in Table 3.

UMTS carriers/GSM **Technologies Transmit power** Site type **TRXs GSM** 4 42dBm per TRX Macro site **UMTS** 3 43dBm per carrier 2 GSM 37dBm per TRX Micro site 2 **UMTS** 34dBm per carrier

Table 3: Characteristics of the macro and the micro layer.



The cell statistics is taken for the exact time of measurements. Measurements were taken for a two hour period, one scenario after the other, during heavy load hours. In this sense, the calculated El values can be considered as the worst case, compared to other periods of the day.

The input data for the El calculation are shown in Table 4 for the scenario with micro layer turned on, and in Table 5 for the scenario with micro layer turned off.

In order to assess the DL component of the EI, field strength samples measured in the field are divided into two groups, one pertaining to the micro area, and another one corresponding to the macro area. The coverage of the micro layer has been verified with the drive-test tool. The recorded samples are first scaled for the indoor attenuation of 18 dB, as explained in section 6.3 of [D6.2-B] (AttFactor = 0.126). Average values are then combined with respect to the percentages of population in the micro and the macro area, by averaging over power. In this way, we can assess the DL components of the EI over each respective area.

Table 4: Input data for scenario Micro ON.

Scenario MICRO ON						
Data	UMTS macro layer			UMTS micro layer		
Avg. UE Tx power [dBm]		-7,19		-23,68		
Fractions of UE Rx power samples for	Good	Medium	Bad	Good	Medium	Bad
good, medium and bad radio conditions [%]	38,73%	39,40%	21,87%	64,19%	31,98%	3,83%
Average voice usage in time (per 1h), all users [Erl]		33,22			1,99	
Average data usage UL in time (per 1h), all users [Erl]	38,13			1,48		
Average data (UL and DL) usage in time (per 1h), all users [Erl]	148		6,02			
Average data volume UL (per 1h), all users [kbits]	3.412.947,00			101.895,00		
Recorded average field intensity [V/m]*		0,152		0,202		
Data	GS	M macro la	ıyer	GSM micro layer		ver er
Avg. UE Tx power for voice service [dBm]	29,79			22,28		
Fractions of UE Rx power samples for	Good	Medium	Bad	Good	Medium	Bad
good, medium and bad radio conditions [%]	15,30%	59,05%	25,65%	35,50%	58,93%	5,57%
Recorded average field intensity [V/m]*	0,103			0,121		

^{*} The value given for the macro layer is related to the macro area excluding micro area, while the value given for the micro layer is for the micro area



Table 5: Input data for scenario Micro OFF.

Scenario MICRO OFF				
Data	UMTS macro layer			
Avg. UE Tx power [dBm]	UE Tx power [dBm] -6,2			
Fractions of UE Rx power samples for	Good	Medium	Bad	
good, medium and bad radio conditions [%]	36,76%	43,15%	20,09%	
Average voice usage in time (per 1h), all users [Erl]		36,52		
Average data usage UL in time (per 1h), all users [Erl]		41,96		
Average data (UL and DL) usage in time (per 1h), all users [Erl]	159			
Average data volume UL (per 1h), all users [kbits]	3	3.452.109,0	0	
Recorded average field intensity in the macro area excluding micro area [V/m]		0,152		
Recorded average field intensity in the micro area [V/m]		0,199		
Data	GS	M macro la	ıyer	
Avg. UE Tx power for voice service [dBm]		29,76		
Fractions of UE Rx power samples for	Good	Medium	Bad	
good, medium and bad radio conditions [%]	14,88%	61,31%	23,81%	
Recorded average field intensity in the macro area excluding micro area [V/m]	0,103			
Recorded average field intensity in the micro area [V/m]	0,107			

Percentages of users per technologies and layers are taken from the signalling messages in the core network, for the exact period of measurements. The corresponding values are shown in Table 6.

Table 6: Fractions of users per technology and layer, extracted from signalling messages.

Fractions of users per technology and layer based on signalling messages	Users
GSM macro	45,59%
GSM micro	1,52%
UMTS macro	52,03%
UMTS micro	0,86%

3.2.2 Evaluation results

The calculated values for the EI over the whole population, for the macro and for the micro area, for the two scenarios, are shown in Table 7.

Version: V1.0



Table 7: El values.

	El over population or over users only [W/kg]	Micro ON	Micro OFF	ΔEI with micro on
Macro area	El for the population	1,37375E-05	1,40383E-05	-2,14%
Micro area	EI for the population	3,27715E-06	1,9014E-05	-82,76%

The overall results show the improvement of the population exposure with the introduction of the micro layer, both for the macro and the micro area. The overall improvement of the EI is more than 80% in the micro area, and more than 2% in the macro area. This is expected, as the micro area represents the zone of bad coverage of the macro layer. Further insight is obtained by observing the EI components per technology and uplink/downlink, over the micro and the macro area. Table 8 shows the percentage share of these EI components in the overall EI (over micro and over macro area), whereas Table 9 shows the absolute values with the growth per component.

Table 8: Shares of the total El per technology and uplink/downlink.

El per population, shares per technology and UL/DL					
Area considered	Technology	UL/DL	Micro ON	Micro OFF	Δshare in total El with micro on
Macro area	UMTS	UL	0,10%	0,14%	-0,04%
		DL	0,29%	0,28%	0,01%
	GSM	UL	99,25%	99,23%	0,02%
		DL	0,36%	0,35%	0,01%
Micro area	UMTS	UL	0,01%	0,07%	-0,06%
		DL	0,30%	0,02%	0,28%
	GSM	UL	97,62%	99,60%	-1,98%
		DL	2,07%	0,28%	1,79%

First, GSM UL causes the major part of the EI. This is expected considering the technology intrinsic characteristics and also due to the fact that a large number of users are actually connected to GSM, since many of them are voice-only users, using a GSM-only device or GSM-only user option on the device. The largest improvement with the introduction of the micro layer is observed over the micro area for the GSM technology.

It is also clear that the DL part of the EI pertaining to UMTS technology is bigger than the UL part, except for the micro area with micro layer turned off. UMTS is an interference limited system, and its efficient power control is one of its most important features. Due to the presence of surrounding base stations and sectors, with up to three carriers, the UMTS DL component is very strong, in both scenarios. In the macro area it is 50% higher than the UL component. In the micro area, the DL component is even stronger with the micro layer turned on, due to the decrease of the UL component (signal quality improved leads to lower UE Tx power levels) and the increase of the DL component due to addition of the new layer. When the micro layer is turned off, UMTS UL component becomes dominant over the DL component in the micro area, since this area is then left with the bad coverage of the macro



layer. If more users were connected to the UMTS, its UL component would be higher, and the GSM UL component would decrease, but due to technology differences, GSM component would still dominate.

El per population, components per technology and UL/DL Area UL/DL **Technology** Micro ON [W/kg] Micro OFF [W/kg] ΔEI with micro on considered UL 1.43648E-08 1,93276E-08 -25,68% **UMTS** -0,43% DL 3,92593E-08 3,94291E-08 Macro area UL 1,36343E-05 1,39304E-05 -2,13% **GSM** DL 0,97% 4,96398E-08 4,91624E-08 UL 2,85246E-10 1,31376E-08 -97.83% **UMTS** DL 9,83112E-09 9,54128E-09 3,04% Micro area UL 3,19936E-06 1,89384E-05 -83,11% **GSM** DL 27,88% 6,76735E-08 5,29195E-08

Table 9: El components per technology and uplink/downlink.

Looking at the absolute values and the growth percentages, it is obvious that the introduction of the micro layer brought huge improvements for most of the El components, but also a slight increase of some of them. UMTS UL component over the macro area is improved (decreased) by 25%, and over the micro area by 97%, due to the improvement of received signal level. The UMTS DL component is somewhat higher over the micro area with the micro layer turned on. Over the macro area, the UMTS DL component is slightly reduced with the addition of the new layer, but this is the result of averaging over the whole population and the increased data usage in the scenario with the micro layer off (laptop usage has somewhat higher SAR values), as the average field strength is of course somewhat higher in the other scenario.

The GSM UL component over the micro area is improved by 83% due to improvement of the received signal, which results in more than 2% improvement over the macro area. The GSM DL component over the micro area is increased by 27%, which is reflected over the macro area as an increase of less than 1%.

Looking per technologies, both UL and DL components, the EI over the micro area is improved for both technologies.

3.2.3 Conclusion

The introduction of the micro layer in both technologies, GSM and UMTS, brings a remarkable decrease in the exposure index for the population in the coverage area of the micro. But it is important to remark that the improvement depends much on the structure of the micro area (building, outdoor), the profile of users and their usage (GSM-only users).

GSM technology causes a huge part of the UL exposure, due to its inherent properties. Introduction of the micro layer increases to some extent the DL component for both technologies, but the improvement of coverage leads to lower powers emitted by UEs and to the significant reduction of the UL component. UMTS



18

DL component is generally higher than the UL one for the given topology, due to various factors: inherent properties concerning power control, the impact of surrounding base stations and sectors with multiple carriers, or the large number of users connected to GSM, thus reducing the UMTS UL component.

As an illustration, for the topology described in [D6.2-A, section 3.4], the improvement in the EI when the micro was turned on compared to the scenario when it was turned off, was about 67%. This improvement is mostly due to the improvement of the GSM UL EI. Given that the studied area was a business building, indoor environment, with distributed antennas on different floors, which are therefore close to users, the DL components for both GSM and UMTS grow drastically when the micro layer is added. The overall UMTS component (UL and DL) grows in fact by a small percentage, but the GSM component decreases.

This leads to the conclusion that the small cells layer should be carefully planned based on usage data and characteristics of the area. For indoor environments, small cells with lower powers are more suitable (pico, femto), while for the outdoor environment cells with higher powers can be used. The needs for capacity, coverage and decreased exposure are mostly in line, and the topology can be thus optimized considering the EI as another KPI.

3.3 Small-cell densification

The small-cell densification that was initially studied in [D5.1] is completed here by the system simulation tool described in section [D6.2-A, section 6.4] run on the Paris scenario of [D6.2-A, section 3.2].

3.3.1 Evaluated solution

Small-cells are small base stations that are expected to increase the broadband service coverage of cellular networks, providing the required capacity in hotspots or high traffic areas. The LTE-A standard from 3GPP release 10 has defined solutions to limit the degradation from co-channel interference in two-tier macro and small-cell networks [WAN], and these should allow dense small-cell deployments. As the field trials became reality in 2015, the first operational deployments are expected very soon. Two-tier topologies might rapidly be a key asset in future networks. Hence, evaluating the impact of such topologies on the EMF exposure is an essential outcome of the LEXNET project.

The scenario that is evaluated here consists in a dense small-cell deployment over a dense urban area, as shown in Figure 5. It was demonstrated in [D5.1] that a significant gain may be reached jointly on the network capacity, user experience and EMF exposure. The [D5.1] results are completed in this deliverable by:

- Considering heterogeneous and time-variant traffic;
- Adding the impact of the small-cell wireless backhaul on EMF exposure;
- Computing the Exposure Index from both DL and UL contributions, and taking into account space and daily traffic variations.

Version: V1.0



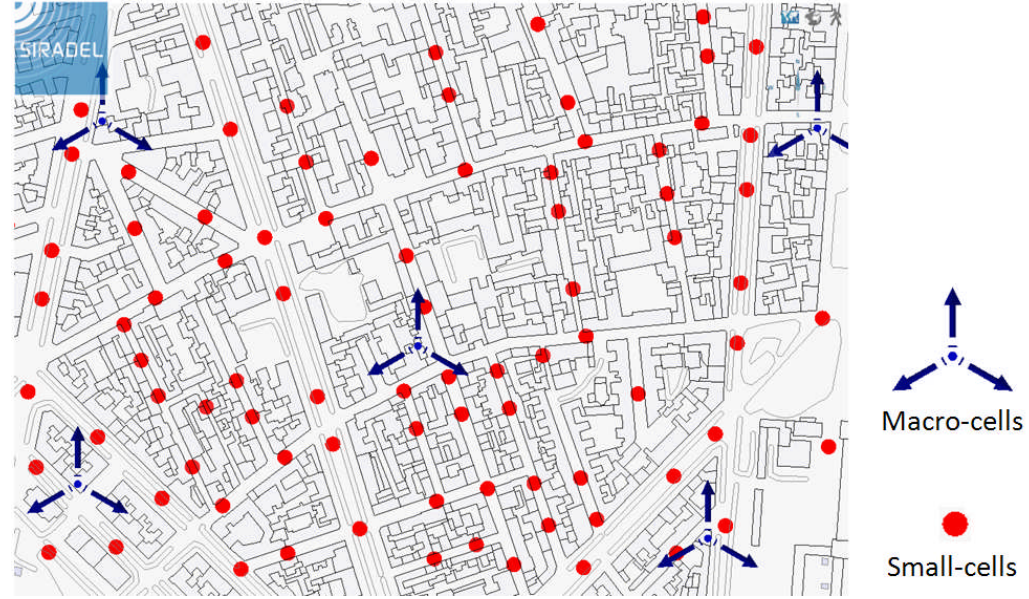


Figure 5: Two-tier network deployment.

3.3.2 Test setup

Small-cells are deployed in addition to the macro LTE-A network described in [D6.2-A, section 3.2]. The properties of the additional small-cells and user traffic are summarized in Table 10.

Table 10: System parameters in the small-cell densification scenario.

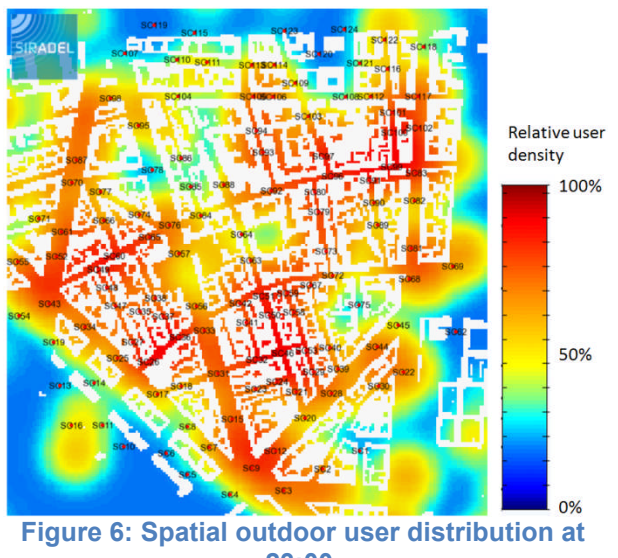
	Spectrum usage: co-channel.
Small-cell layout	SC deployment: Average ISD of 50 m.
	Maximum total transmit power: from 100 mW to 5 W.
	Antenna: omnidirectional, 5 dBi, 6 m above ground.
	UL noise figure: 2.5 dB.
	ABS dedicated resources: 25%
	CRE offset: 12 dB
	DL peak trafic of 55 Mbps/km² or 332 Mbps/km² (see below).
User trafic	UL trafic = 33% of DL trafic.
	20% outdoors, 80% indoors.
	Indoor users distributed into several floors.

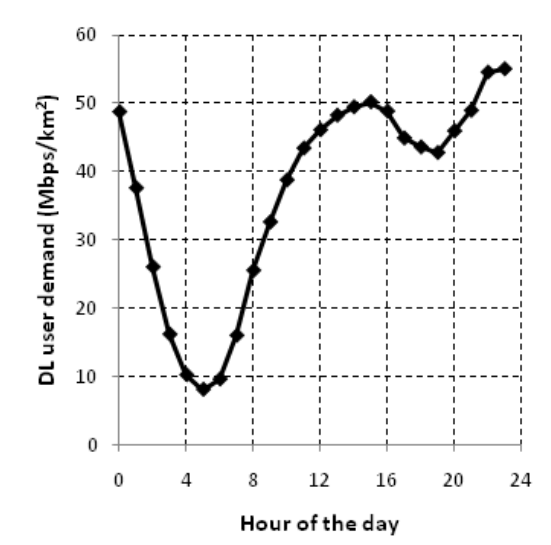
Co-channel interference is managed thanks to the ABS (Almost Blank Subframe) technique, which dedicates some radio resources to the users located at small-cell edges. Besides, the CRE (Cell Range Extension) mechanism gives a priority to small-cell attachment in order to maximize the macro offloading.

A user traffic map is created from geographical and social network data. This map represents the space and daily variations of the users in the 7th district of Paris. It is exploited here to optimize the small-cell deployment (i.e. the distance between antennas is inversely proportional to the local user density) and calculate the EI (note we assume that the relative population and user distributions are similar). Figure 6 shows the map for the outdoor user distribution at 23:00. About the same distribution is considered indoors, but taking into account the building height, i.e. the number of users inside a building is proportional to its height. In average (space and time



average), 80% of users are located inside the buildings. The time variation of the DL user traffic (in Mbps/km²) is given by Figure 7, with a peak demand at 23:00. The considered traffic brings the LTE macro-cell network at its capacity limit, meaning that a small percentage of users (about 1%) cannot be served at peak hour.





23:00.

Figure 7: Time variation of DL user traffic.

Small-cells are linked to the cellular core network by the so-called small-cell backhaul, provided either from an optical fiber connection, a millimeter wave LOS link, or a sub-6 GHz NLOS wireless backhaul. The latter solution is viewed as a relevant candidate when the optical fiber is not available in the deployment area, or the fiber leasing is too expensive; furthermore, the number of deployed small-cells makes the installation of dedicated point-to-point LOS links rather difficult.

The small-cell deployment is completed here with LOS P2P (Point to Point) links at 60 GHz when possible, and a 3.5 GHz P2MP (Point to Multi Points) backhaul in NLOS situations. The backhaul impact on the EMF exposure is assessed and combined with the DL EI contribution of the Radio Access Network (RAN).

The backhaul properties are summarized in Table 11.



Table 11: Backhaul network parameters.

	T	
	LOS V-band P2P:	
Suatam	FDD 2x500 MHz.	
	Central frequency: 60 GHz	
	MIMO configuration: no (single antenna)	
System	NLOS Sub-6GHz P2MP:	
	FDD 2x20 MHz.	
	Central frequency: 3.5 GHz	
	MIMO configuration: Dual-polar. spatial multi-plexing	
	Colocated with macro sites.	
	LOS V-band P2P:	
	Maximum total transmit power: 6 dBm	
	Antenna: directional, 2° HPBW, 40 dBi	
Hub	UL noise figure: 4.5 dB	
	NLOS Sub-6GHz P2MP:	
	Maximum total transmit power: 27 dBm	
	Antenna: directional, 65° horizontal HPBW, 18 dBi	
	UL noise figure: 4.5 dB	
	Colocated with small-cell sites	
	LOS V-band P2P: same as hub node.	
Remote	NLOS Sub-6GHz P2MP:	
Veilloff	Maximum total transmit power: 27 dBm	
	Antenna: directional, 24° horizontal HPBW, 17 dBi	
	UL noise figure: 4.5 dB	

Finally, the evaluation scenario and evaluation metrics are described in Figure 8. The performance of the two-tier scenario is predicted in two different user traffic conditions: 1) same traffic than in the macro-only network, i.e. 55 Mbps/km²; 2) at the maximum network capacity, i.e. 332 Mbps/km². The first results stress how the exposure is reduced when introducing small-cells. The latter ones show how the user performance and the EMF exposure might evolve in time if the user traffic is exploding as expected.

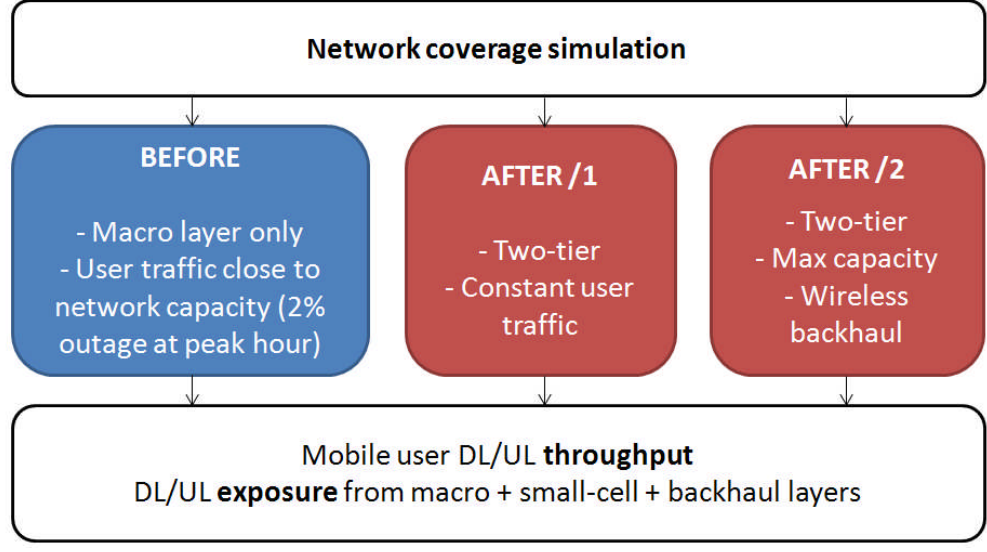


Figure 8: Evaluation scenario for small-cell densification.

Version: V1.0 21



3.3.3 Evaluation results

The simulator generates several maps: per metric of interest, per hour (over a 24-hours total period) and at different floors (from the ground-floor to the 10th floor). Some maps are given in Figure 9 to Figure 11, from the two-tier scenario at constant user traffic.

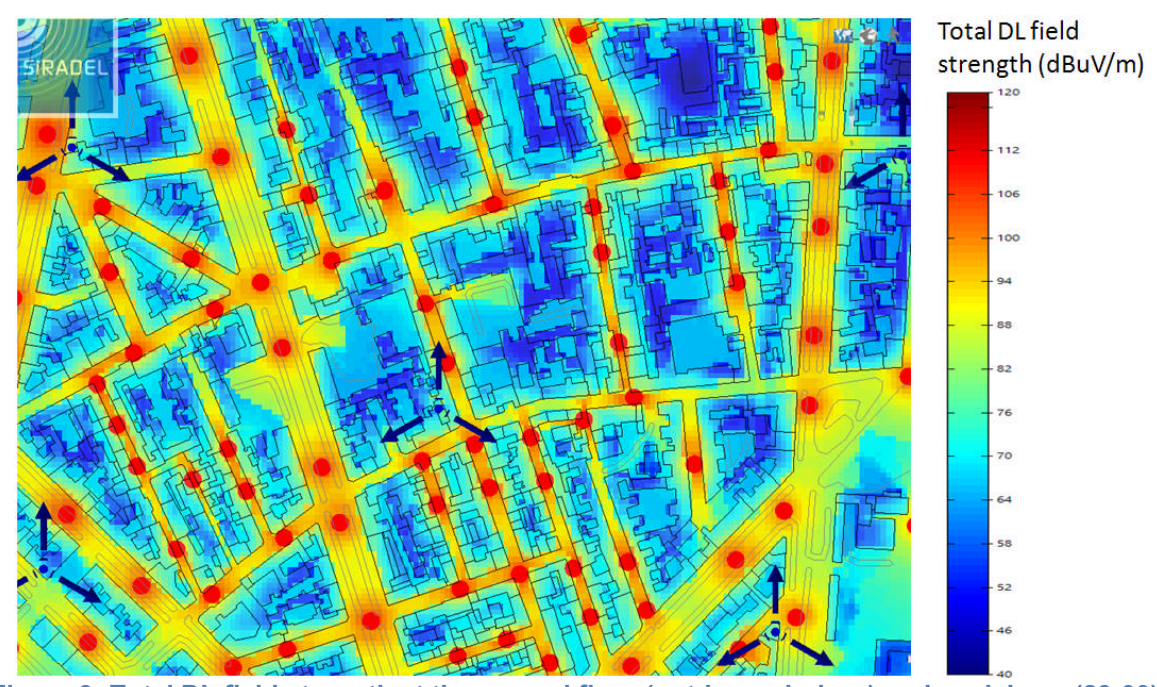


Figure 9: Total DL field strength at the ground floor (outdoor + indoor) and peak hour (23:00).

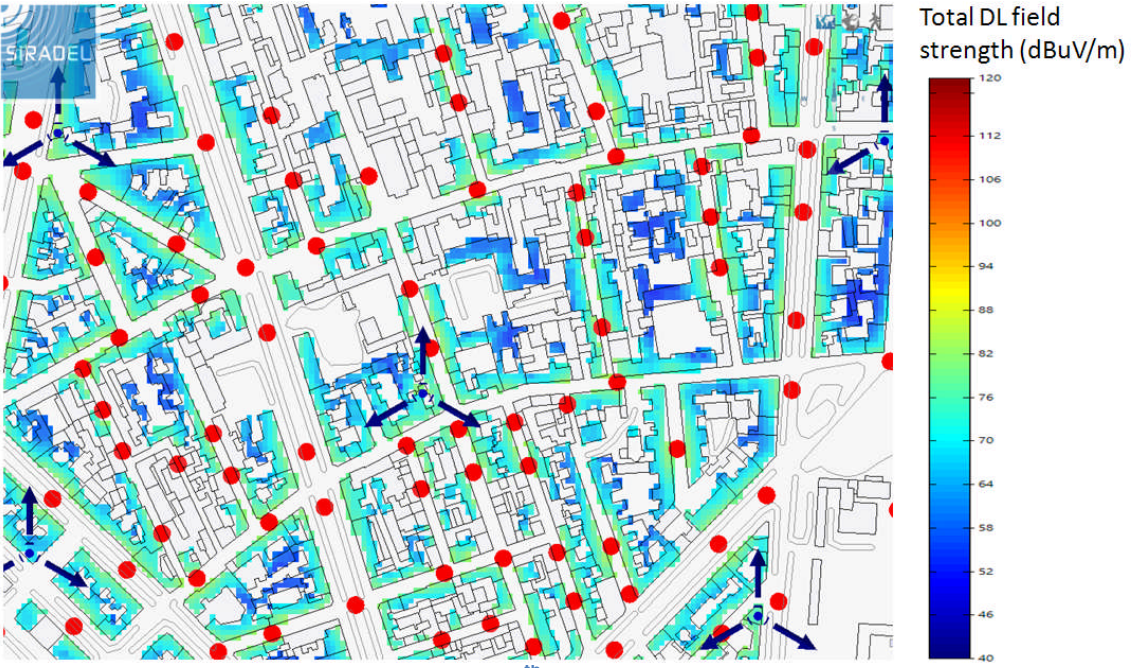


Figure 10: Total DL field strength at the 6th floor (height = 19.5 m) and peak hour (23:00).



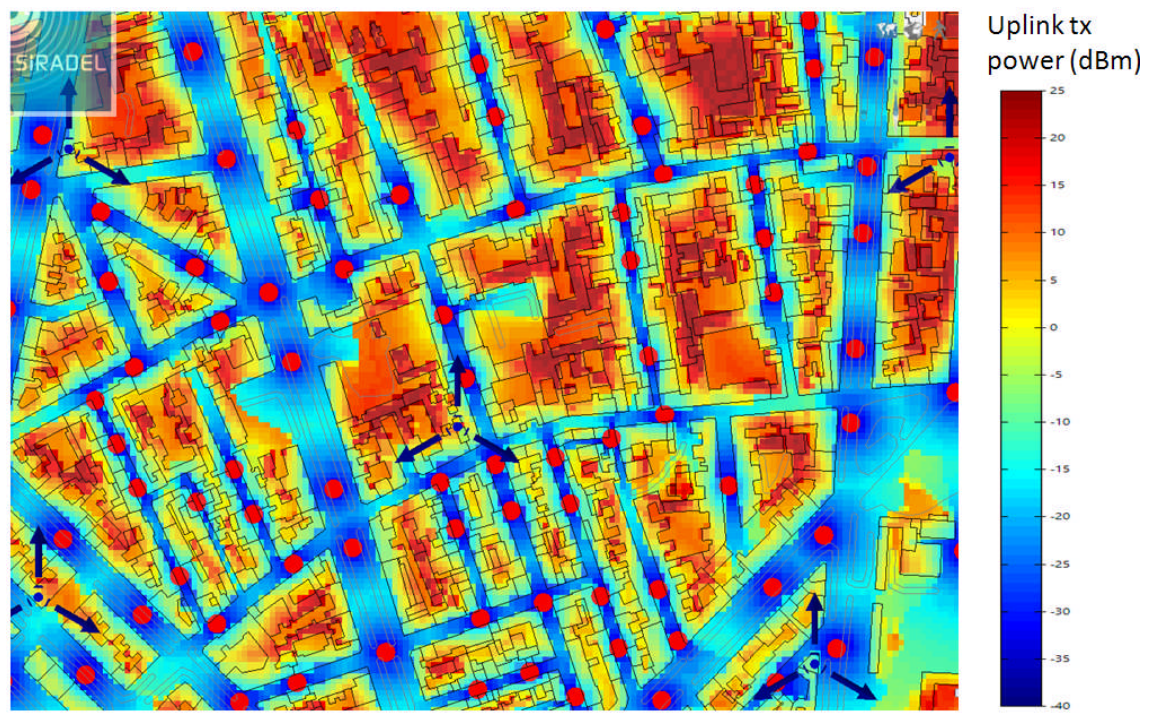


Figure 11: UL transmit power at the ground-floor and peak hour (23:00).

The variations of both DL and UL power values over the day are shown in Figure 12. Those mean values have been obtained from the aggregation of all predicted pixels and floors, taking into account the local user density. The user traffic reduction at night obviously leads to a significant improvement of both the DL exposure (because of a lower cell load) and UL exposure (thanks to a better link performance).

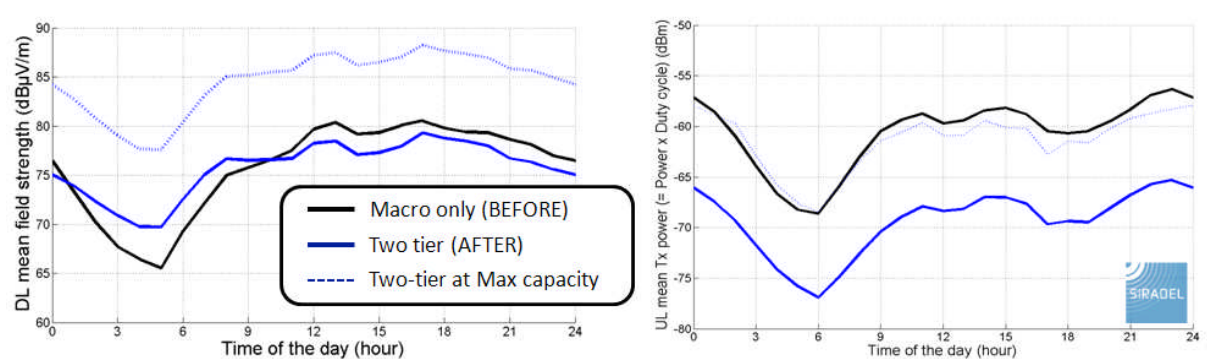


Figure 12: Averaged DL field strength and UL transmit power vs time.

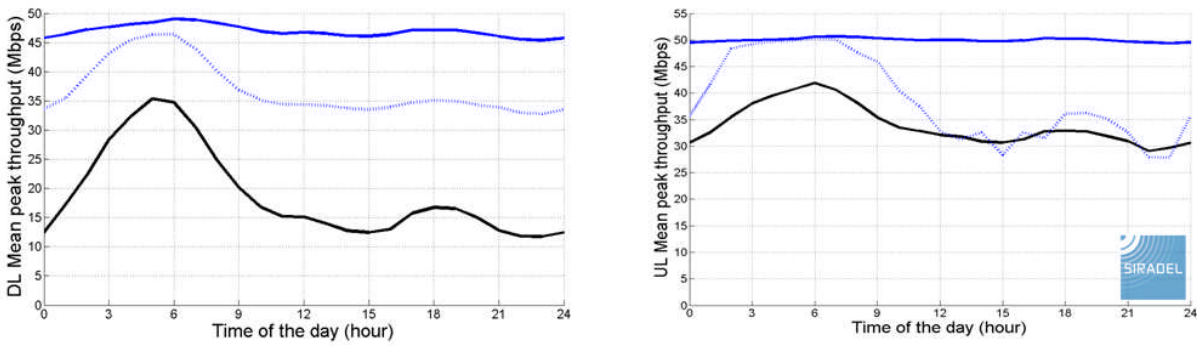


Figure 13: Averaged DL and UL peak throughput vs time.



At constant user traffic, the benefit of the two-tier deployment compared to the macro-only network is obvious for DL and UL peak throughputs. Even with a traffic 6 times higher in the two-tier network (and unchanged in the macro-only network), the DL peak throughput remains significantly better, while the UL peak throughput goes down back to the macro-only level.

Table 12 summarizes how the mean performance of the two-tier network (user QoS, network QoS and EI) changes compared to the macro-only reference. The EI is computed from the LEXNET reference scenario that was briefly described in [D6.2-A, section 3.3] but with the specific user spatial and time variations that were considered here. At constant user traffic, the EI is divided by 4.3, thanks to the strong reduction in the dominant UL component.

Besides, the improvement in the instantaneous transmit power and throughputs is not enough to compensate a 6x increase of the user traffic; the DL field strength is multiplied by 3.4; the UL component and global EI are degraded by 40%.

The conclusion is that a dense small-cell network brings a very significant benefit on user QoS, network capacity and EMF; however it is not sufficient to compensate the effect of a large user traffic rise, i.e. 6 times higher, on the EI.

Table 12: El variations when adding a dense small-cell layout, and increasing the user traffic.

	Constant trafic	Traffic × 6
DL user peak throughput	× 2.4	× 2.0
UL user peak throughput	× 1.5	× 1.1
DL network throughput	=	×6
UL network throughput	=	× 6
EI - DL contribution	÷ 2.3	× 3.4
EI - UL contribution	÷ 4.4	× 1.4
El	÷ 4.3	× 1.4

The backhaul design has been realized with a backhaul planning tool [SIR] that performs automated hub selection, small-cell remote attachment and antenna orientation. The planning aims to provide each small-cell with the required network capacity. In this study, it is computed by aggregating the user throughputs of each small-cell in the busy hour, and in the scenario with maximum network throughput.

The resulting backhaul is presented in Figure 14. The LOS V-band segment is composed of 30 transmitters located at five different macro sites, and serving 30 small-cells. The NLOS sub-6GHz segment is composed of 25 hubs located in nine different macro sites, and connecting 94 small-cells. The proposed hybrid wireless backhaul approach was found specifically suitable for dense outdoor small-cell networks. Small-cells in LOS of hub sites (typically macro-cell sites) benefit from great mean and peak throughputs. Furthermore, the designed sub-6GHz P2MP backhaul network outperforms the mean throughput targets, allowing future traffic demand growth and possibly small-cell BS upgrade with more bands. It also allows the small-cells to provide a good user experience with min and average peak throughputs of 40.0 and 98.72 Mbps respectively.



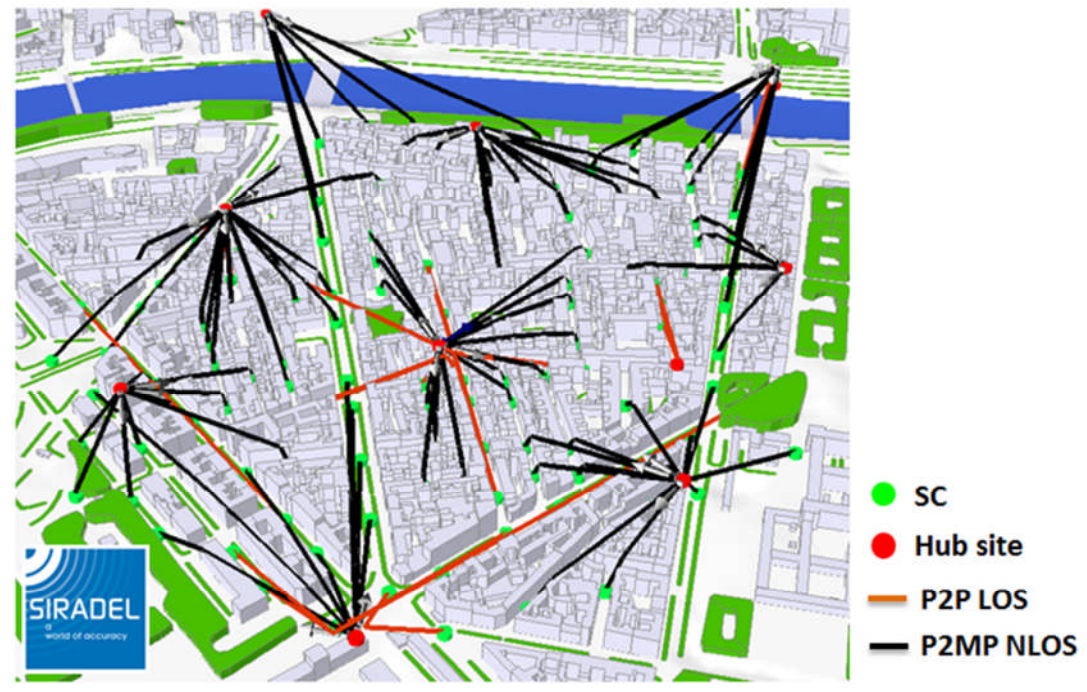


Figure 14: Small-cell wireless backhaul network.

The mean power density from the proposed wireless backhaul is then compared to the mean power density generated by the RAN network (macro and small-cells). The backhaul contribution is computed from only the DL traffic in the NLOS segment. We can state that,

- The contribution from the LOS backhaul links is negligible because of the high antenna directivity;
- The UL contribution of the NLOS backhaul is small compared to the DL contribution, as the backhaul remote antenna installed at the small-cells is directive, and oriented towards the macro hubs.

For simplicity, the comparison is done in the streets only.

The result from Table 13 shows that the backhaul contribution is small: 16% of the total DL exposure. Therefore the proposed backhaul design does not significantly change the conclusions drawn above on the small-cell benefits or limitations. However its impact is not negligible. It is concluded that, in general, the wireless backhaul contribution has to be taken into consideration for a fair EMF small-cell analysis.

Table 13: Mean power density from the RAN two-tier network and the wireless backhaul.

	RAN	Backhaul	Total
Outdoor Mean power	1 025 05	3.58E-06	2 105 05
density (W/m²)	1.83E-03	3.38E-00	Z.13E-03

3.4 Switching off 2G voice

The critical contribution of 2G networks to the population EMF exposure is known from many years; and has been quantified with the LEXNET EI in Santander and Belgrade testbeds as reported in [D6.2-A]. It appears from Trace mobile measurements in Santander that 2G EI is two orders of magnitude higher than any other cellular network, mainly because of the UL transmit power. Another result, from

Document ID: D6.2: Report on validation FP7 Contract n°318273



26

network monitoring in Belgrade, shows that EI-UL from 2G is three orders of magnitude higher than in 3G [D6.2-A, section 7.3.4], knowing that the 3G voice traffic is slightly higher than 2G, and is only a portion of the total UL traffic. The average Tx power during a phone call (in high load hours) is 31 dBm with 2G, while the average transmit power is only -9.4 dBm in the 3G macro network.

Based on [D6.2-A, section 7.3.4], we can estimate that EI-UL would be roughly reduced by three orders of magnitude if 2G was switching off and the associated resources were devoted to 3G voice.

A migration towards VoLTE would have been a more valuable scenario, however no EMF measurement of UL VoLTE was available.

Even in absence of any precise gain quantification, the migration of 2G towards a more recent cellular technology is obviously a mandatory step for EI reduction. The impact of any other technique studied in this document would be negligible as long as a significant part of voice communications will be transmitted with the current 2G transmit power.

Version: V1.0



4 Low EMF COMPONENTS

Several radio components investigated by LEXNET partners have been prototyped and their impact on the link performance and EMF exposure has been evaluated in laboratory testbeds. The validation, characterization and evaluation of two demonstrators are reported in this section: 1) a LTE RF front-end that integrates a compact directive antenna and a reconfigurable low-noise amplifier, suitable for implementation in small-cell base stations; and 2) beamforming antennas whose impact on field radiation and human exposure is assessed through an innovative laboratory testbed composed of EMF probes.

Those laboratory demonstrations are completed with system-level simulations to assess the QoS and EMF performance of steerable directive antennas or beamforming in large-scale small-cell deployments.

4.1 LTE RF front-end and antenna testbed for small-cell BS

4.1.1 Evaluated solution

LTE RF front-end and antenna testbed combines a smart antenna and a reconfigurable low noise receiver based on techniques studied in [D4.3]. The EI evaluation shows the improvement compared to a typical architecture (omnidirectional antenna and reference receiver). The envisaged demonstrator aims to fulfil constraints of dense small cell (SC) base station (BS) deployment in a dense urban environment following the 3GPP guidelines [3GPP]: the SCs form a 3×3 cluster located inside each Macro Cell (MC) sector. However such a density of SC BSs is costly and complicated to deploy on such a wide scale. The idea is to validate the simulated characteristics with a single link experimental characterisation (spatial filtering and noise figure) even if the dense scenario specifications are not reached. As only hardware components have to be validated in this work, it is decided to simplify the validation scenario with only one UL transmission, from a UE to a SC BS, and one UL blocker associated to either the MC BS or another SC BS.

Two separate LTE UL frequency bands are selected for the SC BS demonstration: band 20 (832-862 MHz) and band 3 (1710-1785 MHz). The aforementioned indoor scenario will be emulated during the demonstration.

From the component developments reported in [D4.3], two techniques are appropriately combined for SC BS deployment: the miniature and directive antenna, and the reconfigurable low noise receiver. The combination of both solutions ensures additive gains due to the independency of the individual concepts, which are described below.

4.1.1.1 Miniature and directive antenna concept

Compared to an omnidirectional radiation pattern, the proposed antenna focuses its energy only in the useful angular sector. In the proposed demonstrator, the antenna benefits of a reduction factor of 5 compared to equivalent directivity antenna. This will be integrated into a typical SC BS equipment with an approximate radiating elements cylindrical dimensions 11 x 8 cm (diameter x height) corresponding to 0.28 x 0.2 wavelength at 850 MHz. The major innovation regarding the SotA of the developed



antenna is twofold: first the dual band (band 20 (832-862 MHz) and band 3 (1710-1785 MHz)) and secondly its beam which can be controlled in azimuth for 6 angular directions. This last point is made possible thanks to tunable impedance loads that control the coupling effect between the central driven element and the other parasitic elements. The concept scheme is reminded in Figure 15. A picture of the finale WP6 prototype is given in Figure 16. Notice that the ground plane is quite large (40 cm diameter) for this realisation but will be reduced in future version by re-using the metallic case of the SC BS device. The system-level performance assessment can be found in [D4.2]. It is briefly reminded that to behave super-directive (that is spatial filtering while reducing its dimensions), the antenna efficiency is compromised. Thus, the overall concept of this kind of antenna makes the assumption that in SC BS deployment scenario, the interference impact overrides the budget link impact. Notice that at this stage of development, the prototype does not incorporate omnidirectional pattern mode and thus the allocation of all the surrounding UEs and their tracking for the optimum beam are not addressed in the LEXNET project.

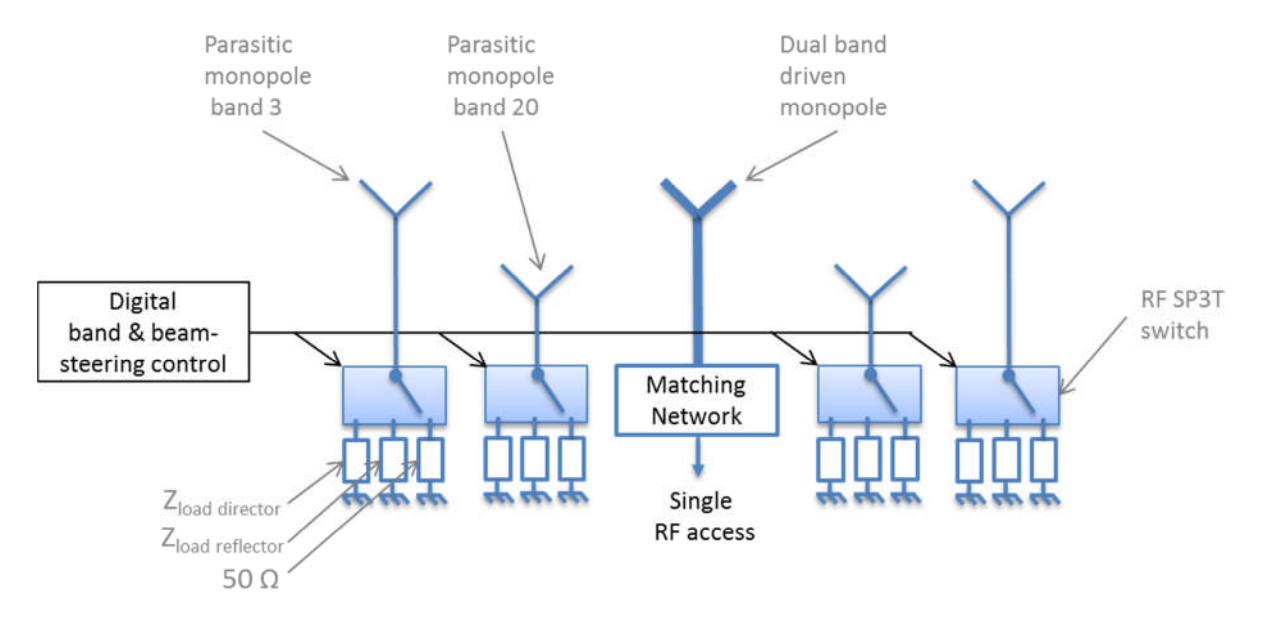
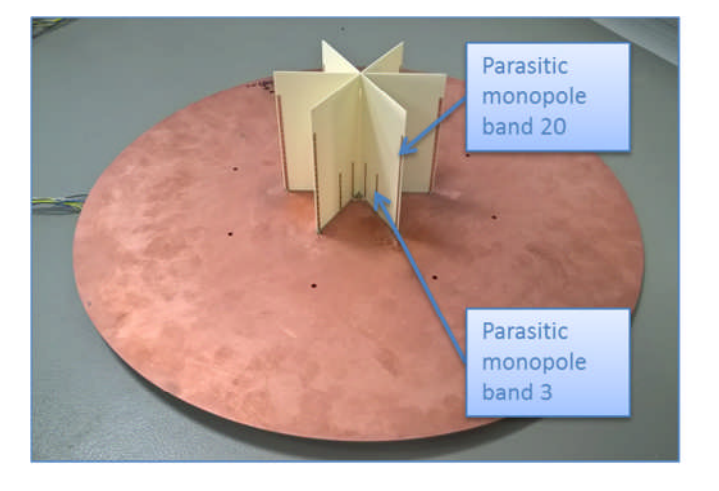


Figure 15: Dual band parasitic antenna array concept with its band and beam-steering implementation.



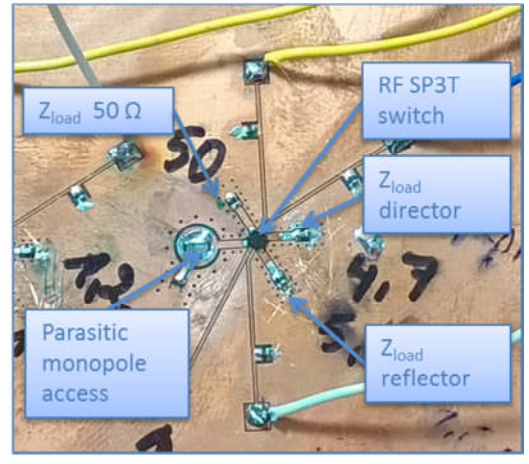


Figure 16: Illustration of the dual band compact and directive antenna in LTE band 3 and band 20: final WP6 prototype top view (left) and details of the impedance load control for the beam steering feature (right).

Version: V1.0



4.1.1.2 Reconfigurable low noise receiver concept

Reconfigurable low noise receiver architecture is proposed to achieve better noise figure (NF) performance. The aim is to reduce the receiver NF compared to reference multi-band receiver architecture. The proposed solution consists of a wideband receiver architecture instead of the narrowband performance presented in traditional multi-band architectures. It implements a reconfigurable band pass filter and a reconfigurable oscillator able to work in different LTE frequency bands, adding a fixed intermediate frequency (IF) at 140 MHz to improve the rejection to interfering signals (Figure 16). More information about the design and initial EI evaluation can be found in [D4.2] [D4.3]. The solution is more promising when a large number of frequency bands are considered in the same receiver, due to its reconfigurability feature. The integration of this solution with the miniature and directive antenna reduces the interferences impact, protecting the first LNA from high power interfering signals and relaxing the maximum input power compared to reference architecture.

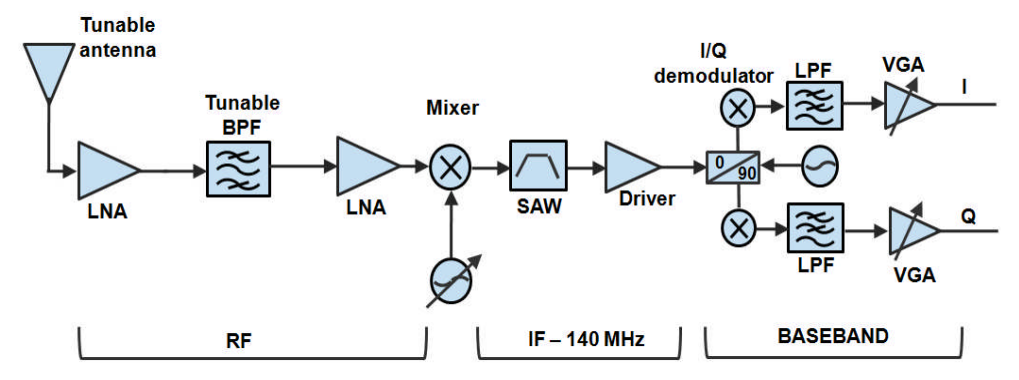


Figure 17: Block diagram of the reconfigurable low noise receiver.

4.1.1.3 LTE SC BS RF front-end and antenna concept

Both previous low EMF techniques are appropriately combined for SC BS deployment. The association of both techniques takes benefit from two independent concepts at the UL: the spatial filtering with interference mitigation (signal-to-interference-plus-noise ratio (SINR) improvement) for the antenna and the sensitivity enhancement (NF reduction) for the receiver. From the antenna view point, the receiver could compensate the potential losses inside the antenna structure. From the receiver view point, the spatial filtering reduces the impact of blockers and eventual spurious signals.

4.1.2 Test setup

The methodology considers the individual evaluation comparing each component with the associated reference component, the so called "SotA" configuration. The super-directive antenna is compared with an omnidirectional antenna, and the reconfigurable low noise receiver is compared with a reference receiver. At last the "LEXNET SC BS" configuration is evaluated and its performance is compared to the three previous configurations. Table 1 summarizes the associated tested configurations. This procedure allows assessing the EI ratio reduction of both individual and combined developed components.



Table 14: Comparison process of the associated tested configurations.

Configuration name	Reference antenna	LEXNET antenna
Reference receiver	"SotA"	"Miniature and directive antenna"
LEXNET receiver	"Reconfigurable low noise receiver"	"LEXNET SC BS"

The test setup for each tested configuration is described below.

4.1.2.1 Miniature and directive antenna test setup

The antenna characterization is carried on in a controlled environment that is the anechoic chamber (6m long) where the antenna can be rotated to measure the radiation pattern in the different cut-planes. The complex impedance is checked by comparing with the simulated one. In a second step the matching network is realized based on the complex impedance measured in both bands. Then the radiation patterns are measured at different frequencies and for two positions of the beam (forward and backward) thanks to the RF switches. Both gain and directivity can be extracted and compared with simulated result.

4.1.2.2 Reconfigurable low noise receiver test setup

The receiver characterization is carried out testing the performance in the proposed solution ("Reconfigurable low noise receiver" configuration) and the reference solution ("SotA" configuration). The reconfigurable low noise receiver is compared to a reference dual band receiver, which includes a RF switch and a bandpass filter before the first LNA (Low Noise Amplifier). Both receivers, whose block diagrams are shown in Figure 18 and Figure 19, operate in LTE band 3 and 20. The green circle shows the scope of the hardware development in LEXNET, which is limited to RF/IF stages.

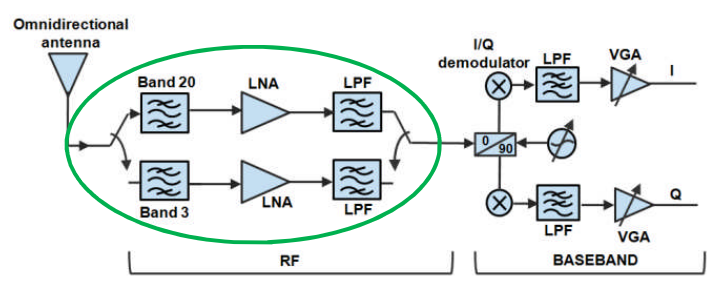


Figure 18: Block diagram of the reference receiver.

Version: V1.0



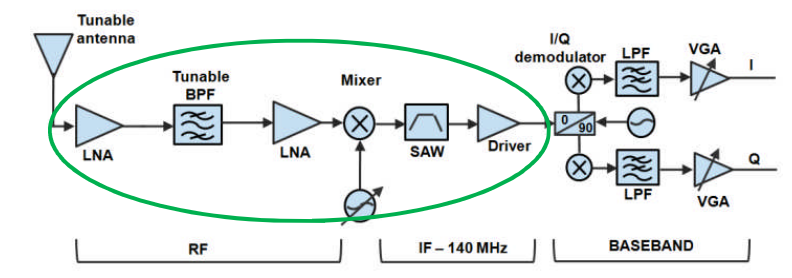


Figure 19: Block diagram of the reconfigurable low noise receiver.

For the receiver validation, EI evaluation is derived from RF signal metrics. The reference receiver and the reconfigurable low noise receiver are compared in terms of NF performance and SNR performance, which eventually derives to EI ratio. The evaluation is performed in RF/IF stages due to lab equipment constraints.

Two different test setups are used to evaluate NF performance (Figure 20a) and SNR performance (Figure 20b).



Figure 20: Test setup to evaluate a) NF performance and b) SNR performance.

Firstly, NF performance was evaluated using the signal analyzer and a noise source. Secondly, SNR performance was evaluated using the vector signal generator, which can generate 10 MHz LTE UL signal, and the signal analyzer.

Moreover, in the reconfigurable receiver, the bandpass filter reconfigurability was also assessed with a network analyzer and the results are shown next.

4.1.2.3 LTE SC BS RF front-end and antenna test setup

Finally, the "LEXNET SC BS" validation is based on SINR and SNR measurements. Thus SINR (UE received signal strength to blocker one plus noise power ratio) comparison corresponds to the EI ratio. Meanwhile SNR (UE received signal strength to noise power ratio when blocker is switched off) comparison is used to assess whether the QoS is maintained.

The global validation has been done in two steps due to the non-availability of the dual-band compact and directive antenna at the time of this document delivery. In a preliminary step the {antenna+receiver} have been tested in typical (not controlled) laboratory conditions (ie not in anechoic chamber). Once the demonstrator will be fully operational, it is planned to install it into the CEA LETI anechoic chamber (22 m long) which is equipped with a 4 m diameter turn table to measure different angular positions of the blocker. In both configurations, an omnidirectional antenna emulates an UE transmission of an LTE signal to the SC BS, Figure 21 Simultaneously on the same frequency band, another UE so-called blocker transmits to another SC or



directly to the MC. The latter interfere with the considered SC when the SC BS has an omnidirectional pattern ("SotA" configuration) and far less with a directive pattern ("Miniature and directive antenna" configuration). Notice that when the blocker is aligned with the UE, the antenna spatial filtering doesn't occure anymore as in the omnidirectional case but this corresponds merely to 1/6 of the directions.

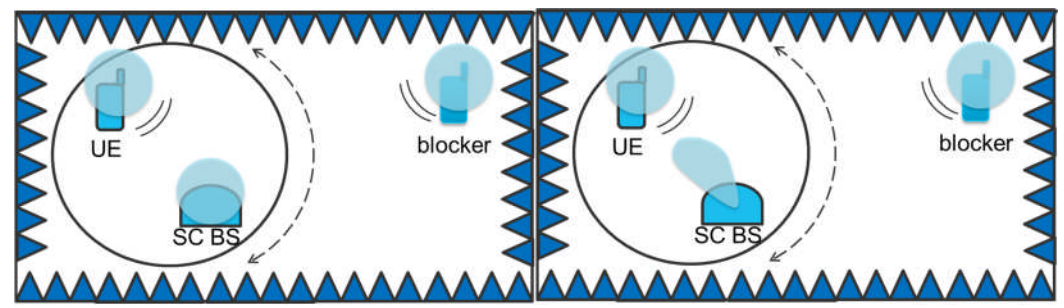


Figure 21Top view illustration of the test setup: "SotA" (left) and "Miniature and directive antenna" configurations (right)

The super-directive antenna ("Miniature and directive antenna" configuration) is compared with a standard 3 dBi omnidirectional dual band (bands 3 and 20) monopole with equivalent dimensions ("SotA" configuration).

For the antenna validation, only RF signals metrics are measured to derive EI ratio and QoS. Thus SINR (UE received signal strength to blocker one plus noise power ratio) comparison corresponds to the EI ratio. SNR (UE received signal strength to noise power ratio when blocker is switched off) comparison is used to check that QoS is maintained.

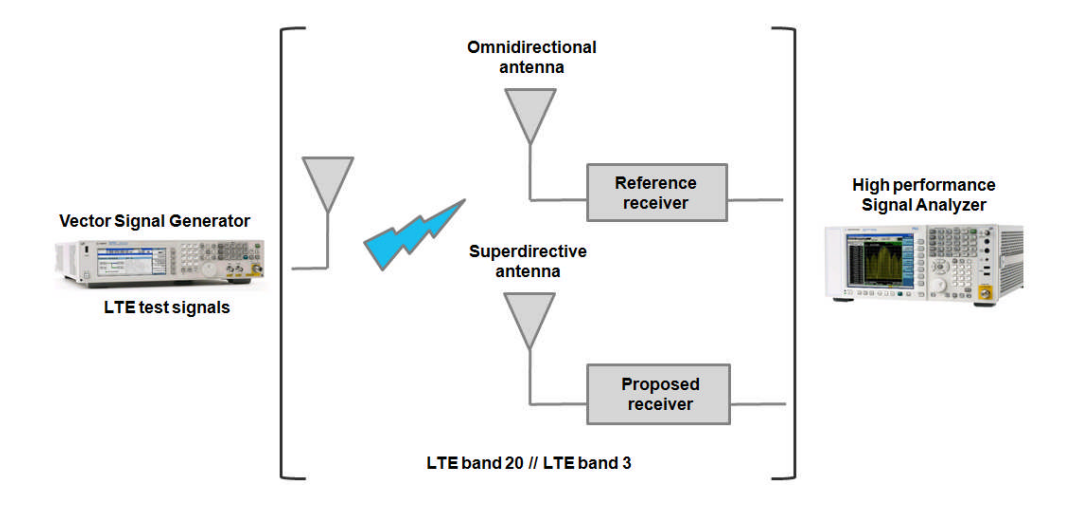


Figure 22: Test setup to evaluate the LEXNET SC BS.

4.1.3 Evaluation results

For proof-of-concept (PoC) validation, different hardware prototypes were manufactured for the miniature and directive antenna, and the reconfigurable low noise receiver. Furthermore, the reference components, i.e. the omnidirectional antenna and the reference receiver, were also manufactured. In the following



sections, the evaluation results of the individual components and the LEXNET SC BS prototype are presented.

4.1.3.1 Miniature and directive antenna evaluation

The complex impedance of the antenna is measured in both bands. In the lower band (band 20), the simulated impedance is retrieved. Antenna gains are measured in two cut-planes and the experimental results fit the simulated one. The -3 dB apertures are well retrieved, despite some difficulties to find the optimal cut-plane where the front-to-back ratio is optimised.

Unfortunately in the higher band (band 3) the results are not available at the time of this document writing. Thus the validation results cannot be shown in this band with the final dual band antenna.

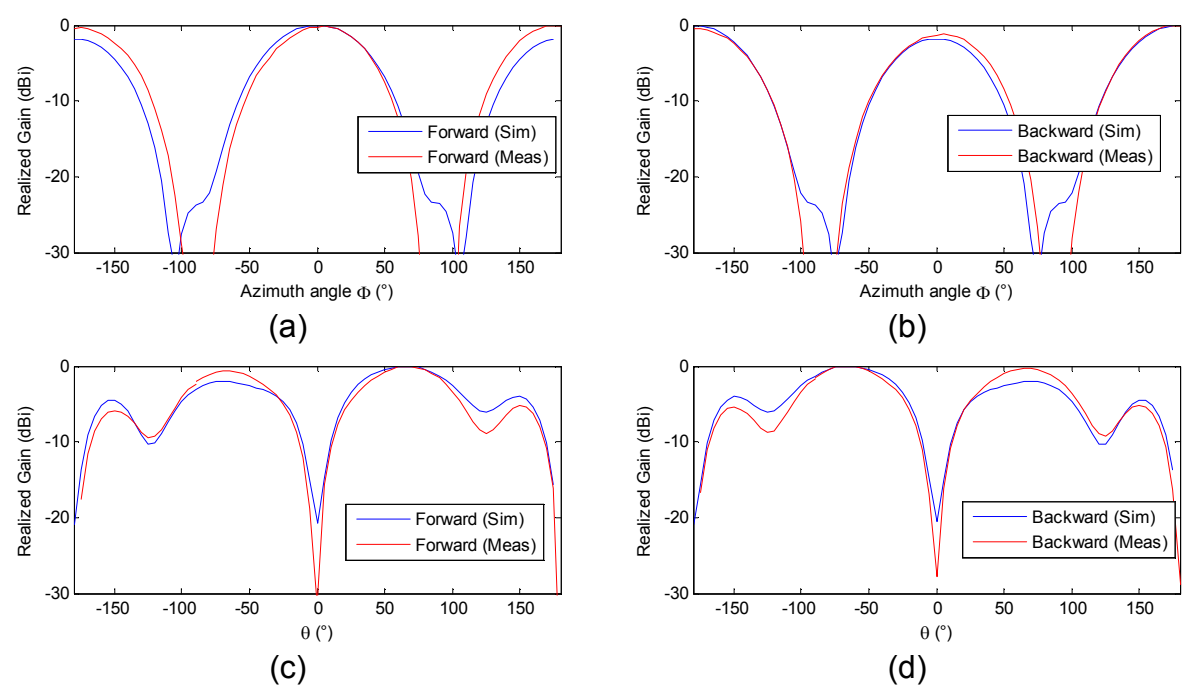


Figure 23: Simulated (blue) and measured (red) normalized realized gain at 855 MHz (central frequency of band 20) in the horizontal cut-plane (a,b) and in the vertical cut-plane containing the beam direction (c,d) for two beam-steering direction: forward (a,c) and backward (b,d).

4.1.3.2 Reconfigurable low noise receiver evaluation

Two hardware prototypes were manufactured, one for the reference receiver and another for the reconfigurable receiver. Both receivers operate in band 3 and band 20. Figure 24 presents the reference receiver prototype which has one RF board and one supply and control board integrated in a single aluminium box. There is a dedicated control circuit to switch between LTE band 20 and LTE band 3.





Figure 24: Reference receiver prototype: a) RF board (top view) and b) Supply and control board (bottom view).

Figure 25 shows the reconfigurable low noise receiver prototype which has also one RF board and one supply and control board. There is also a dedicated control circuit to tune the three varactors which configure the bandpass filter and to program the reconfigurable oscillator. In the reconfigurable receiver prototype, a RF coupler was integrated in order to test the reconfigurable bandpass filter.



Figure 25: Reconfigurable low noise receiver prototype: a) RF board (top view) and b) Supply and control board (bottom view).

To configure and test both prototypes, a console was prepared to select the operating band and tune the varactors. This console can run in a laptop which connects with both prototypes through Inter-Integrated Circuit (I2C) interface. For PoC validation, the console is configured appropriately depending on the frequency band. Figure 26 shows the console to configure the receiver prototypes.



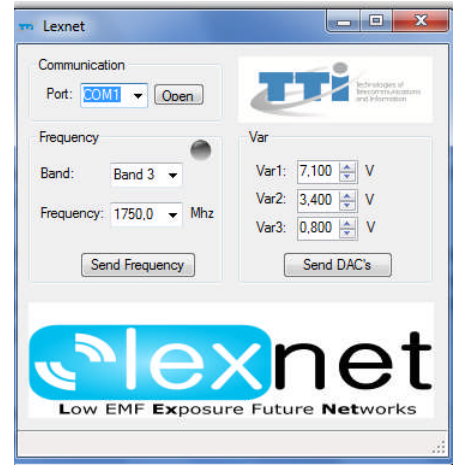


Figure 26: Console to configure both receiver prototypes.

Apart from LTE band 20 and LTE band 3, the reconfigurable bandpass filter was experienced at different operating bands tuning the voltage at three varactors. Figure 27 presents the performance at those frequencies.

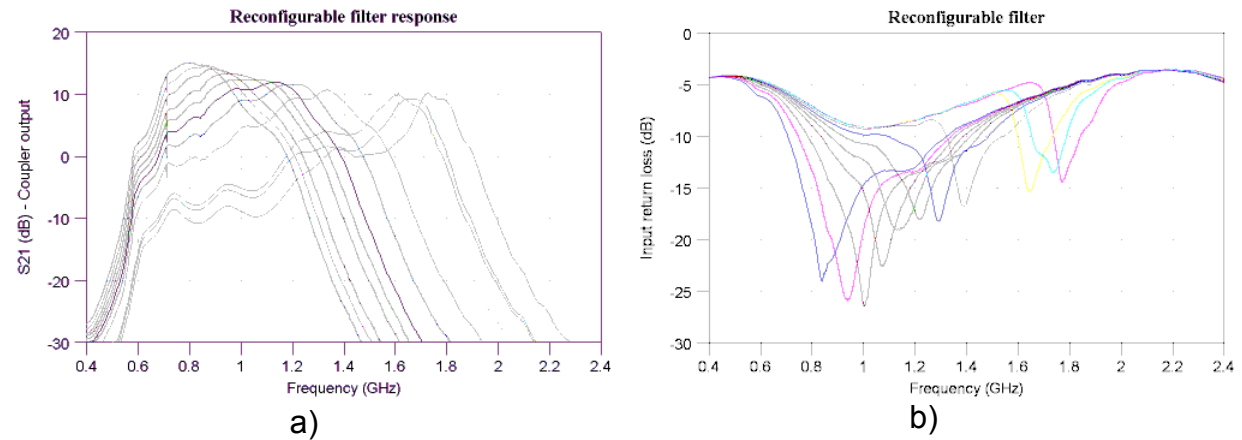


Figure 27: Reconfigurable bandpass filter performance: a) Gain at RF coupler output and b) Input return loss.

The proposed solution enables to operate in different bands without additional RF components. Meanwhile, the reference solution requires RF components for each frequency band. Hence, the reconfigurable solution is more promising when a large number of frequency bands is supported.

Concerning EI evaluation, NF tests were performed in both receivers. Figure 28 shows NF results in the reference receiver and the proposed solution results are depicted in Figure 29.



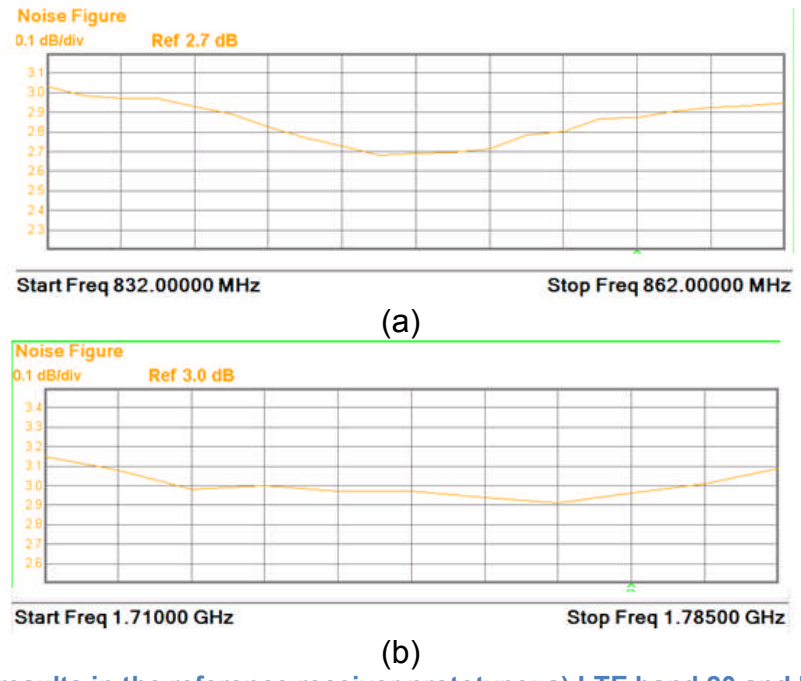


Figure 28: NF results in the reference receiver prototype: a) LTE band 20 and b) LTE band 3.

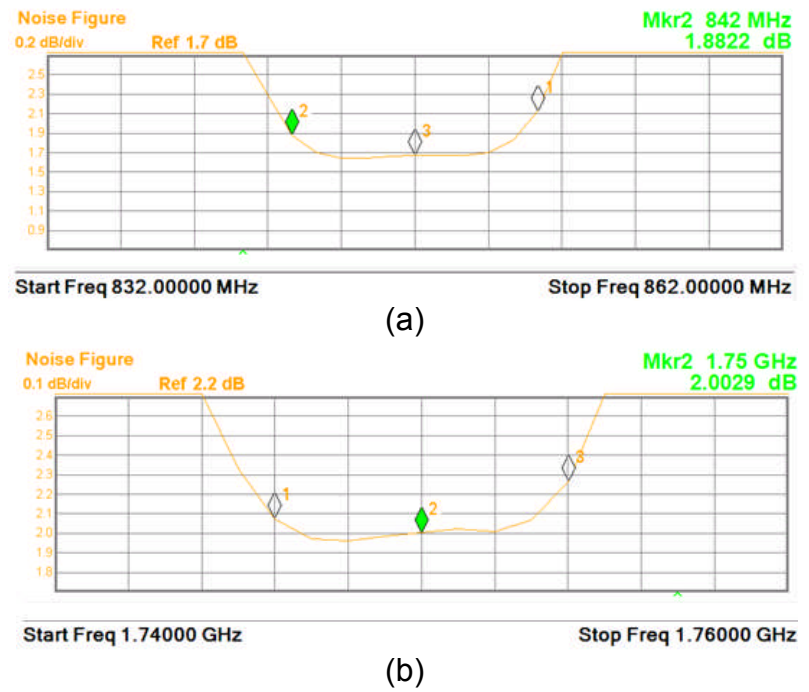


Figure 29: NF results in the reconfigurable low noise receiver prototype: a) LTE band 20 and b) LTE band 3.

Table 15: Comparison in NF performance between the reference receiver and the reconfigurable low noise receiver.

	NF – LTE Band 20	NF – LTE band 3
Reference receiver	2.7 dB (3dB max)	3 dB (3.1 dB max)
Reconfigurable receiver	1.7 dB (1.9 dB max)	2 dB (2.2 dB max)
NF improvement	≈ 1 dB	≈ 1 dB

Version: V1.0



Table 15 summarizes NF results from both solutions. The reconfigurable low noise receiver improves by around 1 dB the NF performance before demodulation stage.

Besides the typical method exposed above, the NF performance can also be calculated as follows:

$$NF = \frac{SNR_{in}}{SNR_{out}}$$

Through this method, both solutions were also evaluated using 10 MHz LTE UL signal. Defining the same SNR_{in} in both prototypes, SNR_{out} improvement works out NF enhancement between solutions. This alternative method allows EI evaluation in the LEXNET SC BS prototype. Firstly, the method was validated with the receiver prototypes. The output signal was measured for -50 dBm input signal and -70 dBm input signal (which represent realistic values) and none input signal which refers to noise floor.

Table 16 summarizes the SNR evaluation in the reference receiver and the reconfigurable low noise receiver prototypes for different input signal level. For each frequency band, SNR results are compared.

Table 16: Comparison in NF performance between the reference receiver and the reconfigurable low noise receiver, based on SNR measurements.

	LTE band 20 @ 850 MHz			LTE band 3 @ 1750 MHz			
Input signal: -50 dBm	Output signal (dBm)	Noise floor	SNR (dB)	Output signal (dBm)	Noise floor (dBm)	SNR (dB)	
Reference receiver	-34.3 dBm	-85.2 dBm	50.9 dB	-36.1 dBm	-86.3 dBm	50.2 dB	
Reconfigurable receiver	-32.5 dBm	-84.6 dBm	52.1 dB	-35.3 dBm	-86.5 dBm	51.2 dB	
SNR improvement			1.2 dB			1 dB	
Input signal: -70 dBm	Output signal (dBm)	Noise floor	SNR (dB)	Output signal (dBm)	Noise floor (dBm)	SNR (dB)	
Reference receiver	-54.3 dBm	-85.2 dBm	30.9 dB	-56.1 dBm	-86.3 dBm	30.2 dB	
Reconfigurable receiver	-52.5 dBm	-84.6 dBm	32.1 dB	-55.3 dBm	-86.5 dBm	31.2 dB	
SNR improvement			1.2 dB			1 dB	

The reconfigurable solution presents around 1dB SNR improvement, regardless of input signal level in line with NF enhancement shown in Table 2. Therefore this alternative method is validated for EI evaluation. This method is proposed mainly to evaluate the LEXNET SC BS prototype because the conventional method to evaluate the NF performance is not applicable.

Based on the simulation-based receiver evaluation in [D4.3], 1 dB NF enhancement before demodulation stage implies about 1.5 dB total NF enhancement comparing



both solutions. As a result, UL EI reduction in small cell scenario using this low EMF technique is 29.2% the one it was studied in [D4.3].

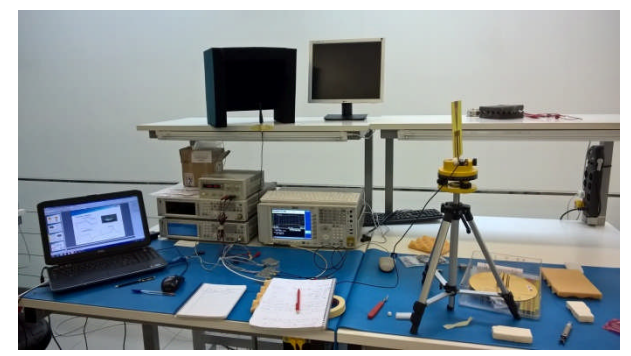
4.1.3.3 LTE SC BS RF front-end and antenna evaluation

To overcome the non-availability of the final antenna prototype in band 3, the previous super-directive single band prototype (developed in the band 3 [D4.3]) has been used temporarily for the common and global evaluation of the antenna and front-end combination.

For simplicity of these preliminary tests, the measurements are not carried on in anechoic chamber but in the large room of TTI RF laboratory, Figure 30. The four configurations are evaluated in term of signal and noise levels, reported in Table 17.

The following analyses can be drawn:

- The swap from standard to super-directive antennas does not disturb the +1 dB improvement on SNR bring by TTI receiver. This +1 dB amount can be directly translated in term of potential EI reduction for the UL at the UE side.
- As expected, the super-directive antenna presents a lower gain (-6 dB measured on the received signal strength) compared to the omnidirectional antenna. However the relevant result will be to measure a SINR improvement once blockers will be introduced, which was not planed at that time of this preliminary campaign.
- Preliminary conclusion seems that there is no noise level degradation due to the
 introduction of the LEXNET super-directive antenna on the noise figure of the
 global receiving chain. This is an important result as it validates that the 5 dB
 loses (due to poor efficiency of the super-directivity mechanism) are not
 completely transduced to the noise figure of the receiver chain. This is not a trivial
 result even inside the antenna designer community. It confirms the potential of
 such super-directive antenna for future deployment.



(a) Testbed with the standard omnidirectional antenna



(b) Testbed with the LEXNET singleband super-directive antenna

Figure 30: Testbed of the LTE RF front-end and antenna evaluation.



Table 17: SNR evaluation and estimated improvements.

		Reference receiver					
	Stand	lard ante	enna	LEX	NET antenna		LEXNET/std
	Noise	Signal	SNR	Noise	Signal level	SNR	Signal level
	level	level	(dB)	level	(dBm)	(dB)	improvement
	(dBm)	(dBm)		(dBm)			(dB)
	-86.0	-50.5	35.5	-87.0	-56.5	30.5	-6.0
			_			_	
				LEXNET	receiver		
	Stand	lard ante	enna	LEX	NET antenna		LEXNET/std
	Noise	Signal	SNR	Noise	Signal level	SNR	Signal level
	level	level	(dB)	level	(dBm)	(dB)	improvement
	(dBm)	(dBm)		(dBm)			(dB)
	-86.5	-50.0	36.5	-87.5	-56.0 (-60.5@+90deg)	31.5	-6.0
SNR improvement (dB)			+1			+1	

4.2 Beamforming antenna testbed

4.2.1 Evaluated solution

As indicated in [D4.3, section 3.3.3], this work presents null steering for the purpose of exposure reduction for a person using a Wi-Fi enabled laptop. The goal is to use experimental data to find a phase offset angle between a pair of transmit antennas that can allow for the implementation of null steering. The work is further extended to facilitate the transmission of a second data stream from the second antenna in a pair of antennas mounted on a laptop. This extension to current techniques [LEN1] [QAM] [KHA] [LEN2] [CHI1] [HOC1] [HOC2] is referred to as the 'hybrid' technique throughout this section since it is a hybrid of very phase-weighted simple null steering and the modulation alphabet technique known as 'SAR Codes' [HOC1] [HOC2]. Null steering technique simply sends copies of the same transmit signal from either RF chain; the hybrid technique uses both this type of simple null steering in conjunction with modulation alphabet design. In order to explain the concept, first consider the modulation alphabet at the output of the two RF chains, i.e. 'Tx 1st stream' and 'Tx 2nd stream' in Figure 31 for the simple case of null steering. The symbol encircled in red is the symbol of choice at this particular sample time; clearly this symbol is the same in both transmit streams, as would be expected.



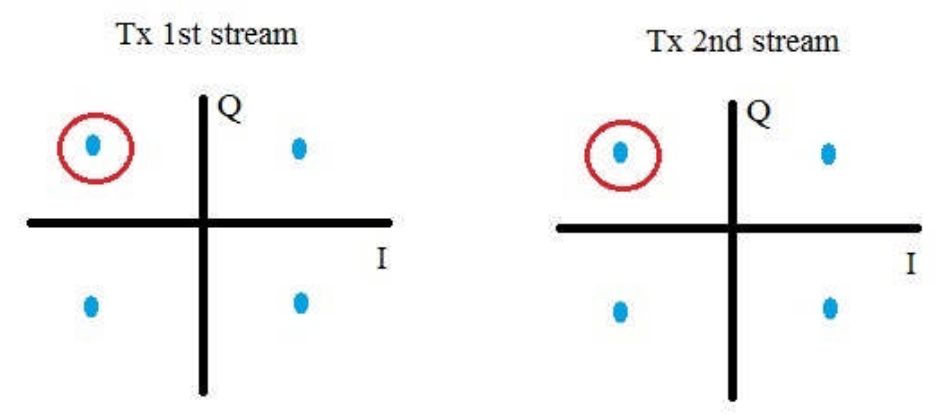


Figure 31: Modulation alphabet at transmit streams when simple null steering is applied.

In contrast to this simple transmission scheme, consider now that the symbol on the second stream is different to that of the first stream but exhibit some dependence. This is shown in Figure 32.

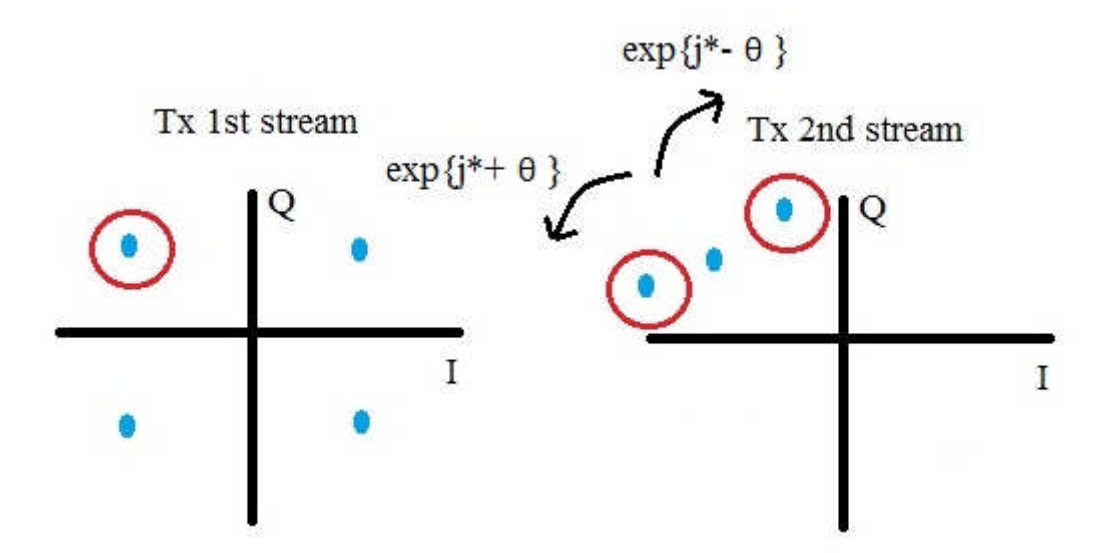


Figure 32: Modulation alphabet at transmit streams where the second stream shows an angular dependence on the first, i.e. the original 'SAR Codes' concept.

The idea is that when a symbol for the first stream is transmitted, it is possible to encode a separate data stream in the second stream whose symbol alphabet is dependent on that of the first stream. In this case when the QPSK from the upper left quadrant is to be transmitted from the first stream, the second stream can transmit one of either two symbols that are phase rotated copies of that of the first stream. These two new symbols are in effect created by phase rotating the symbol from the first stream by $\pm \theta$. This choice of symbol allows for the encoding of information in the second stream. This concept by itself formed the basis for 'SAR Codes'. It was proposed in [HOC1] [HOC2] that the angle θ could be used to steer a null to the user. However a rigorous examination of the SAR Code concept showed that this idea would not work very well in conjunction with the widespread and practical signal transmission scheme OFDM. Also, if the angle to steer the null to the user required a modulation dependence angle, θ , near to 0° or 180°, the scheme would become



impractical since the modulation symbols available on the second transmit stream would be too close to one another in I-Q space.

However as explained in [D4.3, section 3.3.3], when this defunct SAR Code idea with θ fixed at 45° was combined with simple null steering, a workable 'hybrid' system model emerged. It is the goal of this section to implement this system on a testbed demonstrator.

4.2.1 Test setup

The set-up is depicted in Figure 33. A laptop running MATLAB and Xilinx developer studio controls three WARP Virtex II boards [MAN] via a hub. A measure of exposure is made from both a laptop emitting radiation and measured by probes on the chest as well as from a probe inside a skull phantom that has a mobile device attached to it. As the signals are being transmitted from either the laptop or the mobile device, they are being received by an AP antenna, which is also being controlled by WARP Virtex II board. Note that in total, two of the WARP Virtex II are receiving, i.e. one receiving the access point signal and the other receiving signals from either probe configuration (chest or skull phantom). Two signals are implemented: (i) Null steering with selection combining at the receiver and the hybrid signal. In both cases, the signal used is based on 5 MHz MIMO LTE signal thus MIMO-OFDM is implemented. The probe antennas are UWB with 2.3 dBi gain (omnidirectional).

Version: V1.0 41



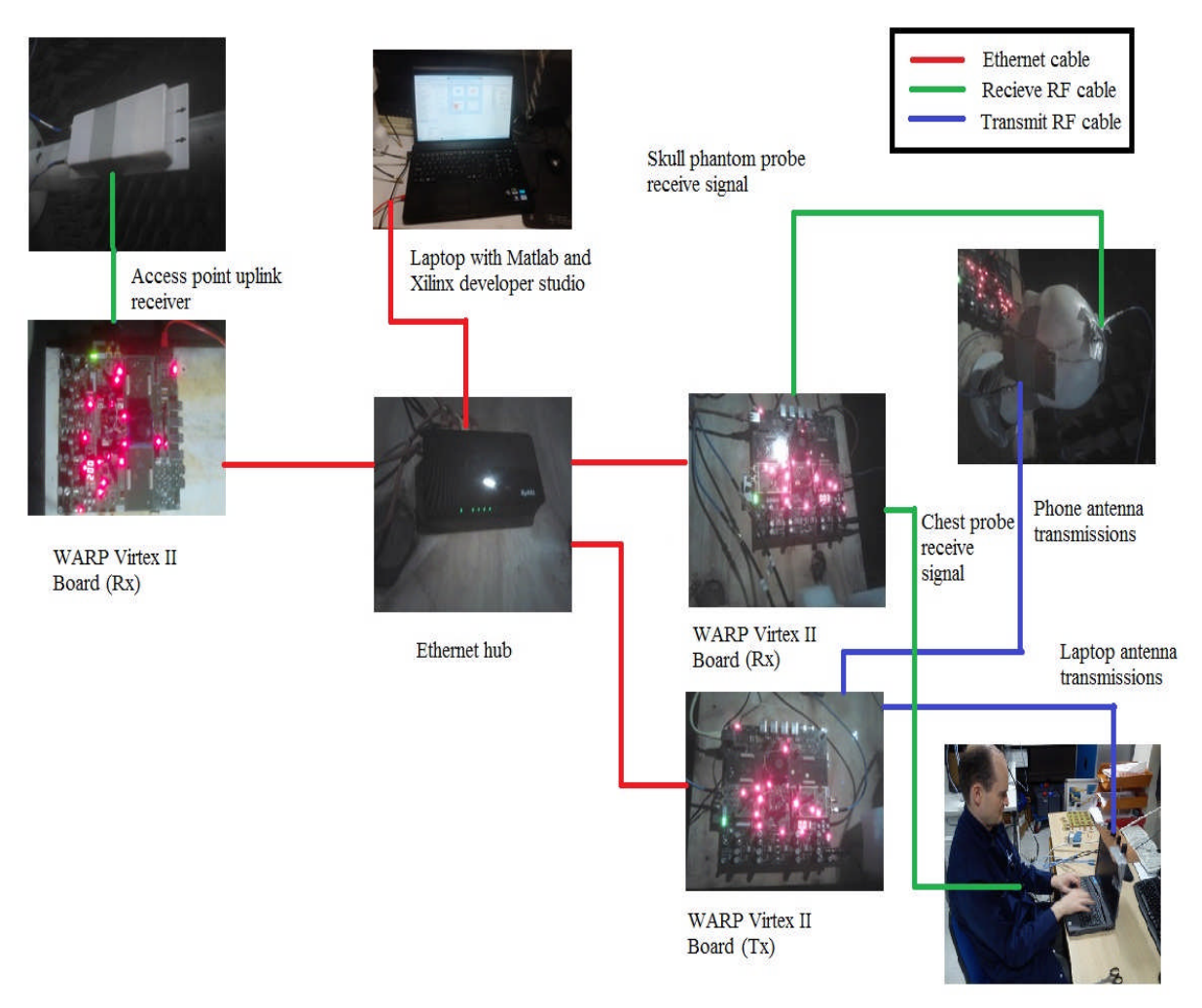


Figure 33: Beamforming testbed set-up.

4.2.2 Evaluation results

The demodulation of the novel waveform of the hybrid system model was successfully achieved. It is shown in Figure 34 for a receive SNR of approximately 20 dB. The BER was zero. In this case, the mobile device at the skull phantom was transmitting but similar results were achieved with the laptop device as transmitter.

Version: V1.0 42



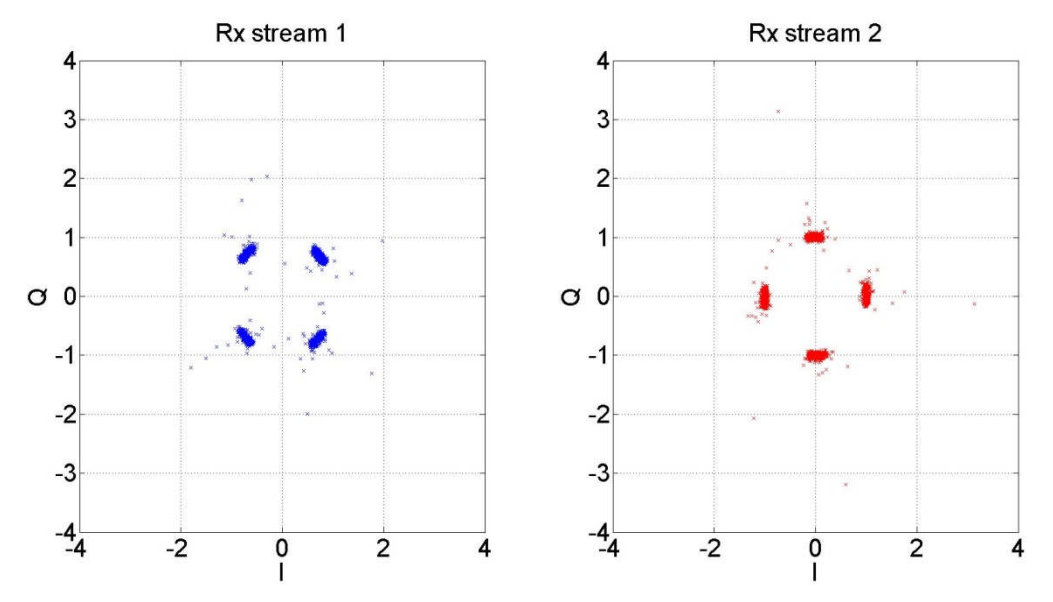


Figure 34: In-phase (I) and quadrature (Q) components of the received signal of the hybrid system model when implemented on the WARP Virtex II based testbed demonstrator. The receive SNR was 20 dB and the uncoded BER was 0.

Next the receive probe power for the case of the laptop as transmitter and for the case of the mobile device as transmitter are examined. Considering firstly, the laptop transmitter, the null angle for null steering and the hybrid system is varied over 0° to 360°. The emitted signal power is received by 4 probe antennas on the user's chest. These 4 signals are combined with a combiner before being attenuated by a 6 dB attenuator to perform an averaging using hardware. The results are given in Figure 35. It should be stressed that the absolute values of the power measurement should be ignored as they are simply decided by manipulating several transmit and receive gains to suit the dynamic range of the input ADC. The point of interest here is the overall pattern, which established quite clearly that a null can indeed be steered to the user at approximately 300°. Each plot is averaged over 5 complete set of probe power vs null angle measurements at the WARP Virtex II probe receiver board.

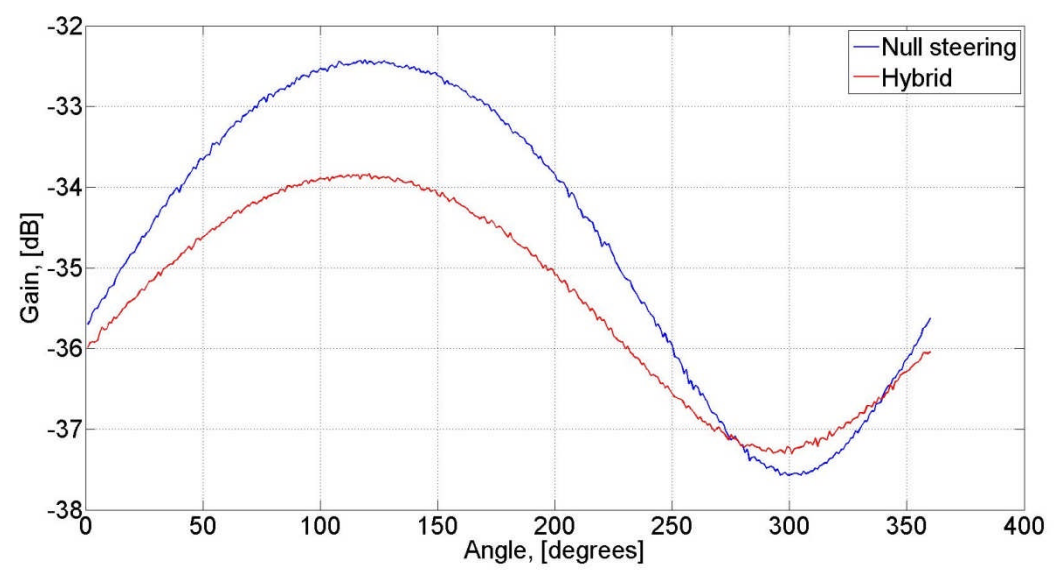


Figure 35: Probe power gain vs null angle for the case of the laptop transmitter and chest mounted probes.



For the case of the mobile device transmission and the skull phantom probe, the angular variation with respect to probe gain is given in Figure 36. Again each plot is averaged over 5 complete set of probe power vs null angle measurements at the WARP Virtex II probe receiver board. Several transmit and receive gains have been manipulated to suit the dynamic range of the input ADC. It is logical that the power gain range is higher for the case of the mobile device since the probe is subjected to less path loss. It is also clear that there is a clear angle where the exposure can be reduced at approximately 25°.

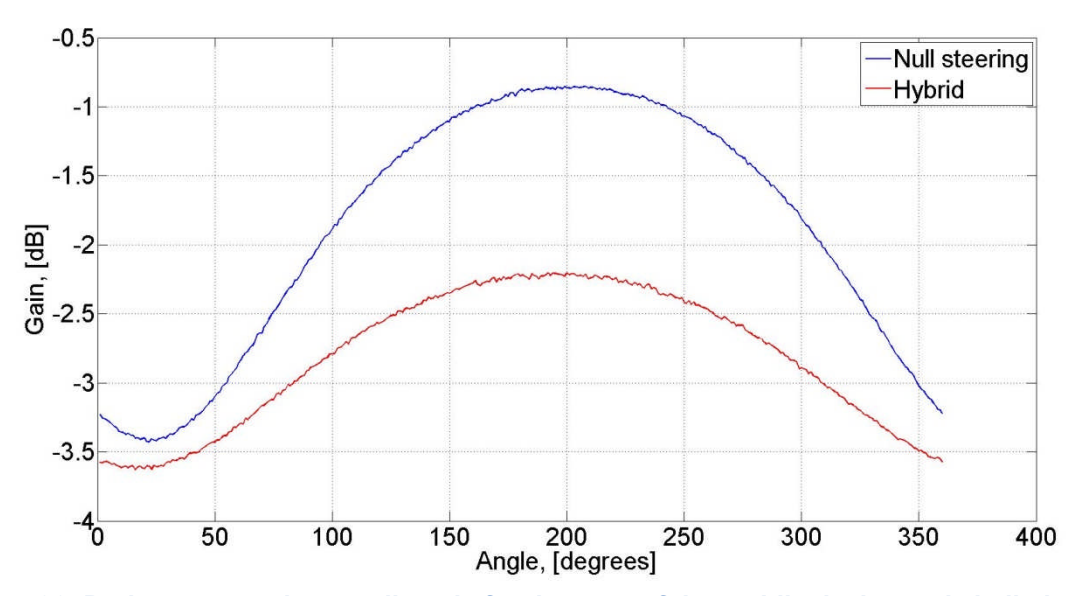


Figure 36. Probe power gain vs null angle for the case of the mobile device and skull phantom probe.

4.2.3 Concluding remarks

In this section, the novel 'hybrid' system model introduced in [D4.3, section 3.3.3] that facilitates simple null steering with more than one transmit data stream was implemented on a testbed demonstrator that is based on WARP Virtex II hardware. It was shown that the novel system model can successfully transmit and receive these new waveforms as well as demodulate two separate data streams while providing a reduction in user exposure due to the null that the system can steer to the user simultaneously to data transmission. It is stressed that, while the results clearly show that such a system is practically viable, this is just demonstrator for the system and that exact values for the nulling angle required and the exposure reduction achieved are not necessarily obtainable using this approach. The work in [D4.3, section 3.3.3] was more rigorous in this regard and the reader is referred here for an examination of the reduction in exposure index that can be achieved.

4.3 Large-scale beamforming simulation

Laboratory evaluations are completed by the simulation of dense outdoor small-cells deployed in an urban environment. Beamforming and steerable antennas are assumed to be installed at the small-cell. The impact on the DL/UL user throughput and EMF exposure are jointly assessed over a scenario with medium traffic load (i.e. the average small-cell traffic load is around 15%).



4.3.1 Evaluated solution

The evaluation consists of the comparison between four different antenna systems at the small-cell:

- 1. Single omni-directional antenna;
- 2. Beamforming with two omni-directional antennas, using LTE TM6 scheme;
- 3. Beamforming with four omni-directional antennas, using LTE TM6 scheme;
- 4. And beamsteering with the directive antenna proposed in section 4.1.

The gain of the omni-directional antenna is 2.15 dBi. The LTE TM6 codebook, with two antennas, proposes four radiation patterns with maximum additional 3dB gain. The codebook with four antennas is composed of 16 possible radiation patterns with a maximum additional gain of 6dB [R&S]. Besides, the directive antenna can be steered in 8 different directions; its maximum gain is 1.3 dB below the one of the omni-directional antenna.

The maximum emitted power is kept constant for all four test scenarios. The total user throughput served by the network is constant as well.

4.3.2 Test setup

The simulation is conducted within the tool presented in [D6.2-A, section 6.4], which relies on a precise description of the urban environment and deterministic ray-based propagation predictions. Here the simulator is set in a specific mode, so-called Monte-Carlo, where discrete users are randomly dropped in the prediction area, and KPI statistics are built from a succession of runs. At each Monte-Carlo iteration, the simulator determines each user attachment (considering an omni-directional antenna pattern at the small-cells and best RSRP), selects the antenna beam that maximizes the useful signal strength for each user, calculates DL/UL interferences, which depend on the antenna beam and user activity, and finally gets the user DL/UL throughput from a mapping with SINR.

The advantage of using a ray-based propagation model in the analysis is two-fold. Firstly, the antenna is 'masking' a dispersive propagation channel, instead of a single-path channel as is often done in large-scale studies. When applying beamforming or beam-steering in a dispersive radio environment, the higher the channel spatial dispersion is, the lower the signal strength, and possibly the stronger the interference. Secondly, the interference between two communications in two neighbour cells does not only depend on the distances or link directions. Still, some correlation might happen between separated links, due to particular reflections, diffractions, or a general canyon effect along the streets. As a result, pointing the beam of a small-cell in a direction opposed to a neighbour-cell user does not guarantee that the interference is null at the user position. Both reasons make the present simulation more realistic than beam-steering studies based on the single direct-path assumption.

As shown in Figure 37, the evaluation is conducted in the Paris downtown with only small-cells (no co-channel macro layout) and 60% indoor users distributed in different floors. Other simulation parameters are given in Table 18.

Version: V1.0



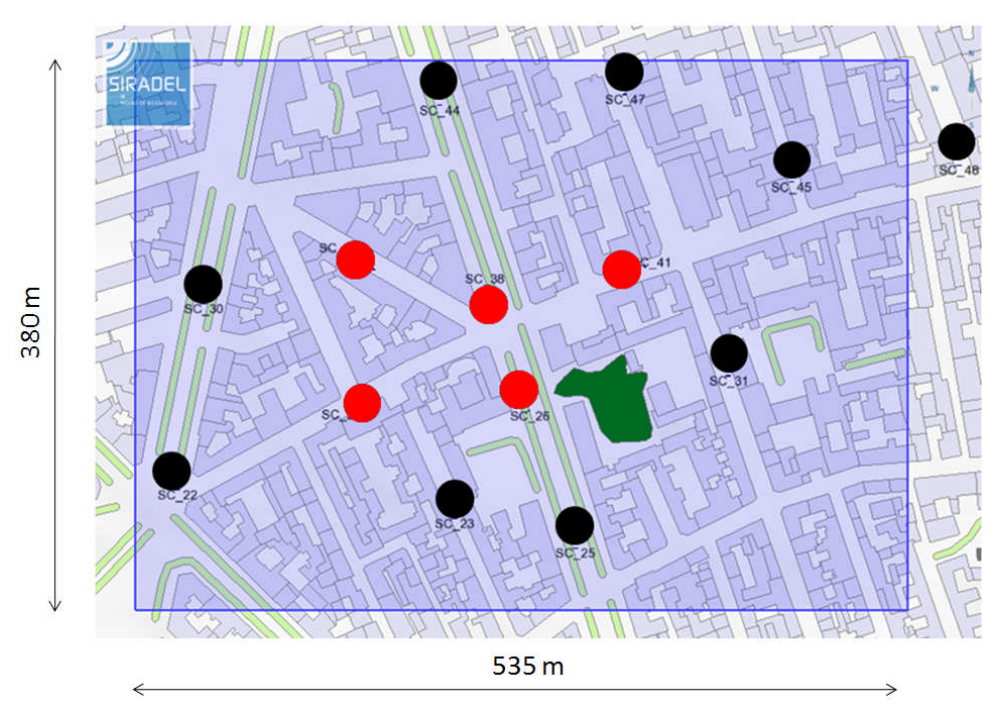


Figure 37: Small-cell deployment in a dense urban environment.

Table 18: System parameters.

System	LTE FDD 2x10 MHz. Central frequency: 2 GHz.
Small-cell layout	SC deployment: 14 small-cells in 0.2 km² (69 cells per km²). Height: 6 m above ground. Maximum transmit power: 5 W. Antenna for cell selection: omnidirectional, 2.15 dBi. UL noise figure: 2.5 dB.
User equipment	UL transmit power: 23 dBm (fixed for simplicity). Antenna: omni-directional, 0 dBi, 1.5 m above ground or floor. DL noise figure: 9 dB.
User trafic	Data trafic. 200 Mbps/km² DL. 33 Mbps/km² UL.

At each Monte-Carlo iteration, a random set of users are positioned in the blue area of Figure 37. As the Monte-Carlo simulation proved to rapidly converge, 30 independent runs were sufficient to reach statistically tight performance results. The performance has been estimated only from the users attached to the five central small-cells represented by red dots in Figure 37. Indeed the interference calculated at the users located close to the external boundary of the simulation area is underestimated and the resulting user performance is therefore not fair.

Besides, in order to capture the DL EMF exposure suffered by the population and not specifically by the users, EMF probes have been distributed into the simulation area independently of the user locations.

Figure 38 gives a short description of the evaluation scenario, where the omnidirectional and LTE beamforming use cases are considered as references; the smallcell with the LEXNET directive antenna is the tested innovation.



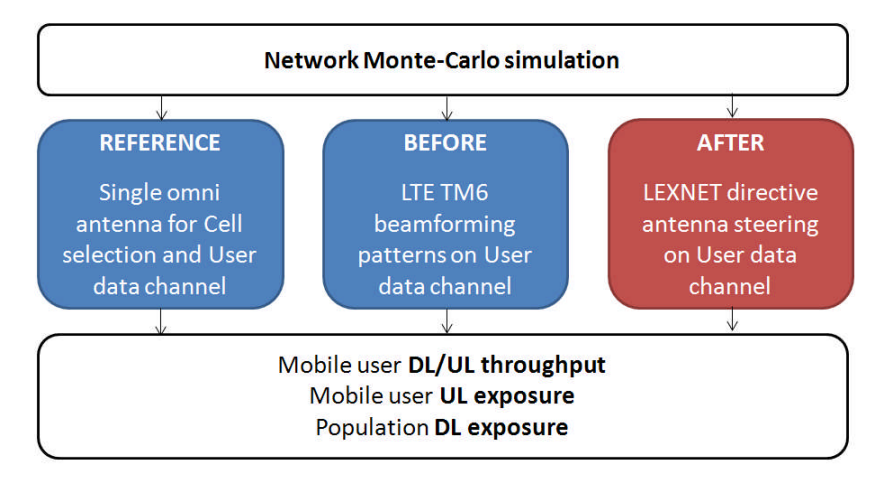


Figure 38: Evaluation scenario for beamforming network simulation.

4.3.3 Evaluation results

Table 19 summarizes the simulation results for both DL and UL directions, including: the DL cell load (ratio of allocated cell resources); the mean DL power density obtained from the sum of DL transmissions at the probe locations; the median peak user throughput; and the peak throughput at the cell-edge (10% worst percentile). The small-cells obviously take great advantage from the beam-forming or beam-steering effect, with a mean DL traffic load reduced by 25%. Compared to the single omni-directional antenna, the steerable directive antenna leads to a significant increase of the median DL peak throughput (+37%), and even more at the cell edge (+78%) where the antenna gain degradation is more than compensated by the reduction of the inter-cell interference. The mean DL power density is divided by 6.3. Getting such a strong exposure reduction factor together with a significant QoS improvement is quite a challenge, and this obviously appears as an interesting gain brought by the directive antenna.

The gain on the UL performance is highly significant as well. The median and celledge peak throughputs are respectively improved by +24% and +714%, while the global transmit power efficiency (UL throughput per unit transmit power) is enhanced by +16%. This latter result means that the EMF exposure of a mobile user, due to its own device transmission, is divided by 1.16 in average (provided its network usage remains constant).



Table 19: Evaluation results from beamforming network simulation.

		Single omni antenna	LTE TM6 – 2 antennas	LTE TM6 – 4 antennas	LEXNETantenna
	Mean traffic load	16 %	12 %	10 %	12 %
Ų	Median SINR	16.1 dB	19.4 dB	22.5 dB	22.0 dB
를	Cell-edge SINR	6.3 dB	9.6 dB	13.2 dB	11.2 dB
Downlink	Median peakthr.	29.8 Mbps	34.1 Mbps	36.9 Mbps	36.9 Mbps
	Cell-edge peakthr.	9.9 Mbps	16.3 Mbps	17.7 Mbps	17.8 Mbps
	Mean power density	93.5 dBμV/m	92.8 dBμV/m	92.5 dBμV/m	85.5 dBμV/m
	Median SINR	17.1 dB	21.1 dB	24.9 dB	22.3 dB
녿	Cell-edge SINR	-5.1 dB	-1.3 dB	2.9 dB	1.1 dB
Uplink	Median peakthr.	29.8 Mbps	36.9 Mbps	36.9 Mbps	36.9 Mbps
	Cell-edge peakthr.	0.7 Mbps	2.5 Mbps	5.7 Mbps	5.7 Mbps
	Tx power efficiency	116 Mbps/W	127 Mbps/W		134 Mbps/W

The LTE TM6 scheme with two antennas also provides good performances, but slightly lower than the ones obtained with the steerable directive antenna on the downlink, and far lower at the UL cell-edge. Besides, the reduction factors on the EMF exposure are limited to 1.17 and 1.09 for DL and UL, respectively.

The gain on user throughput and UL exposure is further enhanced with four antennas; and is very close to the one obtained with the steerable directive antenna. Despite the increased antenna gain in the beam direction (up to 6 dB compared to the omni-directional antenna), the DL exposure improvement is very limited. Besides, the four-antenna beamforming must be of a size much larger than the steerable directive antenna (section 4.1.1.1), which makes its integration into small base stations more complex.

The main conclusion is that beamforming and beamsteering lead to a significant improvement of the user throughput along with a reduction of both DL and UL exposure. In particular, the steerable directive antenna allows the DL exposure to be divided by 6.6.



5 Low EMF NETWORK TECHNIQUES

Two low EMF management techniques, initially investigated by the industry for reducing congestion risks in cellular networks (Wi-Fi offloading), reducing the power consumption in WLAN (switching off some AP's in absence of users) are evaluated here in terms in EMF.

5.1 Wi-Fi offloading

The investigations on the Wi-Fi offloading policy, as it can be implemented in the ANDSF (Access Network Discovery and Selection Function) have been initiated in [D5.2], where it is shown that offloading may significantly reduce the DL exposure contribution coming from a traditional LTE macro layout [D5.2, section 7.1]. A two-tier system-level simulation was also introduced that predicts the user distribution and user performance for different offloading scenarios.

Those results are completed in this document with evaluation of the EI reduction; and the comparison between various scenarios and offloading strategies. The evaluation relies on two complementary system-level simulation platforms: a two-tier dynamic simulator on one hand, using analytical models; and a coverage-based simulator (radio-planning like), using deterministic prediction for the LTE layer and an abstraction model for integration of Wi-Fi offloading.

On the one hand, an accurate analysis is performed by the system-level simulator that makes use of radio-planning techniques, relying on a real urban environment model and a deterministic propagation loss prediction scheme is applied over 3D static maps. By this way, the tool is able to accurately calculate the received field, UL transmit powers and throughput, which allows the estimation of both DL and UL EMF values.

On the other hand, the analysis depicted above lacks from a detailed modelling of network selection and resource allocation procedures based on services demand. In this sense the second tool, whose modelling takes a larger number of abstractions, is able to consider different access policies, carrying out a step-wise service analysis.

5.1.1 Evaluated solution

Traffic offloading from the cellular 3GPP networks (3G or 4G) to Wi-Fi access points is governed by policies defined at the national level in the ANSDF block. The nationwide offloading policy selects a set of services (e.g. video download) that must be, as far as possible, transferred to Wi-Fi with the aim to optimize the core network efficiency in terms of delay, capacity and cost. Several policies are defined for different environments (rural, suburban, urban, dense urban) and time periods. This technique is viewed as a very cost-effective solution to support important traffic increase in the cellular network with only a limited investment in the infrastructure.

A study based on the measured nationwide traffic data in the Orange's French 3G network has shown that 45% traffic offloading was an appropriate target to improve latency and throughput in the core network. This target is used in the evaluation below as an objective given by the ANDSF, but its application depends on radio constraints or criteria. The radio network simulation considers together the ANDSF policy and some QoS measurements that could be made by the user equipment in



order to decide the transfer from 3GPP to Wi-Fi. At the end, the radio network simulator provides a QoS evaluation for users initially connected to the 3GPP network, and the prediction of DL/UL exposure taking both into account the 3GPP and Wi-Fi contributions.

5.1.2 Test setup

The coverage-based simulator is the tool introduced in [D6.2-A, section 6.4], providing outdoor and multi-floor indoor QoS and EMF maps, but extended with introduction of three new blocks devoted to the Wi-Fi offloading study:

- A 2.4 GHz Wi-Fi abstraction model that provides statistics on the maximum Wi-Fi DL/UL PHY throughputs available at indoor locations. Those statistics consider both the backhaul throughput limitations due to fixed internet access and the Wi-Fi max throughputs itself. The abstraction model also gives an estimate of the average DL exposure, both in outdoor and indoor environments, as generated by the Wi-Fi AP layout for a given traffic load.
- 2. A RAT selection module that decides for each user whether the communication is served by the LTE or the Wi-Fi network. First, the type of service (to be offloaded according to ANDSF policy or not) is simulated in a random way. Afterwards, two QoS metrics are involved in the decision: the LTE DL throughput available at the user location, which is predicted in a deterministic way; and the Wi-Fi DL throughput, which is randomly generated from the Wi-Fi abstraction model (i.e. a statistical throughput probability function).
- 3. Finally, the multi-RAT network performance is obtained from the LTE simulation process described in [D62-A, section 6.4] for non-offloaded users; and from the Wi-Fi abstraction model for offloaded users.



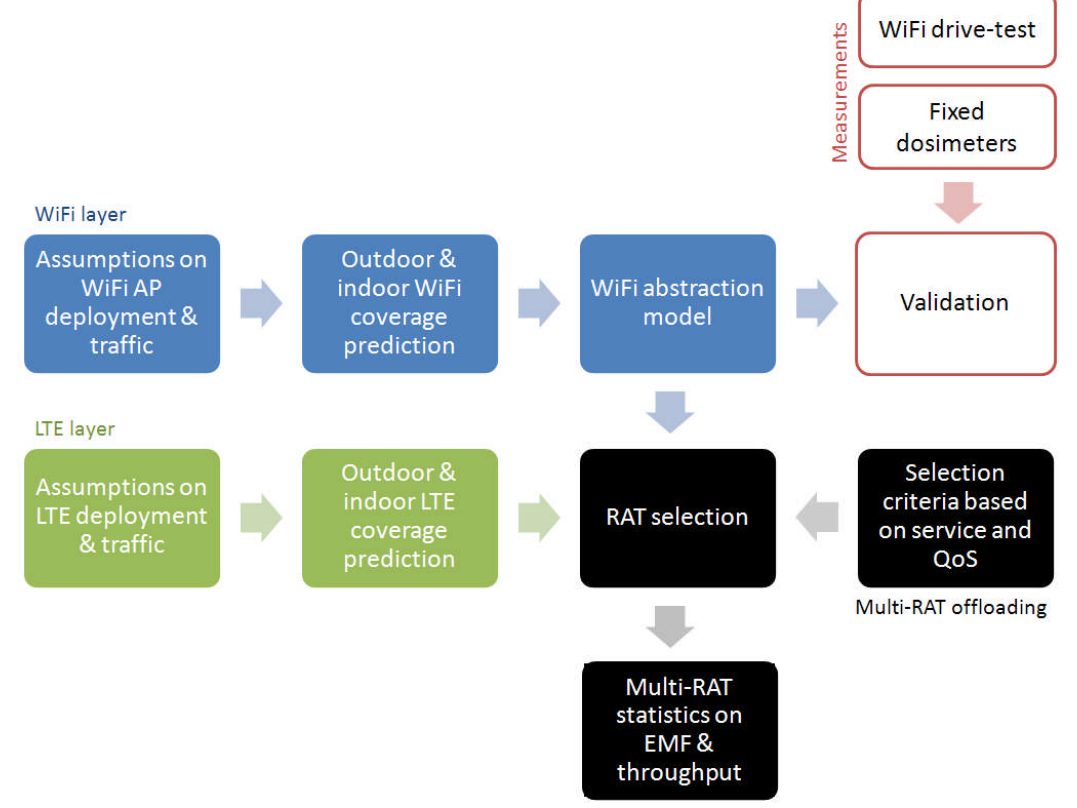


Figure 39: Methodology for Wi-Fi offloading evaluation based on coverage simulations.

The reason why we evaluate the Wi-Fi performance from an abstraction model, even if the LTE network is simulated in a deterministic manner, is two-fold: 1) The spatial distribution of private APs in the environment is unknown, and not controlled by the operator, so it can be seen as random; 2) The evaluation is conducted at a large scale in a dense urban environment, including several macro LTE base stations, which would have required the distribution and prediction of many thousands of APs in a full-deterministic approach.

The elaboration of the Wi-Fi abstraction model and its validation against measurements are detailed in Appendix A3.

The main principles of the Wi-Fi offloading scenario are summarized in Figure 40. The study is conducted in a large dense urban environment, where Wi-Fi and LTE service coverage are reached everywhere. The LTE network is assumed to be highly loaded without having reached its saturation state and we can therefore assume that all users would be eventually served.

Version: V1.0



52

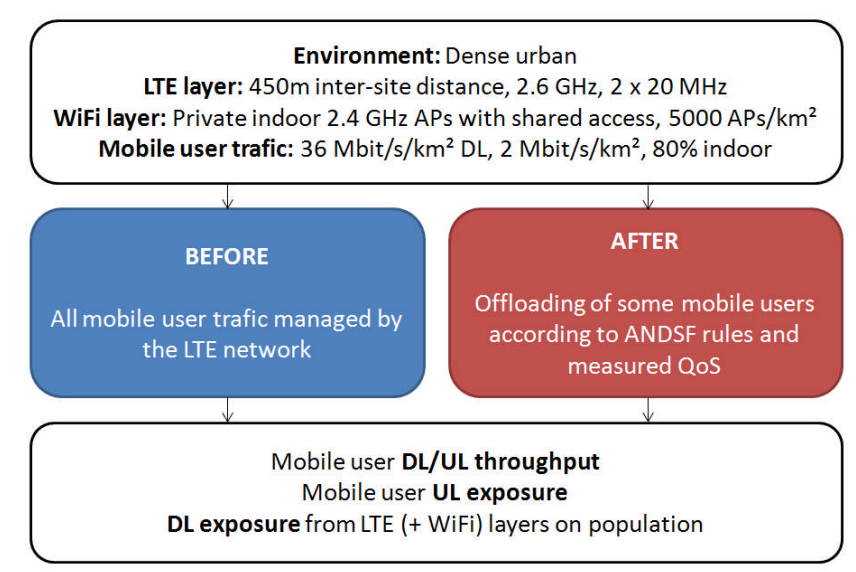


Figure 40: Evaluation scenario for Wi-Fi offloading.

The detailed simulation parameters are presented in Table 20 to Table 22. The offloading is allowed only towards the APs managed by the considered LTE operator. This operator is assumed to be the incumbent fixed access operator in the area, with 40% of APs.

The backhaul performance, from xDSL or optical fiber, is taken into account, such that the xDSL restriction on the peak throughput is integrated in the RAT selection process. The offloading is allowed only for indoor users. Two categories of mobile users are distinguished:

- The ones being located at home with both their fixed Wi-Fi and mobile LTE
 access managed by the same operator. Consequently they can be offloaded to
 the Wi-Fi with full access to the AP bandwidth. Furthermore, as both the AP and
 the user are located in the same location, they most likely benefit from high Wi-Fi
 radio performance.
- The ones who cannot take benefit from a full access to an AP located in their vicinity. Those users can only be offloaded to the Wi-Fi exploiting the shared resources of an AP managed by the cellular operator; hence, depending on the user location from this AP, there might be non-optimal Wi-Fi radio performance.



Table 20: Wi-Fi layout properties.

Wi-Fi technology	802.11n 2.4 GHz
Wi-Fi AP access	Private AP, with $P\%$ of them giving a shared access to the mobile users of the same operator
AP deployment	Indoor 5000 APs/km²
%AP owned by the considered LTE operator	40% (i.e. assuming that is the main nationwide Wi-Fi operator)
Backhaul	Q% APs connected to fiber (100-Q) % APs connected to ADSL
Fiber performance	Assumed to be much higher than mobile user needs
ADSL performance	15 Mbit/s DL
Max bandwidth allowed for shared access	40% on both radio interface and backhaul
Initial traffic on private APs	65 Mbit/s per AP

Table 21: Mobile user properties.

Mobile user traffic	35 Mbit/s/km² DL and 2 Mbit/s/km² UL → LTE layer close to overloading
Mobile user distribution	20% outdoors 80% distributed into the different building floors

Table 22: Offloading rules.

ANDSF policy	Offload video traffic, i.e. 45% of whole traffic
QoS-based selection criteria	Wi-Fi DL max throughput (incl. backhaul limitation) > LTE DL throughput
Mobility	Offloading only allowed for static users For simplicity, all outdoor users are assumed to be moving; and all indoor users are assumed to be static
Mobile user location	Distinction between R% of users with full Wi-Fi access: the user is at home and can be offloaded to their AP with full access. (100-R)% of users with shared Wi-Fi access: the user is not at home or having a different operator for their fixed Wi-Fi access

5.1.3 Evaluation results from coverage-based simulations

The first evaluation scenario assumes unrestricted Wi-Fi broadband access, i.e. Q=100% of private APs are attached to optical fiber and R=100% of indoor mobile users have a full-access to a neighbor Wi-Fi AP. Those assumptions make the simulation setup very close to the one evaluated in section 5.1.4 with the dynamic system-level simulator, and thus allows both simulation tools to provide together an accurate EI estimate with a per-service QoS analysis. Figure 41 gives the EI before (blue) and after Wi-Fi offloading (red), showing a significant EI reduction of 3.3. The distinction is made between DL and UL contributions, as well as between LTE and Wi-Fi components in the case of the two-tier network. It is noticeable that the UL

Version: V1.0



contribution remains almost constant. Indeed, the proximity of the Wi-Fi AP does not lead to any reduction of the UL transmit power, as this power is fixed on Wi-Fi links. Besides, the DL population exposure takes a great benefit from the offloading. The contribution from the Wi-Fi transmissions is negligible, and the average transmit power of LTE macro eNodeB's decreases along with the traffic load.

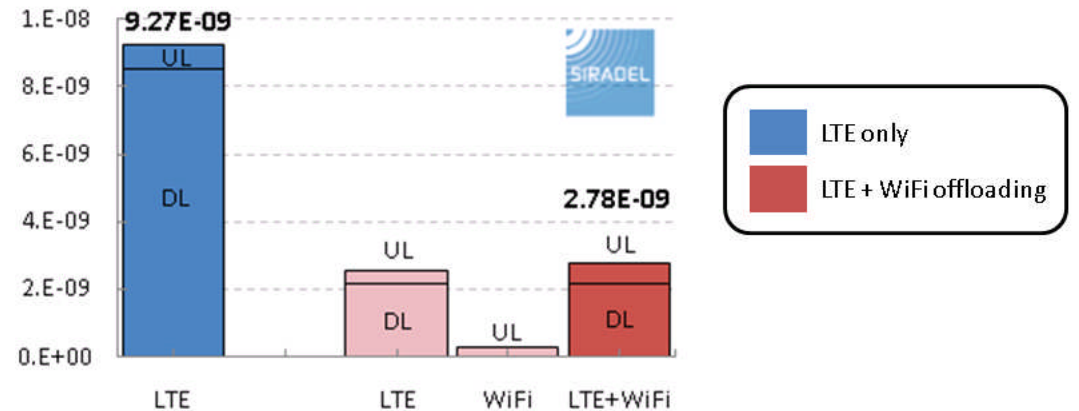


Figure 41: Exposure Index along with Wi-Fi offloading and unrestricted Wi-Fi broadband access.

The evaluation continues with a more realistic and restricted access to the Wi-Fi broadband deployment. Four scenarios are considered. The first one is so-called "reference" offloading scenario and makes the assumptions depicted below:

- P=25% of the private APs permit the external users to have a shared access;
- Q=50% of private APs are connected to the optical fiber, while the others (50%) are fed by xDSL, with maximum throughput of 15 Mbps on the downlink. Note that only 40% of this maximum throughput is available in shared access;
- R=50% of mobile users are considered being at home, and may be offloaded to their own AP without any bandwidth restriction.

Each of the three other offloading scenarios has one input assumption that differs from this reference use case: 1) shared access is allowed with P=100% of the private APs; or 2) Q=100% APs are connected to the optical fiber; or 3) R=90% of mobile users can be offloaded to their own AP with full access.

With those complementary scenarios, we can characterize the EI sensibility to the Wi-Fi AP properties. The analysis is far from being exhaustive, as there is still a large number of sensitive inputs in this evaluation; however, this initial analysis gives us some interesting trends.

The evaluation of the reference offloading scenario leads to the comparison given in Figure 42, which reports on DL/UL throughputs and three EMF metrics:

- Total DL field strength;
- Indoor UL Tx power efficiency, which is defined as the transmit power and the
 user peak throughput; the higher the efficiency value is, the lower is the
 exposure generated per unit data rate;
- El values.

Figure 42 gives the global performance of the two-tier network, but also distinguishes between the performance of users still connected to a LTE eNodeB and users that have been offloaded to Wi-Fi.



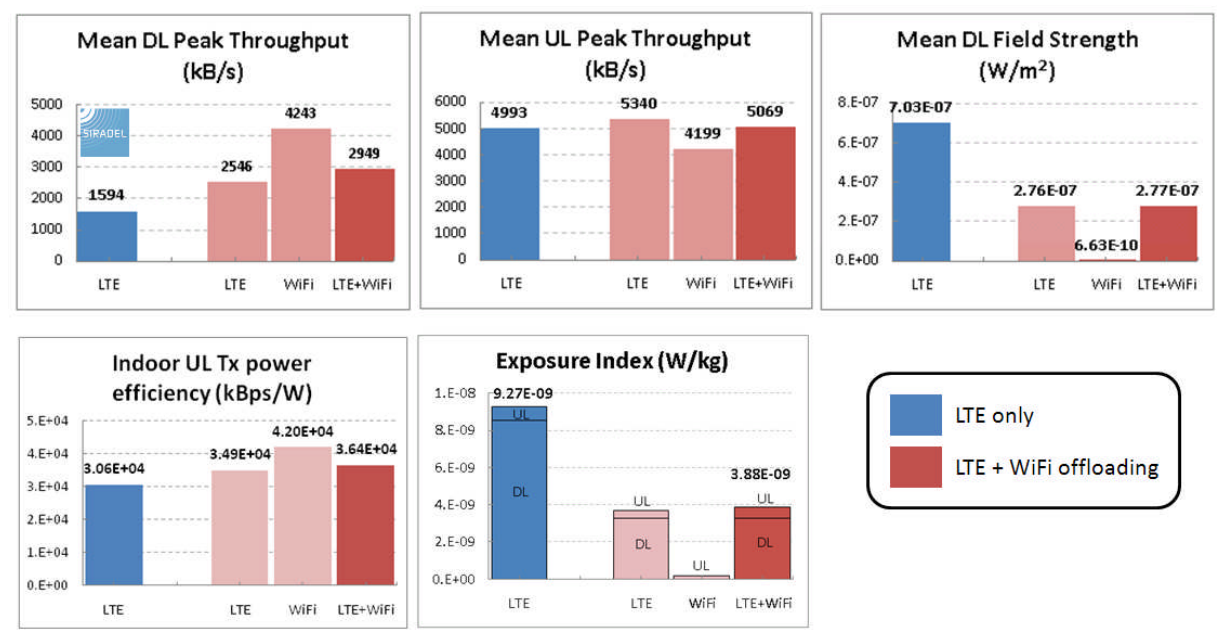


Figure 42: Network QoS and EMF performance before (blue) and after (red) the activation of Wi-Fi offloading.

The benefit of the Wi-Fi offloading is obviously strong on both the mean DL throughput (× 1.8) and the mean DL field strength (÷ 2.5) as the macro eNodeB transmission and the DL interference are both significantly reduced.

The Wi-Fi offloading leads to an increase of the DL exposure in the close vicinity of the AP, but the impact of the additional AP radiation over the whole population remains negligible, compared to the LTE network contribution: 50 times lower inside the buildings, and 450 times lower in the streets.

The Wi-Fi UL performance is slightly worse than the LTE UL performance. But the comparison is very sensible to the SNR-to-throughput mapping tables implemented in the scenario. It is worth recalling that the UL performance is of similar order for indoor LTE users and offloaded Wi-Fi users.

Finally, the global EI is divided by 1.8, mainly because of the DL exposure reduction.

The results from all offloading scenarios are summarized in Figure 43. The El reduction is obviously proportional to the offloading ratio (percentage of users being offloaded). We then illustrate how the AP configuration or user situation can influence the offloading performance and exposure level.



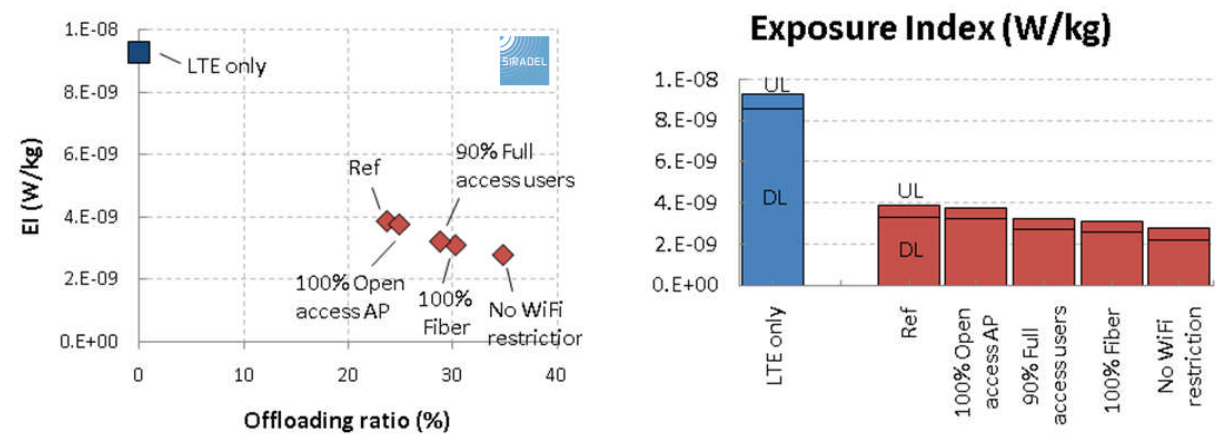


Figure 43: Network EMF performance for different AP configurations or mobile user situations, before (blue) and after (red) the activation of Wi-Fi offloading.

Remark that the strong and linear EI decrease is valid only as long as the DL exposure is predominant compared to the UL exposure contribution.

5.1.4 Evaluation results from dynamic simulations

This section presents the main results obtained by means of analytical system-level simulator. This tool implements analytical models for both the LTE coverage and the corresponding resource allocation schemes, and an abstraction of Wi-Fi technology. More details about the models implemented can be found in [D5.2, section 7.2]. In brief, the tool performs a dynamic analysis over a scenario by applying the access policy on consecutive snapshots. For each snapshot users' position and service activity varies according to a specific pattern, and the output of one snapshot is used to feed the following one (for instance, when a service is dropped); in this way the scenario dynamics and memory can be taken into account.

The scenario studied has a size of 1350x1350m² where the LTE base stations are deployed following a hexagonal deployment; on the other side, the Wi-Fi access points are randomly deployed within the area.

Over this scenario 500 users are moving according to a Random Waypoint model with a speed randomly selected within [1, 3] m/s. Each user is able to initiate 2 types of services: heavy and light, following an ON-OFF model with different parameters. In addition, snapshots are taken every 10 seconds.

The particular values of the user density and services parameters are depicted in Table 23. As can be seen, type 1 users are allowed to connect to Wi-Fi access points, while those belonging to type 2 are limited to the cellular network.

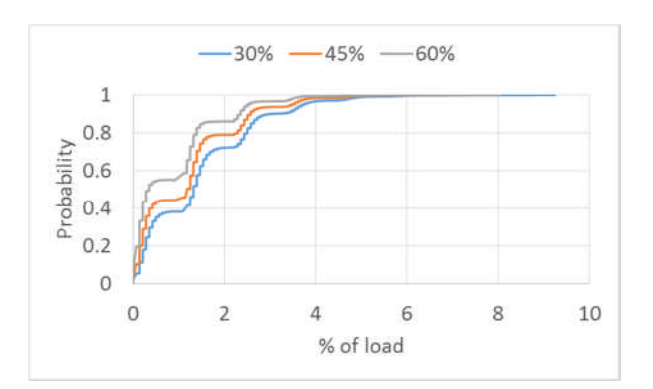
Traffic (Kbps) OFF (sec) **Type** ON (sec.) **Services** Video (V) 1000 300 1200 Internet (I) 64 60 80 **Services** Amount (%) Type Access **Users** V+I 1 [30, 45, 60] All Networks 2 V+I [70, 55, 40] Only Cellular

Table 23: Traffic configuration.



Over this scenario, we have varied the percentage of users of each type, in order to study the impact of the offloading policy. For all the configurations, 10 independent simulations of one hour (i.e. 360 snapshots) are performed. The users who are allowed to connect only to LTE select the cell with higher RSRP; when such cell cannot accommodate enough resources to satisfy the user's demand, the user will try the following and so on. In the case of users allowed to establish Wi-Fi connections, the access point that provides the highest data rate is selected. If the selected access point is saturated, then the user would try connecting to the next one. Only if no Wi-Fi connections are available, the user will try to use the LTE layer.

First, we have analysed how the load of the different access elements vary with the percentage of users that apply the offloading policy; for this first analysis, 100 Wi-Fi access points have been considered. Figure 45 shows the CDF of the relative load of the LTE cells (i.e. each eNB sector) assuming different percentages of offloading; besides, we also study the occupancy of the Wi-Fi access points for the different offloading configurations. In the case of LTE technology, the maximum relative load for the defined scenario is rather low (below 6%) despite the amount of offloaded traffic; nevertheless, we can also observe a load reduction if traffic gets higher. On the other hand, Figure 44 shows that Wi-Fi access points are inactive most of the time, even when 60% of traffic is offloaded. It has been also seen that, even for a 30% of offloaded traffic, some accesses might get temporarily saturated.



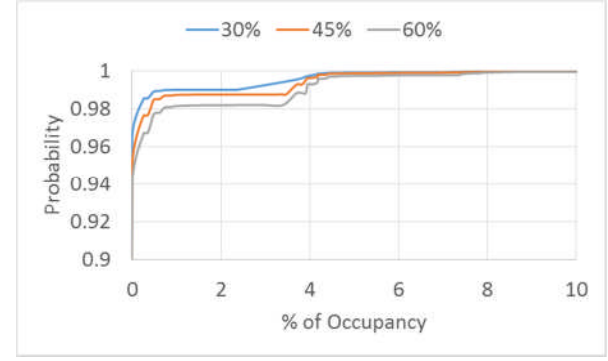


Figure 45: CDF of the LTE cells load.

Figure 44: CDF of the Wi-Fi APs occupancy

Once the influence of the amount of offloaded traffic has been studied, we have focused on the influence of the offloading policy over the different services and the impact of the number of deployed access elements on the QoS parameters.

Figure 46 shows the average service outage (probability that is either rejected or dropped) for different number of deployed access points and for the different types of services: video and internet with and without the possibility of offloading to Wi-Fi. As can be observed, regardless the offloading feature, heavier services (i.e. video) are more likely to fail due to their longer duration and higher demand. Furthermore, it is also shown that services that cannot be offloaded are more likely to suffer a failure, thus leading to a poorer QoE. Last, when increasing the number of access points in the scenario, the failure probability for services that might be offloaded decreases drastically. Interestingly, the higher the number of Wi-Fi access points, the higher the failure probability is for services without offloading. This behaviour is caused by the fact that the network has more traffic (lower failure for offloading traffic), so that the



probability of mutual interference is higher, yielding an increase of the outage probability.

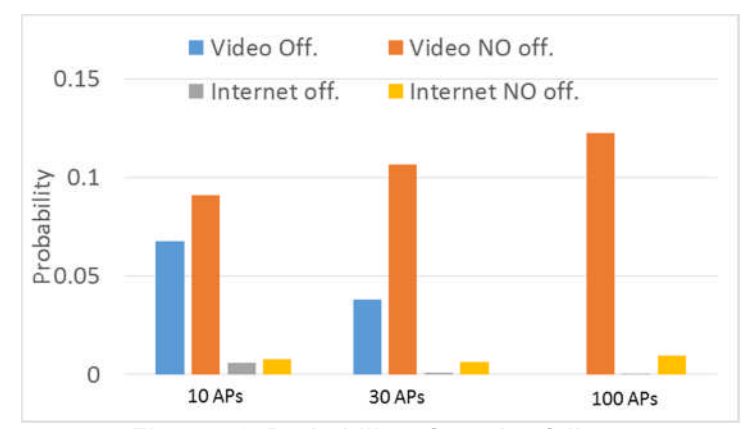


Figure 46: Probability of service failure.

The percentage of time that a particular service is connected to each technology is depicted in Figure 47. This metric is only taken for services that can be offloaded and is measured as the time that a service is connected to one of the technologies divided by the total time the service is active. In general, it is observed that, with low number of access points, services with longer duration spend more time connected to the LTE network.

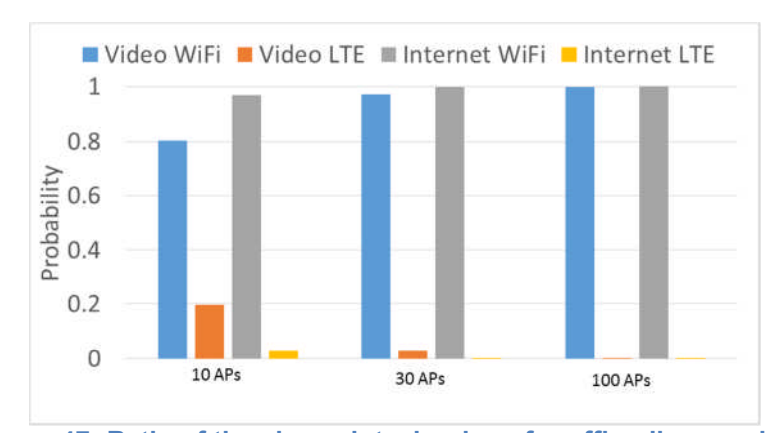


Figure 47: Ratio of time in each technology for offloading services.

Finally, Figure 48 illustrates the number of handovers, both vertical and horizontal, per unit time; again, it is only measured for those services that are allowed to use Wi-Fi. In general, the number of vertical handovers is negligible when compared to the horizontal ones, especially between two different access points. If we analyze these results together with the failure probability seen earlier, we can conclude that in most cases, the reason for dropping services is outage.



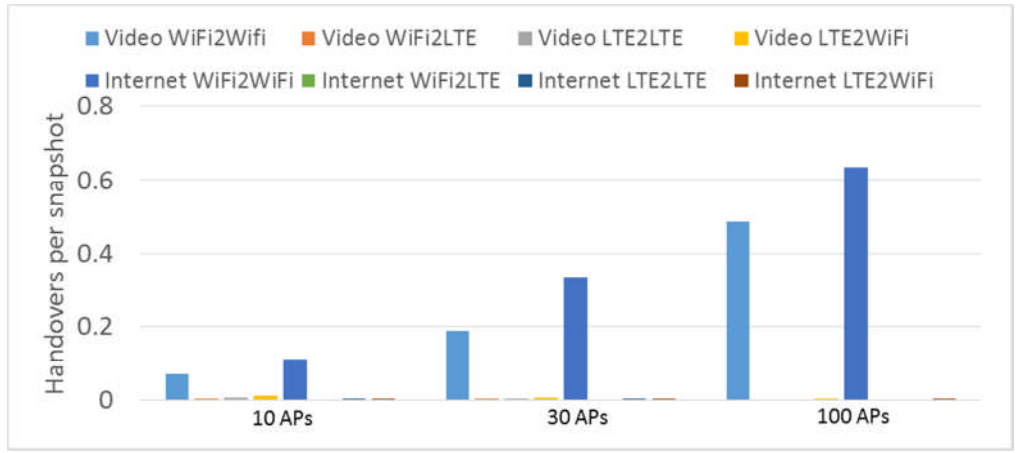


Figure 48 Number of handovers per snapshot vs. the number of access points deployed

5.2 Scheduled On/Off propagation in a wireless mesh network

The scheduled On/Off propagation technique particularly fits a managed WLAN scenario. The main idea is to be able to centrally schedule the switching off or on of one wireless radio of a Wi-Fi AP within a mesh network. The proposed technique, with its associated architecture and specific software development, offers a user-friendly way to schedule on/off periods of Wi-Fi activity for the APs of a mesh network, relying on a smart propagation of these events.

One of the main use case scenarios of this technique could be in a (small) work environment, where mesh-capable Dual Band Dual Concurrent (DBDC) APs are deployed in the meeting rooms. The 2.4 GHz Wi-Fi radio is used to provide service and connectivity inside the room, while the 5 GHz Wi-Fi radio is used for the mesh network in order to connect the APs to each other and eventually to the Wide Area Network (WAN)/Internet.

Assuming one DBDC AP serves one meeting room, when booking a room for a meeting, the time slot can be used as an "on" period of the radio providing the connectivity in the room (2.4GHz). If no meeting is planned, this radio can be in an "off" state. For managed WLAN environment, such procedure must be user friendly, without needing to access physically the AP in the meeting room. It must also be flexible, as booking rooms are often not definitive, with cancelling or changing time slots on the go.

This solution will most likely impact non-users in terms of EMF, which may lead to a small EI reduction. Adjusting the transmit power during the communication as proposed in [D4.3] would lead to higher EI reduction.

5.2.1 Evaluated solution

5.2.1.1 Wireless meshed network

Before presenting the solution itself, it is worth mentioning that the wireless mesh network functionality is based on a proprietary implementation different from what has been standardized in [IEEE]. Each AP being DBDC, the 5GHz radio is used for



the mesh communication. Within our wireless mesh network implementation, a master AP, called Gateway Controller (GWC), plays the role of the portal. It is connected to the WAN and is in charge of giving IP address to any station (STA) associated to the wireless mesh network. Any additional AP added to the mesh will be referenced as APx as shown in Figure 49 with three APs.

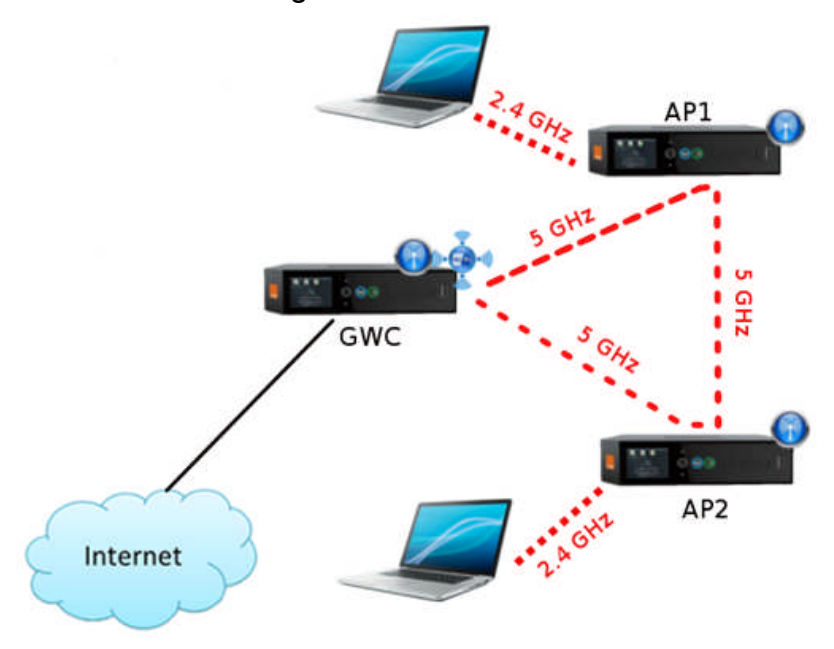


Figure 49: Wireless Mesh Architecture.

Without entering into too much detail, the main building blocks enabling our wireless mesh functionality within the DBDC APs are the following:

- Partial use of the Ad-Hoc feature defined in IEEE 802.11;
- Use of the Optimized Link-State Routing (OLSR) protocol as defined in [IETF1] for the route table construction and update;
- Use of the Dynamic Configuration of Ipv4 Link-Local Address [IETF2] for an automatic address allocation:
- Use of General Routing Encapsulation (GRE) [IETF3] and its extension [IETF4] for encapsulation within the mesh.

5.2.1.2 Calendar-based architecture

The LEXNET deliverable [D6.1] presented the DBDC AP characteristics and the architecture chosen to implement the scheduled on/off technique for a standalone case (no mesh network). The architecture was based on the use of a calendar server and the handling of calendar events, which are known for their footprint optimisation in terms of network load and CPU usage. We extended this architecture to the wireless mesh network as shown in Figure 50.



61

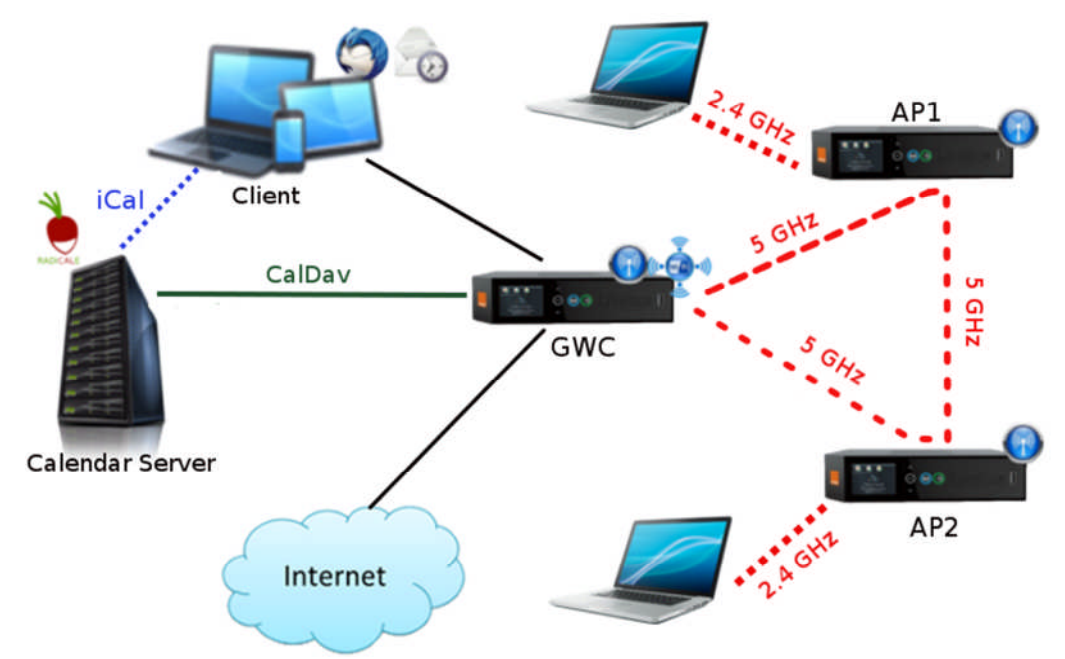


Figure 50: Calendar-based Architecture.

Radicale solution (http://radicale.org/) is used to provide the calendar server as it is a light weight and extremely portable solution to handle CalDAV [IETF5] protocol (a calendar extension of WebDAV [IETF6]).

5.2.1.3 Scheduled On/Off process

In the standalone case, the "lexnet" process running in the AP periodically checks the calendar events stored in the Calendar Server and parses the events introduced by a Client. The event duration represents the time where the 2.4 GHz Wi-Fi radio will be shut down.

The main role of the "lexnet" process is to:

- get events stored in the Calendar Server;
- set the Wi-Fi status accordingly to the events.

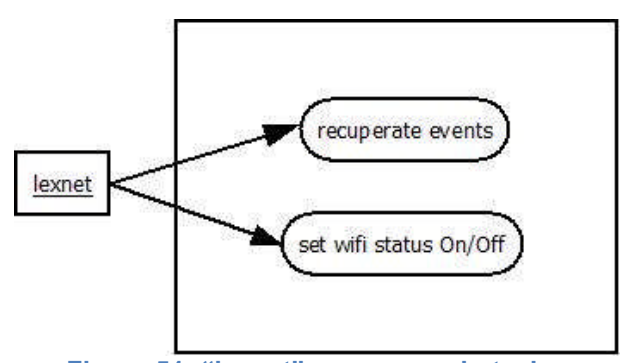


Figure 51: "lexnet" process main tasks.

In the wireless mesh network case, instead of all APs having a "lexnet" module polling the calendar server, we developed a propagation mechanism in which only the main AP (GWC) will poll the Calendar Server for any change in all the calendars (one per AP). If one modification is found for one AP, it will push a notification toward the target AP using the "Software Bus" we developed.

Version: V1.0



A detailed implementation of the "lexnet" process is given in Appendix A2.

5.2.1.4 Propagation through a "Software Bus"

We developed a solution to enable message exchange between threads, process and hosts using a single API, facilitating the software development.

Within different machines, several processes are running and scheduled by the machine operating system. Each process can be made of several threads, each thread running and scheduling different users or system tasks.

We developed a software solution allowing different tasks to exchange messages. For the tasks to communicate we need their processes to be part of a "software bus" and we introduce the following components. Each process contains a bus management module for communication. Each thread also has a bus management module which integrates a scheduler for scheduling the tasks. Finally, we add to each task a FIFO data structure. More details on the implementation of the "Software Bus" are given in Appendix A2.

5.2.2 Test setup

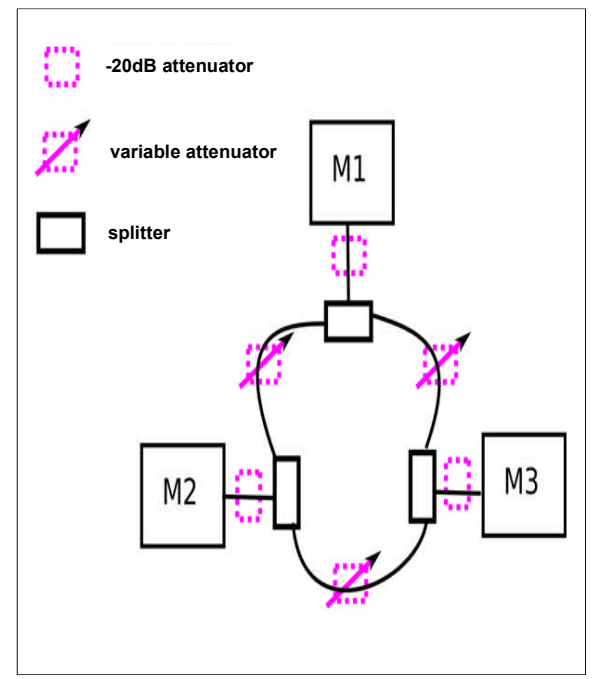
Before testing the scheduled on-off propagation mechanism, we validated the performance of our wireless mesh network solution. As a reminder from [D6.1] our DBDC APs are implementing IEEE 802.11n solutions for both the 2.4 GHz and 5 GHz ISM band.

5.2.2.1 Wireless mesh network performance

We set up the triangle configuration given in Figure 52, where the 5 GHz antenna connectors are wired to be able to reproduce our tests. We use 6 splitters, 6 variable attenuators, 6 fixed attenuators (-20dB), 12 SMA(F)-SMA(M) cables and 6 SMA/ULF cables.

Version: V1.0 62





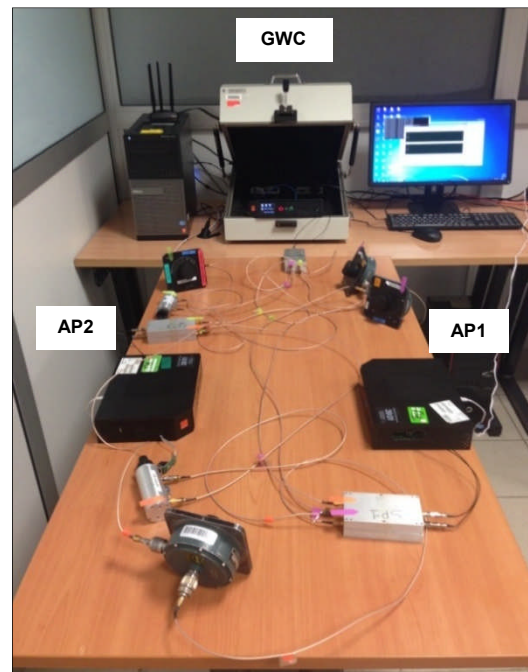








Figure 52: Wireless mesh network setup.

Different configurations were tested, where PCs were either connected to the 2.4GHz radio or to the Ethernet port of the AP to stress the 5GHz link, the 2.4GHz link or both by sending in one direction or in both directions high TCP traffic using IxChariot from Ixia [IXC].

For example when only one PC is connected to the 2.4GHz radio while the other is on the Ethernet, we stress the 2.4 GHz radio where we want a throughput of at least 65 Mbps at the application level. If both PCs are connected to APs through Ethernet cables, we stress the 5 GHz radio where we want a throughput of at least 110 Mbps at the application level. Figure 53 and Figure 54 show the results obtained through the two previous setups, respectively. More simulations results and test results are provided in Appendix A2.



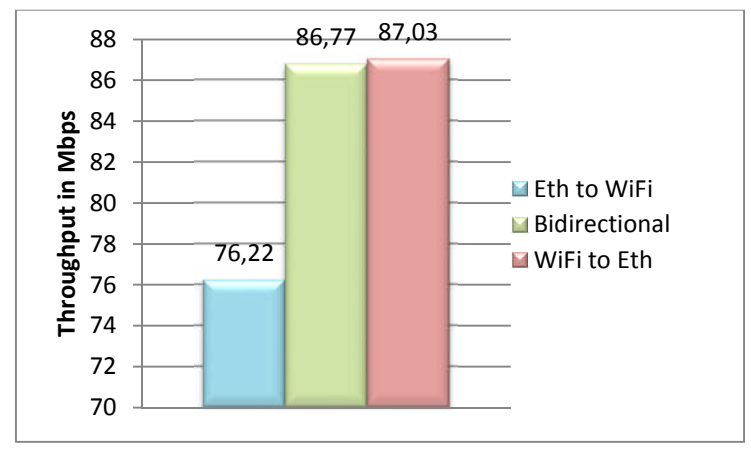


Figure 53: Wireless Mesh Network 2.4GHz stress.

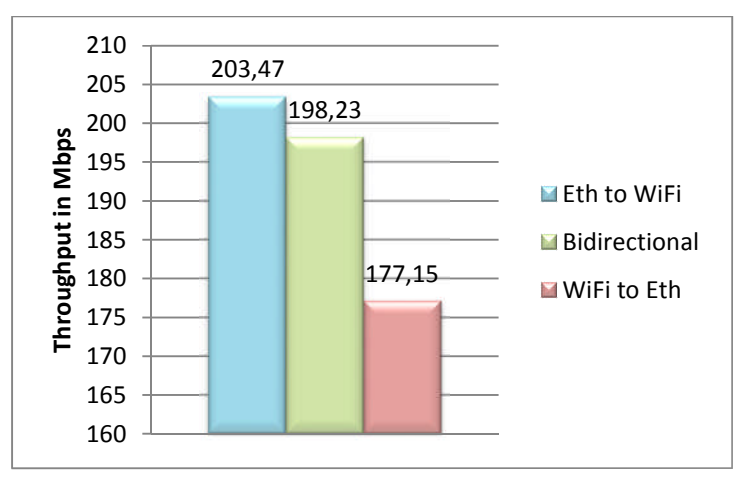


Figure 54: Wireless Mesh Network 5GHz stress.

The wireless mesh network performance being validated, we set up the test bed demonstrating the scheduled on/off solution.

5.2.2.2 Scheduled On/Off set-up

We set-up an over-the-air testbed made of the following equipment:

- One Linux PC: A host and a virtual machine (Qemu) are running on the same hardware.
 - The virtual machine is in charge of emulating the Operator network. This allows the master gateway GWC to set up its Point-to-Point Protocol (PPP) connection and get time synchronization through a Network Time Protocol (NTP) server (which will use the hosting PC clock as a time reference). The operator network emulator is reachable at the IP address 10.0.0.1. The virtual machine also runs the Radical calendar server which is accessible at the IP address 192.168.130.1. Note that the calendar server can be reached by the gateways despite being on another local network because a bridge has been setup on the Ethernet port toward the Qemu machine.
 - The host is running the client in charge of filling event to the data server. This is done through Mozilla Thunderbird in our case which supports the calDAV protocol through its lightning plugin. It has the IP address 192.168.130.10 and will forward any packet to the virtual



machine. Note that the host cannot be reached by the gateways as it is part of another local network (host and virtual machine).

- Three Gateways: The gateways are connected to each other through the 5 GHz Wi-Fi radio and broadcasts the "Lexnet" SSID on the 2.4GHz Wi-Fi radio. The master gateway (GWC) is connected to the Linux PC through an Ethernet link, while additional gateways are named "AP2" and "AP3". GWC receives the IP address 10.67.15.6 for its PPP connection. Any device connected using the LEXNET SSID network will receive an IP address in the form of 192.168.1.x. It will be able to ping the calendar server (192.168.130.1) but not the PC linux host (198.168.130.10). A bridge is setup within the Linux PC to redirect traffic to the Qemu (192.168.130.1), which hosts the calendar server.
- One monitoring PC: This PC captures Wi-Fi SSID presence (and their received power level) using InSSIDer software from metageek [INS].

Figure 55 summarizes the testbed setup while Figure 56 shows when it is deployed in one single meeting room (for convenience).

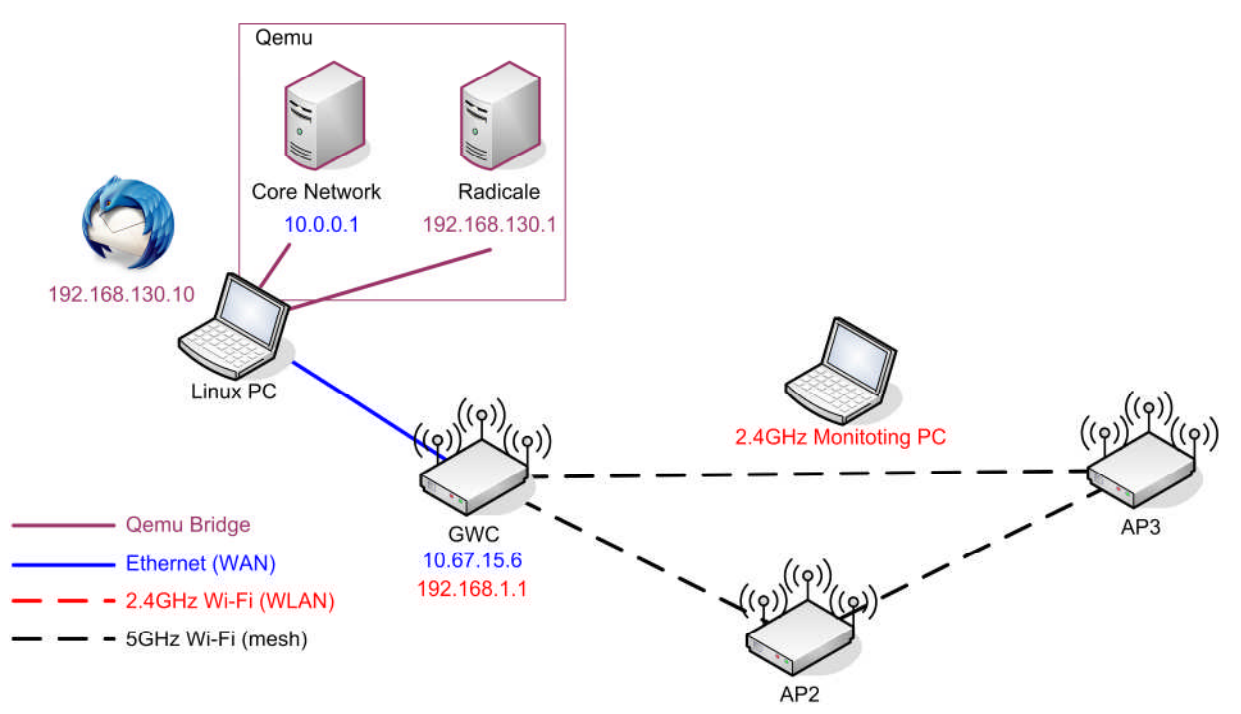


Figure 55: Testbed set-up principle.

Version: V1.0





Figure 56: Over the air testbed set-up.

The test is successful; it is reported with more details in Appendix A2.

5.2.3 Evaluation results

5.2.3.1 *Principle*

Any calDAV client having access to (and thus synchronized with) the three calendars can create an event in any of them. By default, the duration event indicates the time during which the Wi-Fi 2.4GHz radio will be switched off. It is assumed here that the Wi-Fi is always on. Note that the complementary behaviour is possible where the Wi-Fi 2.4GHz radios are off by default and an event indicates when the radio should be switched on.

When the three APs (GWC, AP2 and AP3) are running, we can see the three LEXNET networks operating using InSSIDer as shown in Figure 57.



Figure 57: (GWC-ON, AP2-ON, AP3-ON), probe close to GWC.

We set up through the calendar client three events, one for each gateway as shown in Figure 58. Each event lasts an hour and is separated by 5 minutes from the next one.



67

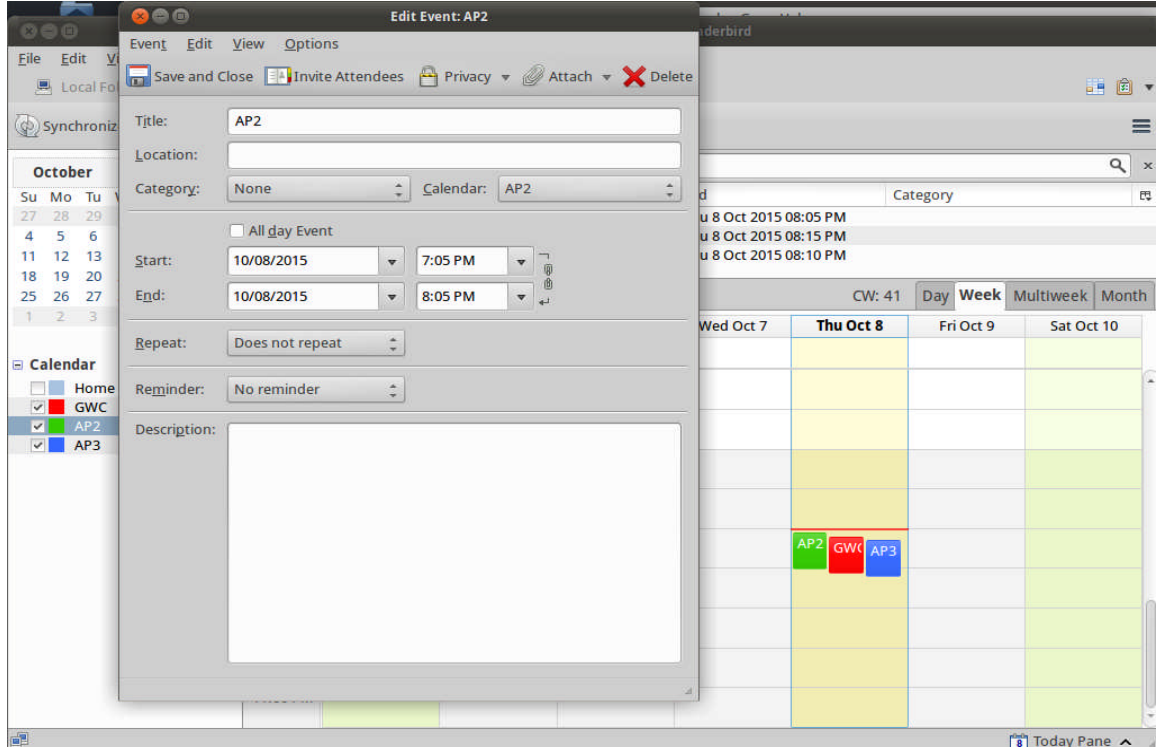


Figure 58: Event scheduling.

The first AP to switch off is AP2 in our planning. So we get the monitoring PC close to AP2 and we wait for the event to occur. Figure 59 shows the 2.4GHz networks operating just before the first event where the three APs are running and broadcast the LEXNET SSID.



Figure 59: (GWC-ON, AP2-ON, AP3-ON), probe close to AP2.

When the event related to AP2 occurs (at 7:05), AP2 switches off. This can be seen on Figure 60, with one network disappearing from the probe.

Version: V1.0



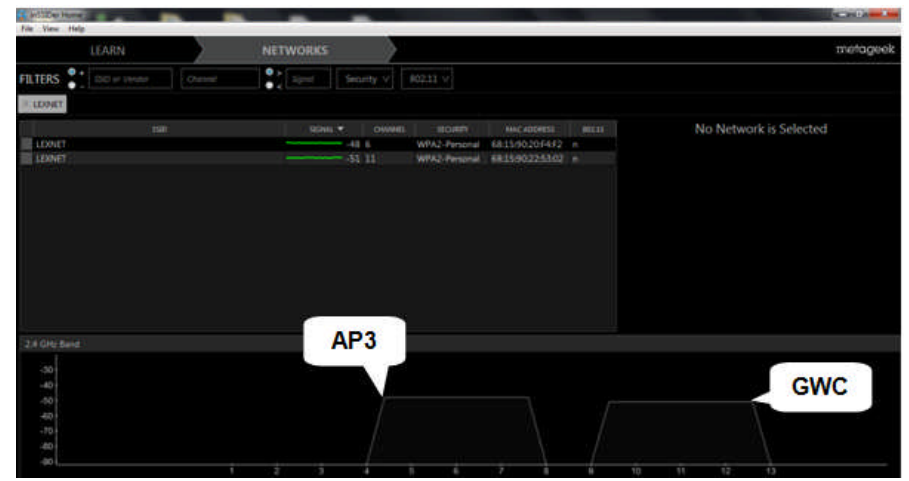


Figure 60: (GWC-ON, AP2-OFF, AP3-ON), probe close to AP2.

Five minutes later (7:10), it is time for GWC to switch off, leaving only AP3 on as shown in Figure 61.

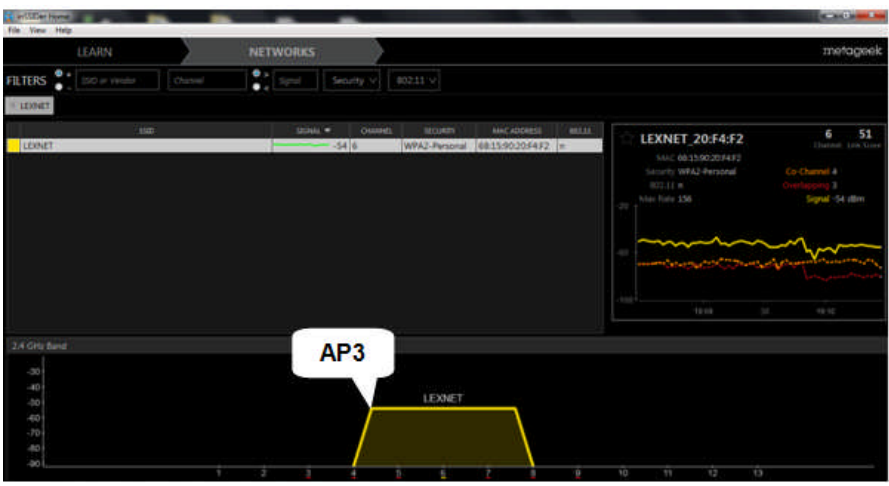


Figure 61: (GWC-OFF, AP2-OFF, AP3-ON), probe close to AP2.

We decide then to remove the event associated to GWC through the calendar client, leaving only AP2 event currently running and AP3 event to be run on the server. The result is that the LEXNET network handled by the GWC goes up again as shown in Figure 62.

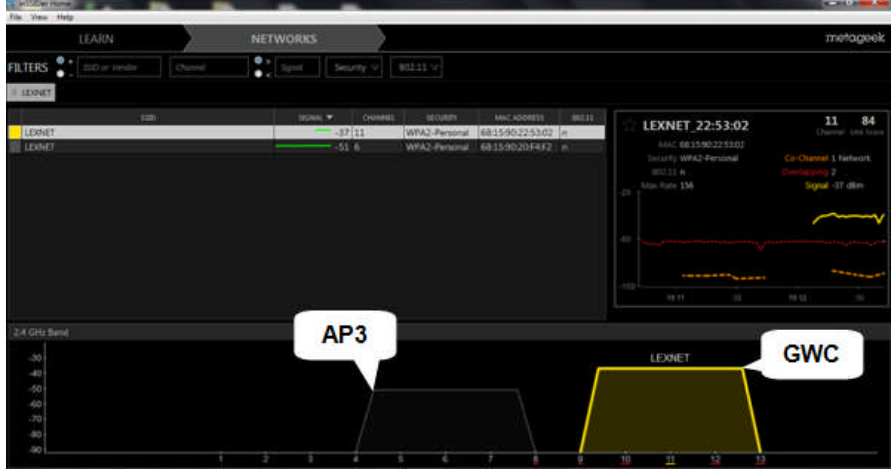


Figure 62: (GWC-ON, AP2-OFF, AP3-ON), probe close to GWC.



When the event associated to AP3 occurs (at 7:15) the only LEXNET network left is the one from GWC.



Figure 63: (GWC-ON, AP2-OFF, AP3-OFF), probe close to GWC.

As shown above, the scheduled on/off mechanism mainly targets places where no Wi-Fi connectivity is needed. Therefore, the EMF will be reduced for passive people (non-user), who are only being affected by "downlink" transmissions. For the EI as defined in LEXNET, considering only active users, the impact of our solution may be minimal.

5.2.3.2 Exposure Index evaluation

In order to evaluate more precisely the impact of this solution on the EI, we mimic our solution within the w-iLab.t testbed in the pseudo-shielded environment (see [D6.1], section 5.3). In this testbed, we have defined three rooms in which an AP is deployed (red circle). The blue circles represent a STA for which transmit and/or receive power will be collected. We only use some of the available nodes as either APs or STAs as shown in Figure 64.

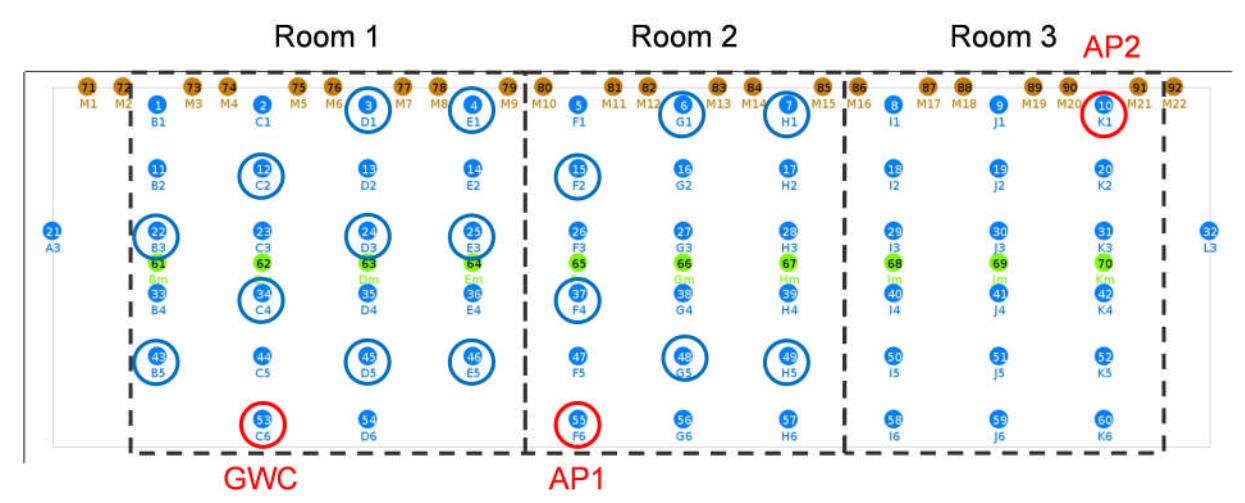


Figure 64: Rooms and nodes assignment.

In our setup, we assume that a meeting is being held in Room #2 with active Wi-Fi users (transmit and received power will be collected), while a training session is



70

ongoing in Room #1 with no active Wi-Fi users (only downlink power will be collected). We consider two air interface loads:

- **low air interface usage**: each STA of Room #2 transmits the equivalent of 1 minutes of uplink traffic (cumulated) and receives the equivalent of 4 minutes of downlink traffic (cumulated). This means that AP1 (node 55/F6) will transmit the equivalent of 24 minutes (+ beacon).
- high air interface usage: each STA of Room #2 transmits the equivalent of 1.5 minutes of uplink traffic and receives the equivalent of 6 minutes of downlink traffic, except one STA (node 49/H5) which will transmit the equivalent of 15 minutes (desktop sharing) and receives the equivalent of 2 minutes of traffic. AP1 (node 55/F6) will then transmit the equivalent of 32 minutes (+ beacon).

For each of the load, we assume that GWC and AP2 are either on (transmitting beacon only) or off which leads to a total of 4 different scenarios:

- Scenario 1: low air interface usage, all APs on.
- Scenario 2: low air interface usage, only AP2 on.
- Scenario 3: high air interface usage, all APs on.
- Scenario 4: high air interface usage, only AP2 on.

Scenario 1 and scenario 3 represent the baseline.

Table 24 summarizes duration chosen for the 4 scenarios. In each one, we assume a transmit power of 16 dBm and the following SAR values for an adult using a laptop:

- SAR DL = 0.0049 W/kg (for an incident power density of 1 W/m²)
- SAR UL = 0.0027 W/kg (for a transmit power of 1 W)

Remark that we have taken into account the downlink exposure from the APs, the uplink exposure of a person to the exposure of its own laptop, and the exposure of a person by the laptop of another person.

Nodes	Exposure	duration (s	sec)		
	S1	S2	S 3	S4	Presence body
C6 (=AP)	72	0	72	0	N
F6 (=AP)	1512	1512	1992	1992	N
G1	60	60	90	90	Υ
H1	60	60	90	90	Υ
F2	60	60	90	90	Υ
F4	60	60	90	90	Υ
G5	60	60	90	90	Υ
H5	60	60	900	900	Υ
K1 (=AP)	72	0	72	0	N

Table 24: Scenario parameters.

When we compute the EI over all users present for the 4 scenarios, we get the values given in Table 25.



71

Table 25: El (in W/kg) evaluation.

DL Exposure in	dex for user at o	corresponding n	ode (see Table	24)
S1	S2	S3	S4	,
1.705E-11	0.000E+00	1.705E-11	0.000E+00	
2.312E-10	2.312E-10	3.046E-10	3.046E-10	
4.575E-12	4.575E-12	6.862E-12	6.862E-12	
2.867E-12	2.867E-12	4.301E-12	4.301E-12	
4.206E-12	4.206E-12	6.308E-12	6.308E-12	
2.258E-12	2.258E-12	3.387E-12	3.387E-12	
3.623E-12	3.623E-12	5.435E-12	5.435E-12	
4.802E-12	4.802E-12	7.202E-11	7.202E-11	
1.414E-13	0.000E+00	1.414E-13	0.000E+00	
				Total DL EI
2.707E-10	2.535E-10	4.201E-10	4.029E-10	(W/kg)
UL Exposure Inc	dex for user at o	corresponding n	ode	
C4				
S1	S2	S3	S4	
51 1.7915E-06	S2 1.7915E-06	S3 2.6872E-06		
_	-			
1.7915E-06	1.7915E-06	2.6872E-06	2.6872E-06	
1.7915E-06 1.7915E-06	1.7915E-06 1.7915E-06	2.6872E-06 2.6872E-06	2.6872E-06 2.6872E-06	
1.7915E-06 1.7915E-06 1.7915E-06	1.7915E-06 1.7915E-06 1.7915E-06	2.6872E-06 2.6872E-06 2.6872E-06	2.6872E-06 2.6872E-06 2.6872E-06	
1.7915E-06 1.7915E-06 1.7915E-06 1.7915E-06	1.7915E-06 1.7915E-06 1.7915E-06 1.7915E-06	2.6872E-06 2.6872E-06 2.6872E-06 2.6872E-06	2.6872E-06 2.6872E-06 2.6872E-06 2.6872E-06	
1.7915E-06 1.7915E-06 1.7915E-06 1.7915E-06 1.7915E-06 1.7915E-06	1.7915E-06 1.7915E-06 1.7915E-06 1.7915E-06 1.7915E-06 1.7915E-06	2.6872E-06 2.6872E-06 2.6872E-06 2.6872E-06 2.6872E-06 2.6872E-05	2.6872E-06 2.6872E-06 2.6872E-06 2.6872E-06 2.6872E-06	Total UL EI
1.7915E-06 1.7915E-06 1.7915E-06 1.7915E-06 1.7915E-06	1.7915E-06 1.7915E-06 1.7915E-06 1.7915E-06 1.7915E-06	2.6872E-06 2.6872E-06 2.6872E-06 2.6872E-06 2.6872E-06	2.6872E-06 2.6872E-06 2.6872E-06 2.6872E-06 2.6872E-06	Total UL EI (W/kg)
1.7915E-06 1.7915E-06 1.7915E-06 1.7915E-06 1.7915E-06 1.7915E-06	1.7915E-06 1.7915E-06 1.7915E-06 1.7915E-06 1.7915E-06 1.7915E-06	2.6872E-06 2.6872E-06 2.6872E-06 2.6872E-06 2.6872E-06 2.6872E-05	2.6872E-06 2.6872E-06 2.6872E-06 2.6872E-06 2.6872E-06 2.6872E-05	
1.7915E-06 1.7915E-06 1.7915E-06 1.7915E-06 1.7915E-06 1.7915E-06	1.7915E-06 1.7915E-06 1.7915E-06 1.7915E-06 1.7915E-06 1.7915E-06	2.6872E-06 2.6872E-06 2.6872E-06 2.6872E-06 2.6872E-06 2.6872E-05	2.6872E-06 2.6872E-06 2.6872E-06 2.6872E-06 2.6872E-06 2.6872E-05	

The DL exposure is reduced when only AP2 is on (scenario 2 and 4) compared to the baseline when all APs are on (scenario 1 and 3, respectively), while UL exposure is not affected. In the low air interface usage scenarios (1 and 2), the DL exposure is reduced by a 6.35% factor, while in the high air interface usage scenarios (3 and 4), the DL exposure is reduced by a 4.09% factor.

However, the global EI computations show almost no reduction at all, since EI is highly dominated by the uplink and our approach tends to reduce the downlink EMF.



6 CONCLUSION AND RECOMMENDATIONS

Part-B of the LEXNET deliverable D6.2 was devoted to the demonstration and evaluation of some promising low EMF techniques, either relying on new topologies, new components or new management techniques. This work was carried out based on preliminary evaluations and specifications coming from [D4.3] and [5.2], and via the implementation into real wireless networks, laboratory testbeds and HetNet simulation platforms.

Network local improvement

It was demonstrated that a local network densification (i.e. by adding a macro or micro base station) with the objective to improve the service in a poor coverage area, or to offer higher capacity in a hotspot, creates a local increase in DL exposure but this may be positively balanced by the UL exposure reduction.

Small-cells

In order to raise the coming challenge of sustaining the demanding throughput in dense or ultra-dense scenarios without increasing the EMF level, a novel small-cell component architecture (compact and directive antenna & low noise RF front-end) has been developed and demonstrated in LEXNET. The combination of both techniques takes benefit from two independent concepts at the UL: First the spatial filtering (interference mitigation via a SINR improvement) for the antenna; and secondly the sensitivity enhancement (NF reduction) for the receiver. From the antenna view point, the receiver compensates the 0.5 dB losses inside the antenna structure. From the receiver view point, the spatial filtering reduces the impact of blockers and eventual spurious signals. A system-level simulation has validated the overall benefit at both UL and DL on a large-scale SCBS deployment scenario, showing 20% EMF reduction while increasing the mean SINR (+6 dB). The beamforming with low antenna complexity and compact form factor appears as a promising solution in this specific context but need to increase its technological maturity before it can be integrated into commercial hardware equipment.

The impact of a wireless small-cell backhaul, in particular for NLOS situations, was also quantified in terms of EMF exposure and proved to represent about 10% of the overall DL small-cell contribution.

Beamforming antennas

The main benefit of the antenna beamforming method is that it achieved comparable SNR benefit from using multiple antennas with the new hybrid beamforming proposed in LEXNET, to that of conventional diversity gain that is achievable from multiple antennas applied together with the modulation and coding schemes used in 4G.

The technology would be applicable to tablet devices and laptop computers as it would reduce the exposure towards the user assuming the device is aware of the user direction. Such devices require omni-directionality on their antenna elements due to their changing orientation and position, hence it would be necessary to apply a suitable beamforming adaptively based on the direction of the user. It is possible to ascertain or estimate the direction of the user using other appropriate technologies such as image recognition with optical cameras typically existent in such devices.

Version: V1.0



Wi-Fi offloading

Enabling Wi-Fi offloading will mainly be driven by the need to avoid congestion in the core network or access network. We demonstrated in two complementary HetNet simulations that such offloading is beneficial for both the user QoS and the DL exposure, which is divided by 2.5 in our scenario (the reduction in the macro-cell traffic load has a larger impact than the distributed increase in Wi-Fi duty cycles). Of course, the density of Wi-Fi access points compatible with such offloading, the fixed backhaul performance, and the Wi-Fi offloading large-scale policy, do all influence the EMF reduction. We evaluated the impact of some of those parameters through a parametric study.

On/off

The main innovation in the scheduled on/off propagation technique is the "software bus" solution we developed. This solution allows a propagation of any kind of messages in a simple way from our middleware. In the LEXNET project, we used the "on/off message" as a visible way to validate and demonstrate our software implementation but its impact on EMF after evaluation is very limited. Instead of sending on/order message through the software bus, we can think about messages affecting for instance the transmit power during communication as we have done in [D4.3]. Indeed an evaluation of the EI (for active users) through system-level simulations shows in [D4.3] that significant EI reduction can be achieved while maintaining quality of service.

As a first main output of this validation work, it appears that the experimentation generally confirmed the expected low EMF performance.

Comparing the different evaluated techniques is not a straightforward exercise (those technologies cannot all be applied at the same scale or do not have similar technical maturity) however we can stress some benefits and make recommendations:

- 2G is today the access technology that generates the highest exposure, as measured by EI; this mainly comes from the strong mean UL transmit powers during the voice calls.
 - Migrating the voice calls from 2G to a more recent access technology is obviously the most beneficial evolution for EMF.
- Small-cell densification leads to strong El reduction, mainly on the UL contribution.
 - However this strong reduction is true at constant traffic. And small-cells will obviously be deployed to offer higher capacity and then enable higher mobile traffic. The conclusion must then be reformulated as follows: small-cells are to be preferred to macro-cells (in terms of QoS, power consumption but also EMF exposure) to answer the expected mobile traffic rise.
- Implementing beamforming or beamsteering systems at the small-cells can reduce the DL exposure in a very significant way.
- The reduction of the UL exposure by high-efficiency low noise amplifiers at the base station is a very interesting low EMF solution that converts a reduction of the noise figure into a reduction of exposure (when noise is the limiting factor). This solution is of interest whatever the access technology and deployment are.



- Wi-Fi offloading leads to a significant DL exposure reduction, while its impact on UL is uncertain.
- Finally, and contrary to usual perception, a local network densification done from careful planning does not necessarily degrade the population exposure, even with the introduction of a new macro-cell.

For a summary on the EI reduction factors for each evaluated low EMF technology, go to section 2.

Version: V1.0 74

Dissemination level: PU



7 REFERENCES

- [3GPP] 3GPP TSG RAN, TR 36.872, Small cell enhancements for E-UTRA and E-UTRAN-Physical layer aspects (Release 12), V12.1.0, Dec. 2013.
- [CHI1] K.-C. Chim, R.D. Murch, "Investigating the effect of smart antenna on SAR", IEEE International Symposium on Antennas and Propagation, pp.432-435 vol.1, 2002.
- [CHI2] K-C.Chim, K.C.L. Chan, R.D. Murch, "Investigating the impact of smart antennas on SAR", *IEEE Transactions on Antennas and Propagation*, vol. 52, no. 5, May 2004.
- [COR] Y. Corre, J. Stéphan and Y. Lostanlen, "Indoor-to-outdoor path-loss models for Femtocell predictions", 22nd IEEE PIMRC, Toronto, 2011.
- [D2.8] LEXNET Deliverable D2.8: *Global wireless exposure metric definition*, 2015.
- [D4.2] LEXNET Deliverable D4.2: Performance evaluation of low exposure index solutions for components and transmission techniques, 2014.
- [D4.3] LEXNET Deliverable D4.3: Final validation and recommendations for smart low exposure index radio techniques, 2015.
- [D5.1] LEXNET Deliverable D5.1: Smart Low EMF architectures: novel technologies overview, 2014.
- [D5.2] LEXNET Deliverable D5.2: Smart Low EMF architectures: results and recommendations, 2015.
- [D6.1] LEXNET deliverable D6.1: Validation platform framework and initial assessment, 2014.
- [D6.2-A] LEXNET deliverable D6.2: Report on validation, Part A, 2015.
- All LEXNET deliverables are available at http://www.lexnet.fr/scientificoutputs/ publicdeliverables.html.
- [HOC1] B.M. Hochwald, D.J. Love, S. Yan, J. Jin, "SAR codes", Information Theory and Applications Workshop (ITA), 2013.
- [HOC2] B.M. Hochwald, D.J. Love, S. Yan, P. Fay, J-M Jin, "Incorporating specific absorption rate constraints into wireless signal design", *IEEE Communications Magazine*, vol.52, no.9, pp.126-133, 2014.
- [IEEE] IEEE 802.11s, "Specifications Amendment 10: Mesh Networking", 2011.
- [IETF1] RFC 3626, Optimized Link State Routing Protocol (OLSR), 2003.
- [IETF2] RFC 3927, Dynamic Configuration of IPv4 Link-Local Addresses, 2005.
- [IETF3] RFC 2784, Generic Routing Encapsulation (GRE), 2000.
- [IETF4] RFC 2890, Key and Sequence Number Extensions to GRE, 2000.
- [IETF5] RFC 4791, Calendaring Extensions to WebDAV (CalDAV), 2007.
- [IETF6] RFC 4918, HTTP Extensions for Web Distributed Authoring and Versioning (WebDAV), 2007.
- [IXC] IxChariot, available online at http://www.ixiacom.com/products/ixchariot



- [KHA] M.R.R. Khan, V.Tuzlukov, "Null-steering beamforming for cancellation of Co-channel interference in CDMA wireless communication system", *Proc. of 4th International Conference on Signal Processing and Communication Systems (ICSPCS)*, 2010.
- [LEN1] S. Leng, W. Ser, C.C. Ko, "A simple constrained based adaptive null steering algorithm", *Proc. of 16th European Signal Processing Conference*, 2008.
- [LEN2] S. Leng, W. Ser, "Adaptive null steering beamformer implementation for flexible broad null control", *Elsevier Signal Processing*, vol. 91, pp. 1229–1239, 2011.
- [MAN] Information available online at http://mangocomm.com.
- [QAM] R.A. Qamar, N.M. Khan, "Null steering, a comparative analysis", *Proc. of* 13th IEEE International Multitopic Conference (INMIC), 2009.
- [R&S] Rohde&Schwarz, *LTE transmission modes and beamforming*, White paper, 2015, available online at https://www.rohde-schwarz.com/en/applications/lte-transmission-modes-and-beamforming-application-note-56280-15744.html.
- [SIR] Information on S_Backhaul by SIRADEL available online at http://www.siradel.com/wireless-3d-design/software/s backhaul/.
- [WAN] J. Wannstrom, *Heterogeneous networks in LTE*, available online at http://www.3gpp.org/technologies/keywords-acronyms/1576-hetnet.

Document ID: D6.2: Report on validation FP7 Contract n°318273



APPENDIX A1: INTERNAL REVIEW

		Reviewer 1: Nadège Varsier		Reviewer 2: Ramon Agüero			
		Answer	Comments	Type*	Answer	Comments	Type*
1.	1. Is the deliverable in accordance with						
(i)	the Description of Work?	⊠ Yes □ No		□ M □ m □ a	⊠ Yes □ No		□ M □ m □ a
(ii)	the international State of the Art?	⊠ Yes □ No		□ M □ m □ a	⊠ Yes □ No		□ M □ m □ a
2. Is the quality of the deliverable in a status							
(i)	that allows to send it to EC?	⊠ Yes □ No		□ M □ m □ a	⊠ Yes □ No		□ M □ m □ a
(ii)	that needs improvement of the writing by the editor of the deliverable?	⊠ Yes □ No	See my comments	□ M □ m □ a	⊠ Yes □ No	Comments were made in the deliverable to be considered before submitting to the EC	□ M ⊠ m □ a
(iii)	that needs further work by the partners responsible for the deliverable?	⊠ Yes □ No	See my comments and recommendations	□ M □ m □ a	☐ Yes ⊠ No	Most of my comments were editorial and related to presentation; there was anything requiring additional work	☐ M ⊠ m ☐ a

^{*} Type of comments: M = Major comment; m = minor comment; a = advice



APPENDIX A2: SCHEDULED ON/OFF PROPAGATION

Appendix A2 gives additional detailed information on the scheduled on/off propagation scenario presented in section 5.2.

- 1. Description of the "lexnet" process.
- 2. Description of the innovative "software bus".
- 3. Details on the on/off propagation validation.
- 4. Additional evaluation results.

1. Scheduled On/Off module description: the "lexnet" process

For the "lexnet" process to operate, we introduced many new modules as highlighted in red in Figure 65.

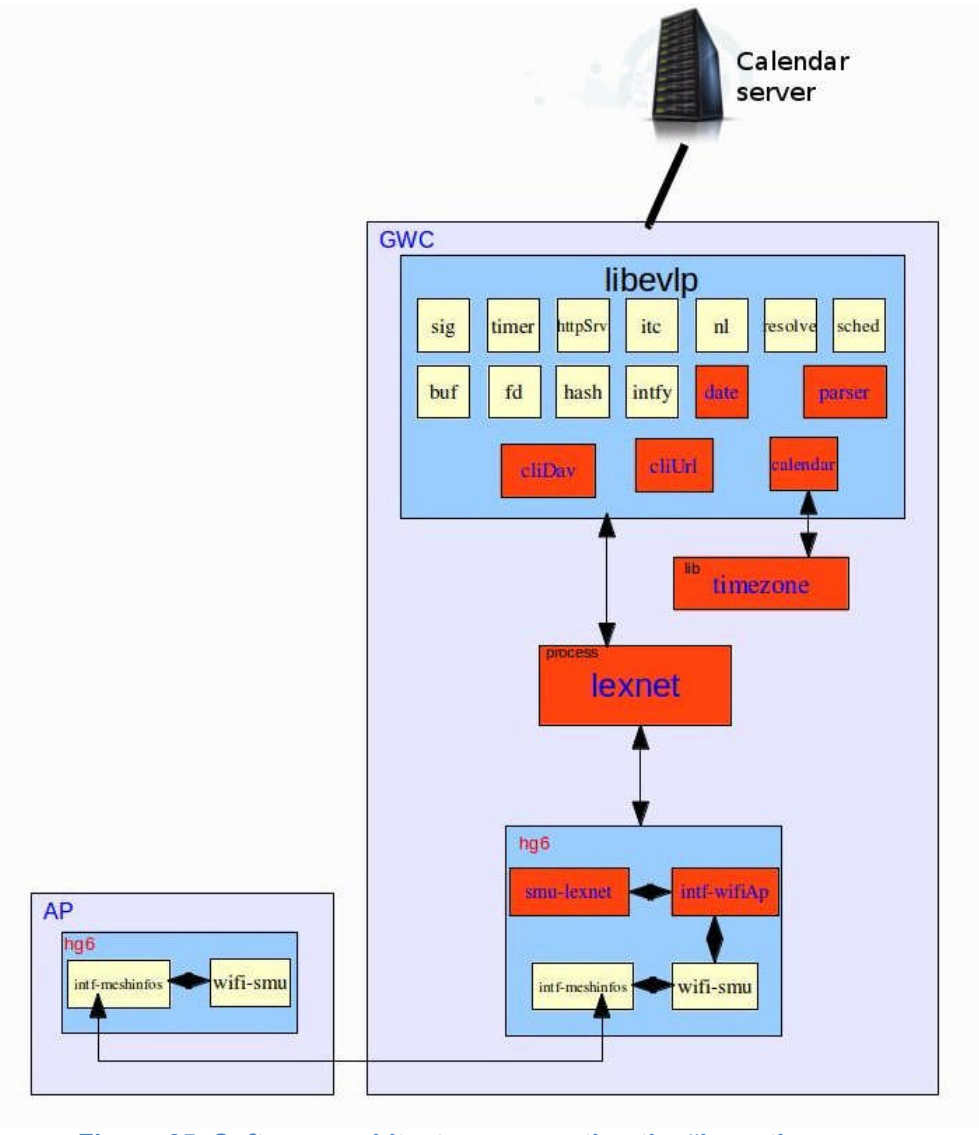


Figure 65: Software architecture supporting the "lexnet' process.

The role of each module is as follows:

- **lexnet**: The process responsible of getting the events and setting the status of the Wi-Fi based on the starting and ending dates.
- cliUrl: A library responsible of managing the webDay requests.



- parser: A library responsible of parsing the webDav responses.
- **cliDav**: A library which uses **cliUrl** to make the requests and receives the webDav responses from parser module.
- calendar: A library that receives the events from cliDav and parses them using iCal format.
- date: A context needed by the module calendar to make the events calls at the right time.
- **timezone**: A library to interpret correctly the time zone of the events.
- **Intf-Wi-FiAp**: The interface responsible on setting the state of the 2.4 GHz Wi-Fi radio.
- lexnet-smu: The interface which communicates with intf-wifAp.
- intf-meshInfos: The interface which facilitates the communication between gateways on a mesh network (which will be later explained as it is used for the propagation).

For the two main roles of the "lexnet" process, the following message sequence charts are followed:

- To get an event, the following blocks are involved as shown in Figure 66:
 - 1. lexnet process executes cliDav.
 - 2. **cliDav** executes **cliUrl** by specifying the URL of the CALDAV server.
 - 3. **cliURL** sends a CALDAV request to the calendar server.
 - 4. The server sends the CALDAV response to parser.
 - 5. parser parses the CALDAV responses using libexpat.
 - 6. parser sends the parsed response to cliDav.
 - 7. cliDav sends the responses to calendar.
 - 8. **calendar** parses the iCal events using the library timezone and stores them.

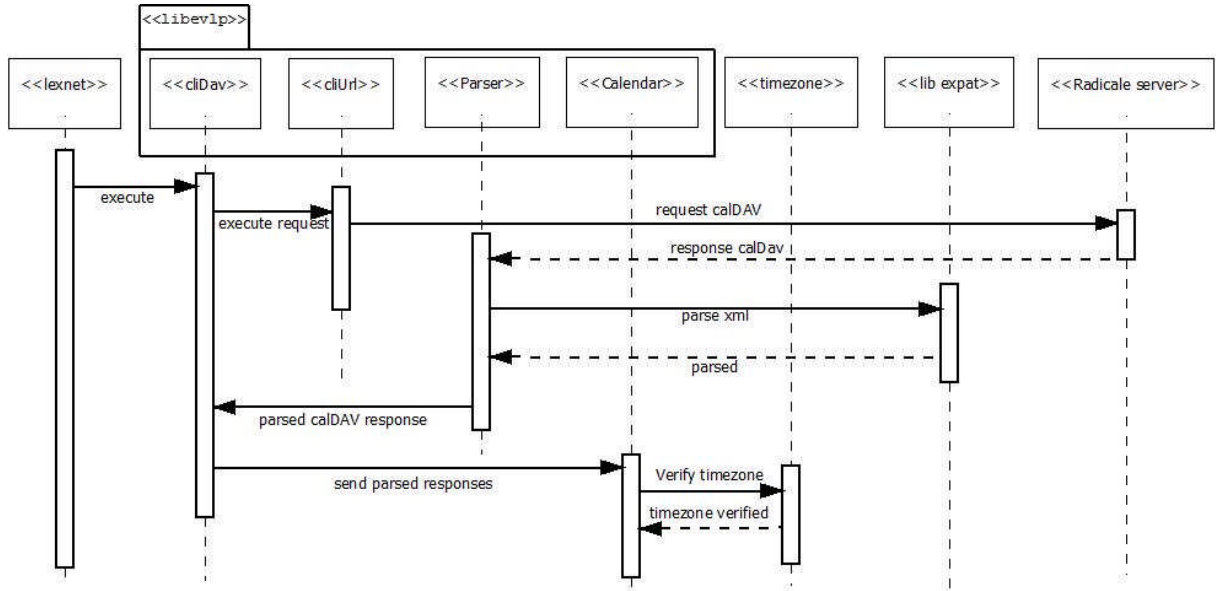


Figure 66: Getting an event from the Calendar Server (Radicale).

- To set the Wi-Fi status, the following blocks are involved as shown in Figure 67:
 - 1. **calendar** verifies the date of the events using the library **date**.



- 2. When the date is matched, **calendar** calls the iCal event.
- 3. **lexnet** sets the Wi-Fi status by sending a request to **intf-Wi-FiAp**.

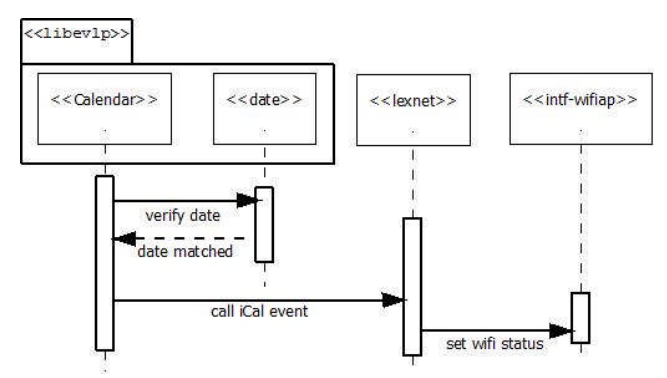


Figure 67: Setting the Wi-Fi Status.

In the wireless mesh network case, instead of all APs having a "lexnet" module polling the calendar server, we developed a propagation mechanism in which only the main AP (GWC) will poll the Calendar Server for any change in all the calendars (one per AP). If one modification is found for one AP, it will push a notification toward the target AP using the "Software Bus" we developed through the **intf-meshInfos** interface.

2. "Software Bus" Description

Within different machines, several processes are running and scheduled by the machine operating system. Each process can be made of several threads, each thread running and scheduling different users or system tasks.

For the different tasks to communicate (exchange message) we need their processes to be part of a "software bus" and we introduce the following components. Each process contains a bus management module for communication. Each thread also has a bus management module which integrates a scheduler for scheduling the tasks. Finally, we add to each task a FIFO data structure.

Afore any message exchange between tasks is possible, an initialization step is performed where one process is designated as master of the software bus while the others are all slaves.

Before a source task transmits a message to a destination task, the bus management module of the thread owning the source task will check if it also owns the destination task. If this is the case, then the message will be posted on the FIFO data structure of the destination task, waiting for scheduling and processing.

Otherwise the bus management module of the thread owning the source task asks the bus management module of the master process to search for the destination task:

If the bus management module of the master process determines that the
destination task is handled by a thread of the master process, then it sets up a
remote relay task within this thread and advertises the bus management
module of the thread owning the source task that a path has been found
(through the remote relay task). Otherwise, the bus management module of



the master process broadcasts to the other bus management modules of the slave processes a message seeking the destination task.

• If the bus management module of a slave process determines that the destination task is handled by a thread of its slave process, then it sets up a remote relay task within this thread and advertises the bus management module of the master process that a path has been found (through the remote relay task). The bus management module of the master process forwards this information to the bus management module of the thread owning the source task.

Once the bus management module of the thread owning the source task knows that the destination task has been found, it creates a relay task within the thread owning the source task to communicate with the remote relay task running in the thread owning the destination task. Through this relay link, the message will be posted on the FIFO data structure of the destination task, waiting for scheduling and processing.

As shown in Figure 68, software buses can be interconnected with each other and the unicity of the users will be preserved through the pair made of the bus name and the user (task) name. As long as the buses and the user names are known, everything is handled internally as previously described for a message to reach its destination.

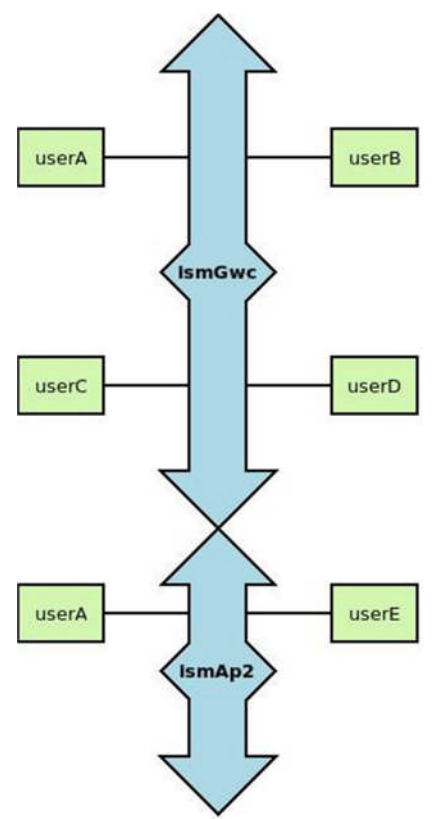


Figure 68: Software bus principle.

Version: V1.0



The messages are exchanged through a client/server model using the FIFO data structure, where two types of message can be sent and placed in the queue of the user waiting to be processed.

• **Command**: One user (here B) plays the client and sends a command to another user (here A) which plays the role of the server. The command can request or not an immediate response.

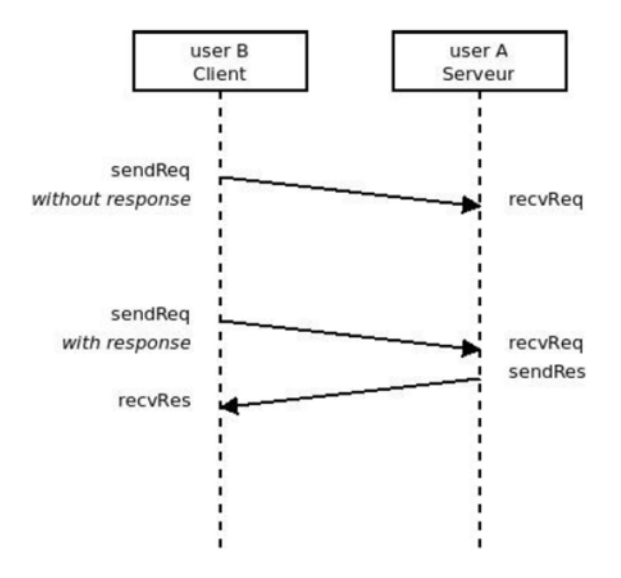


Figure 69: "Command" message.

 Notification: One user (here A) plays the server and sends a notification to other users (here B and C) which play the role of the clients. The notification can request or not an immediate response.

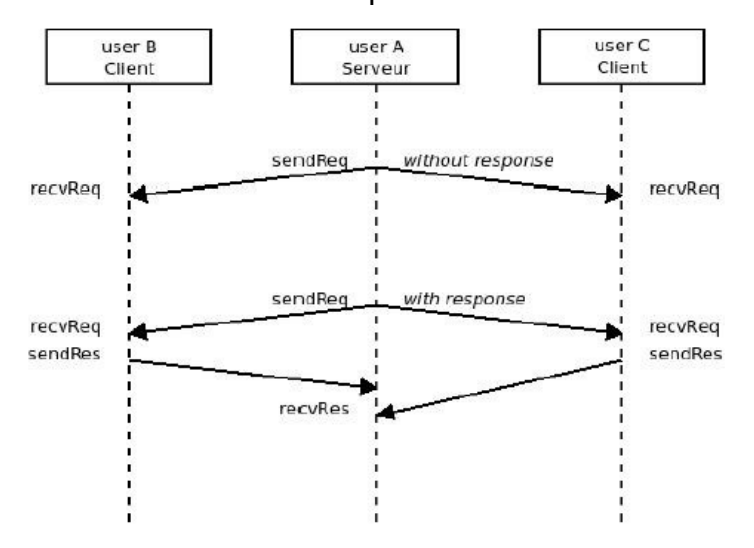


Figure 70: "Notification" message.

In our solution, the notification messages are used by the GWC to send to the APs the events through this "software bus" to trigger a change in their 2.4 GHz Wi-Fi radio.

Version: V1.0



3. Test on the on/off scheduling

The on/off scheduling is validated from the test setup described in section 5.2.2.2. Details are given below.

The calendar server is launched on the virtual machine using the following command: ~# ./radicale.py -D

The calendar server can be reached on the IP address 192.168.130.1 and will listen on the port 5323 by default. To check that this server is reachable, opening a browser and entering the web address http://192.168.130.1:5232 should return a page with the message "Radicale works!".

The calendar client (Mozilla Thunderbird) is launched on the Linux PC. It is configured such that it will interact with three different calendars on the network hosted by the calendar server (one per gateway). If those calendars are not present, Radicale will create them.

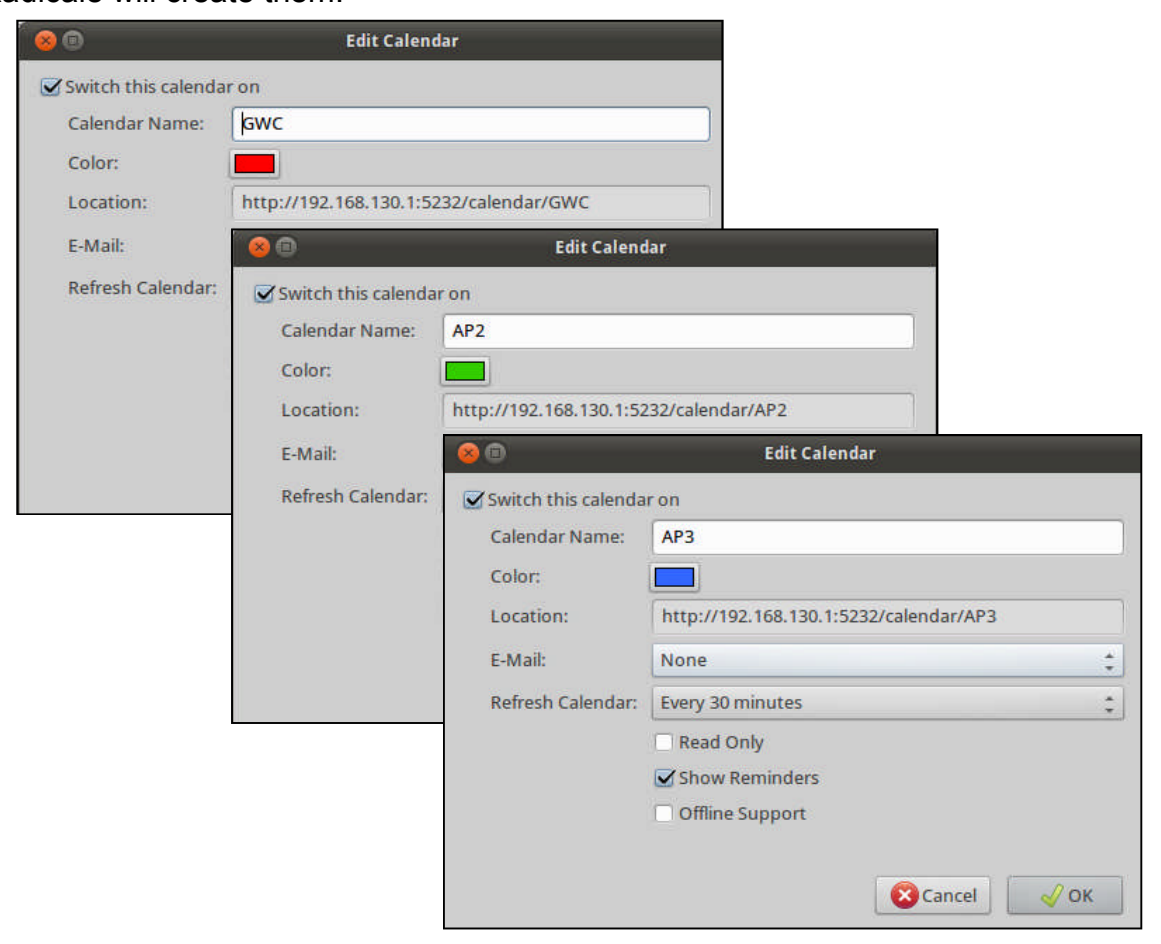


Figure 71: Mozilla Thunderbird calendar configuration.

Finally, the "lexnet" module is launched from the master gateway (GWC) using the calendar address and its listening port as follows in our example:

~#lexnet http://192.168.130.1:5232

Once running, the GWC (10.67.15.1) periodically requests any modification on any of the three calendars to the calendar server (192.168.130.1) through the PROPFIND



method in the same way as the one described in described in [D6.1]. The following is an output example produced by the Radicale server when a request is received on its port 5232 (see part bolded in green).

PROPFIND request at /calendar/GWC/ received

Request headers:

{'HTTP_HOST': '192.168.130.1', 'REMOTE_ADDR': '10.67.15.1', 'REQUEST_METHOD': 'PROPFIND',

'SERVER_PORT': '5232',

Sanitized path: /calendar/GWC/}

PROPFIND request at /calendar/AP2/ received

Request headers:

{'HTTP_HOST': '192.168.130.1', 'REMOTE_ADDR': '10.67.15.1', 'REQUEST_METHOD': 'PROPFIND',

'SERVER_PORT': '5232', Sanitized path: /calendar/AP2/}

PROPFIND request at /calendar/AP3/ received

Request headers:

{'HTTP_HOST': '192.168.130.1', 'REMOTE_ADDR': '10.67.15.1', 'REQUEST_METHOD': 'PROPFIND',

'SERVER_PORT': '5232',

Sanitized path: /calendar/AP3/}

4. Additional Wireless Mesh Network Performance

This section describes some tests on the mesh performance, in addition to the results presented in section 5.2.2.1. Two connected clients can communicate whatever their positions are in the mesh network and whatever their local connection technology is: 2.4GHz Wi-Fi (WLAN) or Ethernet (LAN). Figure 72 reminds the Wireless mesh network structure.

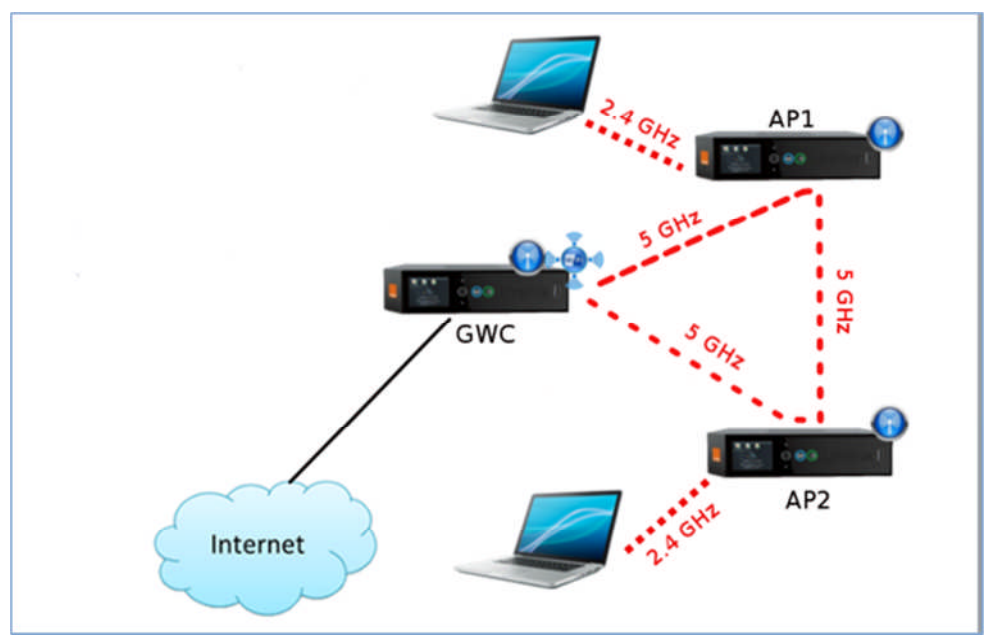


Figure 72: Wireless Mesh Network setup.



The following tests have been performed to assess the data traffic performance.

Table 26: LAN-LAN traffic.

Steps	Expected results	Result	Throughput
1- Build a three Livebox Mesh network (GWC, AP1,AP2) with a star topology. ==> GWC then AP1 and AP2.	1- Mesh network is operational		
2- Connect with Ethernet PCLAN0 on GWC and PCLAN2 on AP2. Ping from one to other.	2- Ping successful.		
3- Start a bidirectional TCP High_Throughput Chariot traffic between PCLAN0 and PCLAN2 for 2 minutes	3- The bidirectional traffic is launched correctly.	Passed	166.03 Mbps
4- Connect with Ethernet PCLAN0 on GWC and PCLAN1 on AP1. Ping from one to other.	4- Ping successful.		
5- Start a bidirectional TCP High_Throughput Chariot traffic between PCLAN0 and PCLAN1for 2 minutes	5- The bidirectional traffic is launched correctly.	Passed	127.40 Mbps
6- Connect with Ethernet PCLAN2 on AP2 and PCLAN1 on AP1. Ping from one to other	6- Ping successful.		
7- Start a bidirectional TCP High_Throughput Chariot traffic between PCLAN1 and PCLAN2for 2 minutes	7- The bidirectional traffic is launched correctly.	Passed	207.50 Mbps

Table 27: WLAN-WLAN traffic.

Steps	Expected results	Result	Throughput
1- Build a three Livebox Mesh network (GWC, AP1,AP2) with a star topology. ==> GWC then AP1 and AP2.	1- Mesh network is operational		
2- Connect with Wi-Fi STA0 and STA1 on GWC. Ping from one to other.	2- Ping successful.		
3- Start a bidirectional TCP High_Throughput Chariot traffic between STA0 and STA1 for 2 minutes	3- The bidirectional traffic is launched correctly.	Passed	30.92 Mbps
4- Connect with Wi-Fi STA0 on GWC and STA2 on AP2. Ping from one to other.	4- Ping successful.		
5- Start a bidirectional TCP High_Throughput Chariot traffic between STA0 and STA2 for 2 minutes	5- The bidirectional traffic is launched correctly.	Passed	15.41 Mbps
6- Connect with Wi-Fi STA2 and STA3 on AP2. Ping from one to other.	6-Ping successful.		
7- Start a bidirectional TCP High_Throughput Chariot traffic between STA2 and STA3 for 2 minutes	7- The bidirectional traffic is launched correctly.	Passed	34.71 Mbps
8- Connect with Wi-Fi STA0 on GWC and STA4 on AP1. Ping from one to other.	8- Ping successful.		
9- Start a bidirectional TCP High_Throughput Chariot traffic between STAO and STA4 for 2 minutes	9- The bidirectional traffic is launched correctly.	Passed	25.56 Mbps
10- Connect with Wi-Fi STA2 on AP2 and STA1 on AP1. Ping from one to other.	10- Ping successful.		
11- Start a bidirectional TCP High_Throughput Chariot traffic between PCLAN2 and PCLAN4 for 2 minutes	11- The bidirectional traffic is launched correctly.	Passed	18.11 Mbps

Table 28: WLAN-LAN traffic.

Steps	Expected results	Result	Throughput
1- Build a three Livebox Mesh network (GWC, AP1,AP2) with a star topology. ==> GWC then AP1 and AP2.	1- Mesh network is operational		
2- Connect with Wi-Fi STAO and with Ethernet PCLANO on GWC. Ping from one to other.	2- Ping successful.		
3- Start a bidirectional TCP High_Throughput Chariot traffic between STAO and PCLANO for 2 minutes	3- The bidirectional traffic is launched correctly.	Passed	82.38 Mbps
4- Connect with Wi-Fi STA0 on GWC and with Ethernet PCLAN1on AP1. Ping from one to other.	4- Ping successful.		
5- Start a bidirectional TCP High_Throughput Chariot traffic between STAO and PCLAN1 for 2 minutes	5- The bidirectional traffic is launched correctly.	Passed	74 Mbps
6- Connect Wi-Fi STA1 and Ethernet PCLAN1 on AP1. Ping from one to other.	6-Ping successful.		
7- Start a bidirectional TCP High_Throughput Chariot traffic between STA1 and PCLAN1 for 2 minutes	7- The bidirectional traffic is launched correctly.	Passed	90.66 Mbps
8- Connect with Ethernet PCLAN1 on GWC and with Wi-Fi STA1 on AP1. Ping from one to other.	8- Ping successful.		

Document ID: D6.2: Report on validation FP7 Contract n°318273



86

9- Start a bidirectional TCP High_Throughput Chariot traffic between STA1 and PCLAN1 for 2 minutes	9- The bidirectional traffic is launched correctly.	Passed	69.29 Mbps
10- Connect with Wi-Fi STA2 on AP2 and with Ethernet PCLAN3 on AP3. Ping from one to other.	10- Ping successful.		
11- Start a bidirectional TCP High_Throughput Chariot traffic between STA2 and PCLAN3 for 2 minutes	11- The bidirectional traffic is launched correctly.	Passed	72.9 Mbps

Version: V1.0

Dissemination level: PU



APPENDIX A3: WI-FI ABSTRACTION MODEL FOR OFFLOADING STUDIES

The abstraction model presented in this Appendix was built for the LTE to Wi-Fi offloading scenario (section 5.1). It was elaborated in the medium-size area shown in Figure 73. The number of APs, distributed in the different floors of this area, was deduced from a typical Wi-Fi penetration rate, i.e. 5000 private AP/km². The location of APs is drawn from a random generator, but with some constraints to prevent from having two APs in the same "apartment".

The propagation around all those APs is simulated from the Volcano ray-based model using parameters calibrated for the prediction of dense femto-cell coverage and interference. These parameters have been derived from advanced studies in the frame of the European project FREEDOM few years ago [COR]. The propagation loss is predicted inside the building where the AP is located, but also in surrounding streets and other buildings.

The simulation is validated by comparison to 2.4 GHz Wi-Fi measurements collected in Santander downtown. A perfect match is not expected, as the uncertainties on the AP density and Wi-Fi traffic are too much strong. However the objective is to check that the metrics of interest are well simulated with a realistic order of magnitude.



Figure 73: Deployment of Access Points within the Wi-Fi study area (blue polygon). All APs from different floors are superimposed in the view.

The signal propagation from the AP deployment towards the streets is simulated and compared to the statistics extracted from the Santander drive-test measurements. One particular metric is used: the total beacon power, which is computed from the Wi-Fi scanner measurements by summing the received beacon power from all detected APs. Figure 74 shows the CDF built from the measurements (black line) and the same CDF built from the simulations (red line). The shapes of CDFs do not perfectly match but the median values are very close; and the RMSE is only 6.8 dB. This conclusion makes us confident in the ability of the Wi-Fi abstraction model to represent (with simplifications) the reality.



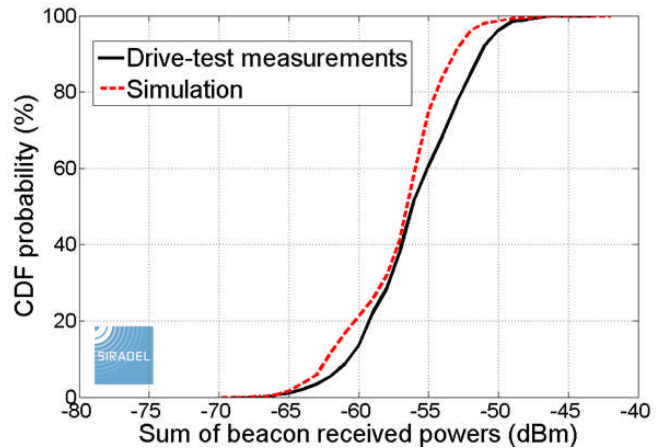


Figure 74: Comparison between outdoor Wi-Fi simulations and measurements (Santander downtown) based on the total beacon power.

The measurements at 2.4 GHz from the fixed dosimeters of the SmartSantander platform have also been compared to the simulations, considering the total received signal power instead of the total beacon power. This received power depends on each AP duty cycle, which relies on the user traffic conditions. There is thus an additional uncertainty that is related to the coherence between the real traffic during the measurement and the one assumed in the simulation inputs. Here again, the highest part of the CDF (high signal levels) does not match: the simulation is pessimistic. But the difference at the 60% percentile (about 75 dB μ V/m) is less than 2 dB. The measurements below this 60% percentile are not available.

Even if the comparison shows strong uncertainty, it is confirmed that the Wi-Fi signal level simulated in the street is of a good order of magnitude.

After this validation, the final step in the construction of the Wi-Fi abstraction model is the calculation of DL exposure and DL/UL max throughput maps in the streets and at the different floors (Figure 75) from which indoor and outdoor statistic distributions are derived.

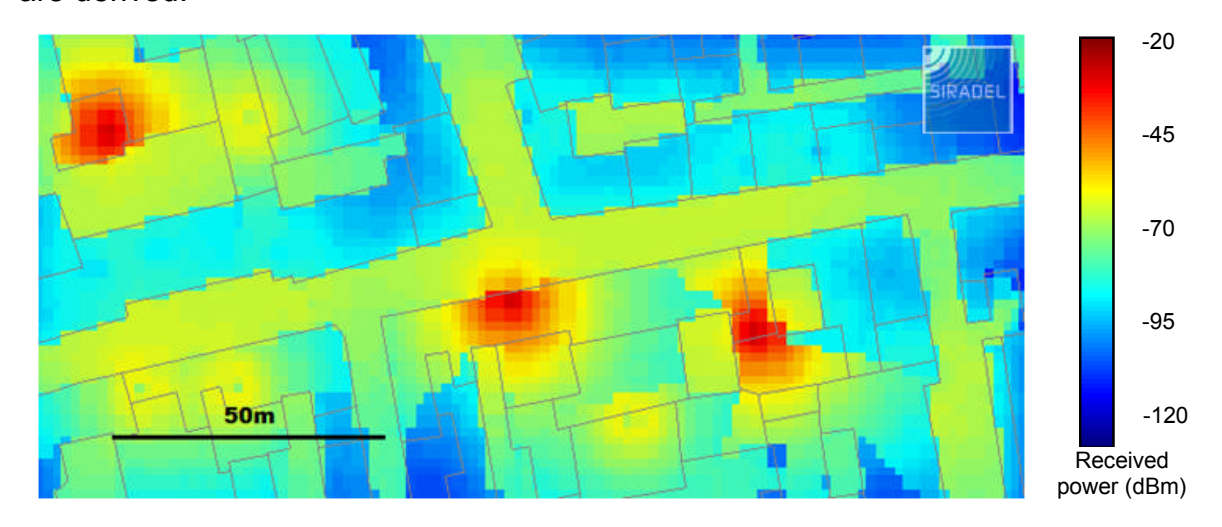


Figure 75: DL field strength generated at the ground floor by the Wi-Fi Access Points.